Synthesis and Photoluminescence Properties of Bi^{3+} activated Novel Single Phase Full Color Emitting Phosphors for White Light Emitting Diode Applications

Thesis submitted to

KERALA UNIVERSITY

In partial fulfillment of the requirements for the award of the degree of

DOCTOR OF PHILOSOPHY
IN PHYSICS
UNDER THE FACULTY OF SCIENCE

by

SUCHITHRA V.G.

Materials Science and Technology Division
CSIR - National Institute for Interdisciplinary Science and Technology (NIIST)
Thiruvananthapuram – 695019
Kerala, India

2020

DECLARATION

I hereby declare that the PhD thesis entitled "**Synthesis and Photoluminescence Properties of Bi^{3+} activated Novel Single Phase Full Color Emitting Phosphors for White Light Emitting Diode Applications**" is an independent work carried out by me and it has not been submitted anywhere else for any other degree, diploma, or title.

Suchithra V.G.

Thiruvananthapuram
Date:

NATIONAL INSTITUTE FOR INTERDISCIPLINARY SCIENCE AND TECHNOLOGY (NIIST)

Council of Scientific & Industrial Research
(Formerly Regional Research Laboratory)
Industrial Estate P.O., Trivandrum - 695 019
Kerala, INDIA

Dr. P. Prabhakar Rao
Chief Scientist & Head
Materials Science and Technology Division

Tel: 91-471-2515311
E-mail: padala_rao@yahoo.com

CERTIFICATE

This is to certify that the work embodied in the thesis entitled "**Synthesis and Photoluminescence Properties of Bi^{3+} activated Novel Single Phase Full Color Emitting Phosphors for White Light Emitting Diode Applications**" has been carried out by Mrs. Suchithra V.G. under my supervision at the Materials Science and Technology Division of National Institute for Interdisciplinary Science and Technology (NIIST-CSIR), Thiruvananthapuram and the same has not been submitted elsewhere for any other degree.

Dr. P. Prabhakar Rao
(Thesis supervisor)

Thiruvananthapuram
November, 2020

To my Parents…

Acknowledgements…

The period of completing PhD was full of hurdles to me. It was a great effort to overcome all those things. During this journey I lost my mother…my ever best well wisher, my greatest supporter, my all in all. Completing my work without her support and timely advices was very hardship to me. Still I maintained it to keep myself on the path, I continued the journey till now…managed things anyway, finally I am submitting my thesis. I am thankful to all good hearts for their timely support and care they extended towards me. I am extremely thankful to my guide Dr. P. Prabhakar Rao, for giving me an opportunity to conduct my research work with him and for the support and guidance given to me.

I am grateful to Dr. A. Ajayghosh, Director CSIR-NIIST, and former directors Dr. Suresh Das and Dr. Gangan Prathap for allowing me to carry out my research in this esteemed laboratory. I also express my gratitude to Dr. Savithri S, Dr. Harikrishna Bhat, Dr. P. Prabhakar Rao and Dr. M. L. P. Reddy, present and former Head of Materials Science and Technology Division, for extending the research facilities. Also, I sincerely thank all scientists and staffs of MSTD for all the help and support extended to me.

It is my pleasure and privilege to thank Department of Science and Technology, INSPIRE Program for the financial support granted to me to undertake this research work and also for attending many conferences and explore myself. Also I am thankful to Council for Scientific and Industrial Research (CSIR) for providing me all the facilities and infrastructure to perform my research work.

Here I also express my thankfulness to Mr. M. R. Chandran, Mrs.Soumy Valsalam and Mr, Harish Raj for SEM imaging. I wish to thank Mr. Mr. Pruthiviraj, Mr. M. P. Varkey and Mr. Shanoj for the technical support. In this context I gratefully remember my senior colleagues Dr. Linda Francis, Dr. Vaisakhan Thampi, Dr. Mahesh, Dr. Sumi S, Dr. Bradha, Dr. SreenaT.S, Dr.Athira K V Raj, Ms. Parvathy S Babu, Ms. Renju for lending me their expertise to my scientific and technical problems. Special thanks to my colleague Mrs. Aswathi B A for her companionship in the days of

loneliness. I am also thankfully remembering Ms. Aju Thara T. R. and Ms. Haritha in this occasion. Here I express my sincere gratitude to all the NIIST family for their various supports.

I am extremely indebted to all my teachers who opened me the new doors to knowledge and made me capable of thinking in new ways, and made me self confident, especially my beloved professor Dr. Sudarsan Kumar, who made initial pavements to this journey of doing PhD. I am also thankful to Dr.Deepthi Rajendran for introducing NIIST and Dr.P.Prabhakar Rao to me.

Next…how can I express my gratitude to my family with these limited words…I don't know. My Amma Mrs. Geetha Kumari G, in the other world might be seeing her kid completing her task. Dear Amma… please be with me always… I bow my head in front of my father, Mr.K.Viayakumaran Nair, with respect for giving me good education, allowing me pursue my Phd degree, he is there for all my needs anytime. My Ammumma Ms.Madhavikkutty Amma, chechi Sukannya V.G, and Chettan Ajith kumar, my Devu and Ami my anti depressants during this period. My husband Mr. Prasanth kumar, who stand with me to overcome the difficulties, it is his support and cooperative nature which helped me a lot in completing my thesis work. Finally I extend my whole hearted acknowledgement to my three month old little champ Ms.Niranjana S.P., my bundle of joy for adjusting her sleeping schedules for me…otherwise I couldn't complete the writing procedure of this thesis work.

Above all I thank almighty for letting me to do all the things and making everything successful.

Suchithra V.G.

CONTENTS

Declaration	ii
Certificate	iii
Acknowledgements	v
Contents	vii
List of Tables	xiii
List of Figures	xvii
Abbreviations	xxix
Preface	xxxi
Chapter 1: PHOSPHORS –INDRODUCTORY FACTS	**1-22**
1.1 Introduction	1
1.2 Luminescence	4
1.3 Principles of Lanthanide Luminescence	7
1.4 Solid State Lighting	9
1.5 Phosphor introducing facts	10
1.6 Basic Terminology	10
1.6a Correlated Color Temperature (CCT)	
1.6b CIE chromaticity coordinates	
1.6c Color Rendering Index (CRI)	
1.6d Luminous Efficacy	
1.7 Different Strategies for White Light Generation	11
1.8 Challenges of existing technology	11
1.9 Single Phase Phosphor for WLED, prerequisites, need and relevance	13
1.10 Energy transfer mechanism	14
1.11 Importance of Ln_3MO_7 structures	15
1.12 Luminescence Properties of Bi^{3+}	17
1.13 Literature review	20
1.14 Goals & Objectives of the Work	22

Chapter 2: Studies on photoluminescence properties of weberite type phosphors with different cationic modifications

2.1 Introduction 23

2. 2 Experimental 25

2.3 Results and discussion 26

2.3.1 Variation in A site cation 28

2.3.1.1 Powder X-ray diffraction studies 30

2.3.1.2 Morphological studies 32

2.3.1.3 Photoluminescence studies 34

2.3.2 Variation in B site cation 35

2.3.2.1 Powder X-ray diffraction studies 36

2.3.2.2 Absorption studies

2.3.2.3 Photoluminescence studies

2.3.3 La3NbO7: Bi3+

2.3.3.1 Morphological studies

2.3.3.2 Absorption studies

2.3.3.3 Photoluminescence studies

2.4 Conclusions

Chapter 3: Color - Tunable Phosphors in Weberite Type System, $La_3SbO_7:Bi^{3+}$, Eu^{3+} for Near-UV LED Applications

3.1 Introduction 51

3. 2 Experimental 53

3.3 Results and discussion

3.3.1 XRD refinement and crystal structure 73

3.3.2 Morphological studies 73

3.3.3 Absorption studies 73

3.3.4 Photoluminescence properties, energy transfer and chromaticity 74

3.4 Conclusions 74

Chapter 4: New full color emitting phosphor through energy transfer in Bi^{3+} and Eu^{3+} co - doped La_3TaO_7 weberite system

4.1 Introduction 77

4. 2 Experimental 79

4.3 Results and discussion 80

4.3.1 Effect of partial substitution 82

4.3.1.1 XRD analysis 85

4.3.1.2 Photoluminescence studies 85

4.3.2 Eu^{3+} co-doped $La_3TaO_7:Bi^{3+}$ 86

4.3.2.1 XRD analysis and crystal structure 87

4.3.2.2 Morphological studies 89

4.3.2.3 Absorbance, Photoluminescence properties, energy transfer and chromaticity 90

4.4 Conclusions 91

Chapter 5: Novel $LaGaGe_2O_7$ single phase phosphors for WLED applications 93

5.1 Introduction 93

5. 2 Experimental 95

5.3 Results and discussion 96

5.3.1 Luminescence properties of Bismuth doped LaGaGe2O7 98

5.3.1.1 Powder X-Ray diffraction studies 98
5.3.1.3 Photoluminescence studies 100
5.3.2 Effects of Cerium substitution into Monoclinic $LaGaGe_2O_7$ 107
5.3.2.1 Powder X-Ray diffraction studies 109
5.3.2.3 Photoluminescence studies 109
5.3.3 Europium co-doping and photoluminescence studies 110
5.3.2.4 Morphological studies 111
5.3.3.2 Absorption studies
5.3.2.6 Photoluminescence and Energy Transfer 111
5.4 Conclusions 111
Chapter 6: Full color emission in Pyrochlore type phosphor 113
$La_2 Y_{0.66} Sn_{0.66} Sb_{0.66}O_7$: Bi^{3+}, Eu^{3+}
6.1 Introduction 114
6.2 Experimental 117
6.3 Results and discussion 123
6.3.1 Powder X-Ray diffraction studies 125
6.3.2 Morphological studies 126
6.3.3 Absorption studies 128
6.3.4 Photoluminescence studies 130
6.4 Conclusions
Chapter 7: Conclusions And Future Aspects
7.1 Conclusions 137
7.2 Future scope 138
References 139
List of publications 163

LIST OF TABLES

Table No.	Table Caption	Page No.
2.1	Average crystallite size of L*B*O compounds	46
2.2	Band gap values of La_3NbO_7: Bi^{3+} samples	50
2.3	CIE values of La_3NbO_7: Bi^{3+} samples	60
3.1	Starting structure model of $La_{2.93}SbO_7$:0.04 Bi^{3+}, 0.03Eu^{3+}	75
3.2	Refined parameters obtained from Rietveld analysis of LSO: $x$$Bi^{3+}$, $y$$Eu^{3+}$	80
3.3	Band gap energy of LSO: 0.04Bi^{3+}, $y$$Eu^{3+}$($y$ = 0.005, 0.01, 0.02, 0.03, 0.04)	85
3.4	Color coordinates of LSO: $x$$Bi^{3+}$($x$ = 0, 0.025, 0.04, 0.05, 0.06, 0.075).	90
3.5	CIE color coordinates and lifetime values of La_3SbO_7: $x$$Bi^{3+}$, $y$$Eu^{3+}$($x$ = 0.04, y = 0.005, 0.01, 0.02, 0.03, 0.04).	93
4.1	Lifetime values of LSTO:Bi^{3+},Eu^{3+} samples	124
4.2	CIE values of LSTBE samples	131
4.3	Band gap values of LTO: 0.04Bi^{3+}, $y$$Eu^{3+}$	135
4.4	Lifetime values of LTO: Bi^{3+}, Eu^{3+}	
4.5	CIE values of LTO : Bi^{3+}, Eu^{3+}	
5.1	Band gap energy of LGG: Bi^{3+}, $y$$Eu^{3+}$.	147
5.2	Lifetime values LGG: 0.05Bi^{3+}, $y$$Eu^{3+}$ samples	151
5.3	CIE values of LGG: Bi^{3+}, Eu^{3+} samples	153
6.1	Band gap energy of LYSSO: 0.04 Bi^{3+}, $y$$Eu^{3+}$ (0.01 to 0.075) samples.	176
6.2	CIE values of LYSSO: 0.04Bi^{3+}, $y$$Eu^{3+}$ samples	180
6.3	Lifetime values of LYSSO: 0.04Bi^{3+}, $y$$Eu^{3+}$ samples	183

LIST OF FIGURES

Figure No.	Figure Caption	Page No.
1.1	Energy level diagrams of the lanthanide ions.	3
1.2	History of lighting	5
1.3	Comparison of different light sources	6
1.4	CIE chromaticity coordinate diagram	11
1.5	Example for color rendition(Franz Mark "Blue horse"(1911))	13
1.6	Luminous efficacy timeline of different light sources	19
1.7	Representation of Weberite structure	22
1.8	Representation of Pyrochlore structure	23
1.9	Energy level Diagram of Bismuth ions	26
2.1	Powder X-ray diffraction patterns of A_3SbO_7 (A = Y, La, Lu, Gd) samples.	45
2.2	SEM images of A_3SbO_7 (A = Y, La, Lu, Gd) samples	46
2.3	PLE spectra A_3SbO_7 (A = Y, La, Lu, Gd) samples	48
2.4	PL spectra A_3SbO_7 (*A* = Y, La, Lu, Gd) samples	49
2.5	Powder X-ray diffraction patterns of La_3BO_7 (*B*= Sb, Ta and Nb) samples	51
2.6	Powder X-ray diffraction patterns of La_3BO_7: Bi^{3+}(*B*= Sb, Ta and Nb) samples	52
2.7	Absorption spectra La_3BO_7: Bi^{3+} (*B* = Sb, Ta and Nb) samples	52
2.8	Photoluminescence Excitation spectra of La_3MO_7: Bi^{3+}(M = Sb, Ta and Nb) samples	53
2.9	Photoluminescence emission spectra of La_3MO_7: Bi^{3+}(M = Sb, Ta and Nb) samples	53
2.10	SEM images of LNO: xBi^{3+} (x = 0.01, 0.02, 0.03, 0.04, 0.05)	54
2.11	EDS spectra of LNO:Bi^{3+} sample	56

2.12	X-ray dot mapping images of LNO: Bi^{3+}	58
2.13	Absorption spectra La_3NbO_7: Bi^{3+} samples	59
2.14	Photoluminescence excitation spectra of La_3NbO_7: xBi^{3+} samples	61
2.15	Photoluminescence emission spectra of La_3NbO_7: xBi^{3+} samples	62
2.16	CIE Diagram of La_3NbO_7: Bi^{3+} samples	63
3.1	Crystal structure of La_3SbO_7.	75
3.2	Powder XRD patterns of LSO:$x$$Bi^{3+}$($x$ = 0, 0.025, 0.04, 0.05, 0.06, 0.075	76
3.3	Powder XRD patterns of LSO: 0.04Bi^{3+}, $y$$Eu^{3+}$($y$ = 0.005, 0.01,0.02, 0.03, 0.04) samples, the inset illustrates the enlarged 2θ range around 30- 34°.	77
3.4	EDS spectra of LSO:$x$$Bi^{3+}$($x$=0,0.04)	78
3.5	SEM images of LSO: $x$$Bi^{3+}$, $y$$Eu^{3+}$ (x = 0.04, y = 0.005, 0.01, 0.02, 0.03, 0.04)	78
3.6	EDS spectra of LSO: 0.04Bi^{3+}	78
3.7	EDS spectra of LSO: 0.04Bi^{3+}, 0.03Eu^{3+}	79
3.8	Absorption spectra of (a) LSO: $x$$Bi^{3+}$ and (b) LSO: 0.04Bi^{3+}, $y$$Eu^{3+}$	80
3.9	PLE spectra of LSO: 0.04Bi^{3+}under λ_{em} = 517 nm, 560 nm, 570 nm	81
3.10	PL spectra of LSO: 0.04Bi^{3+}under different excitations	82
3.11	PLE spectra of LSO: $x$$Bi^{3}$ for λ_{em} = 517 nm	84
3.12	PL spectra of LSO: $x$$Bi^{3+}$($x$ = 0, 0.025, 0.04, 0.05, 0.06, 0.075) under λ_{ex} = 315 nm	86

3.13	PLE spectra of LSO: 0.04Bi^{3+}, 0.03Eu3+ under λ_{em} = 517 nm, 575 nm, 581 nm, 606 nm, 616 nm	87
3.14	PLE spectra of LSO: Bi^{3+}, Eu^{3+} samples with different Eu^{3+} concentration	87
3.15	EDS of $Gd_{2-x}Ce_2O_7$: xEu^{3+}; x = (a) 0.05 and (b) 0.20red phosphors.	88
3.16	PL spectra of LSO: Bi^{3+}, Eu^{3+} samples under λ_{ex} = 303 nm	88
3.17	PL spectra of LSO: Bi^{3+}, Eu^{3+} samples under λ_{ex} = 390 nm	89
3.18	Energy transfer mechanism in LSO: xBi^{3+}, yEu^{3+} samples	90
3.19	Dependence of η_T on Eu^{3+} concentration	91
3.20	Dependence of ln(Iso/Is) on total concentrtion of dopants and Iso/Is on $C^{n/3}$ for n = 6, 8, 10.	92
3.21	Fitted curves of dependence of Iso/Is on $C^{n/3}$ for n = 6, 8, 10	94
3.22	Decay curves of LSO: xBi^{3+}, yEu^{3+}(x = 0.04, y = 0.005, 0.01, 0.02, 0.03, 0.04) at λ_{ex} = 303 nm and λ_{em} = 616 nm	95
3.23	Plot of lifetime values against Eu^{3+} concentration	96
4.1	The powder XRD patterns of $La_3Sb_xTa_{1-x}O_7$: Bi^{3+}, Eu^{3+} samples	112
4.2	PLE spectra of LSTO: Bi^{3+}, Eu^{3+} samples at 582 nm emission wavelength	114
4.3	PLE spectra of LSTO: Bi^{3+}, Eu^{3+} samples at 517 nm emission wavelength	116
4.4	PL spectra of LSTO: Bi^{3+}, Eu^{3+} samples at 315 nm emission wavelength	117
4.5	PL spectra of LSTO: Bi^{3+}, Eu^{3+} samples at 332 nm emission wavelength	118
4.6	PL spectra of LSTO: Bi^{3+}, Eu^{3+} samples at 337 nm emission wavelength	119
4.7	PL spectra of LSTO: Bi^{3+}, Eu^{3+} samples at 390 nm emission wavelength	120
4.8	Lifetime decay curve of LSTO:Bi^{3+},Eu^{3+} samples	121
4.9	Crystal structure of LTO	123
4.10	Powder XRD patterns of LTO samples	124

4.11	SEM images of LTO: 0.04 Bi^{3+}, yEu^{3+} samples	125
4.12	X-ray dot mapping of LTO: 0.04 Bi^{3+}, 0.02 Eu^{3+}	126
4.13	EDAX image of LTO: 0.04 Bi^{3+}, 0.20 Eu^{3+}	127
4.14	Absorption spectra of LTO: 0.04Bi^{3+}, yEu^{3+}	128
4.15	Emission spectra of LTO: xBi^{3+}(x = 0.04, 0.05, 0.06, 0.075) samples	128
4.16	Excitation spectra of LTO host and LTO: 0.04Bi^{3+} sample for an emission corresponding to 454 nm	129
4.17	Emission spectra of LTO: 0.04Bi^{3+} samples at different excitations, the inset shows host emission peak	130
4.18	PL and PLE spectra of LTO: Bi^{3+}, Eu^{3+}	131
4.19	PLE spectra of LTO: 0.04 Bi^{3+}, yEu^{3+}	136
4.20	PL spectra of LTO: 0.04 Bi^{3+}, yEu^{3+}	
4.21	Spectral overlap between PL spectra of LTO: 0.04Bi^{3+} and PLE of LTO: yEu^{3+}	
4.22	Lifetime measurements of LTO: Bi^{3+}, Eu^{3+}	
4.23	Energy transfer efficiency determination plot	
4.24	Fitted curves of intensity ratios Vs concentration	
5.1	XRD patterns of $LaGaGeO_7$: xBi^{3+} samples	147
5.2	Emission spectra of LGG : Bi^{3+} sample for different excitations	148
5.3	PLE of LGG: Bi^{3+} for different emission wavelengths	148
5.4	Powder XRD pattern of cerium substituted $LaGaGe_2O_7$:Bi^{3+} sample	149
5.5	Excitation spectra of $La_{0.95}GaGe_{1.8}Ce_{0.2}O_7$ sample for λ_{em} =382 nm and λ_{em} = 455 nm	149
5.6	Emission spectra of $La_{0.95}GaGe_{1.8}Ce_{0.2}O_7$ sample for λ_{ex} =252 nm and λ_{ex} = 315 nm	150

5.7	Powder XRD patterns of LGG: xBi^{3+}, yEu^{3+} samples	151
5.8	SEM images of $LaGaGe_2O_7$: 0.05Bi^{3+}, yEu^{3+} samples	152
5.9	X-ray dot mapping images of $LaGaGe_2O_7$: 0.05Bi^{3+}, 0.04yEu^{3+} samples	154
5.10	EDS spectra of LGG: Bi^{3+}, Eu^{3+} samples	155
5.11	Absorption spectra for LGG: Bi^{3+}, yEu^{3+} samples	156
5.12	PLE and PL spectra for LGG: Bi^{3+}, Eu^{3+} sample	156
5.13	PLE spectra of $LaGaGe_2O_7$: Bi^{3+}, Eu^{3+} samples at an emission wavelength of 452 nm	157
5.14	PL spectra of $LaGaGe_2O_7$: Bi^{3+}, Eu^{3+} samples	158
5.15	Lifetime decay curves of $LaGaGe_2O_7$: Bi^{3+}, Eu^{3+} samples	159
5.16	CIE diagram of LGG: Bi^{3+}, Eu^{3+} samples	161
5.17	Fitted curves of dependence of I_{so}/I_s on $C^{n/3}$ for n = 6, 8, 10 and total concentration of Bi^{3+} and Eu^{3+} ions.	161
6.1	XRD pattern of LYSSO : xBi^{3+}, yEu^{3+} ((a)x = 0, (b)x = 0.04, (c)x = 0.04, y = 0.01, (d)x = 0.04, y = 0.05)	174
6.2	SEM images of LYSSO: xBi^{3+}, yEu^{3+} samples	175
6.3	EDS spectra for LYSSO: xBi^{3+}, yEu^{3+} for (a) x = 0, y = 0 (b) x = 0.04(c) x =0.04, y =0.05	175
6.4	X-ray dot mapping images of LYSSO: xBi^{3+}, yEu^{3+} for (x = 0.04, y = 0.05)	177
6.5	Absorption spectra for LYSSO: 0.04Bi^{3+}, yEu^{3+}(0.01 to 0.075).	178

6.6	PL and PLE spectra for LYSSO: 0.04Bi^{3+} samples for different excitation (307 nm, 322 nm) and emission (424 nm, 500 nm) wavelengths	179
6.7	PLE spectra for LYSSO: xBi^{3+} samples for emission at 520 nm	181
6.8	PL spectra for LYSSO: xBi^{3+} samples for excitation at 322 nm	181
6.9	PLE spectra of LYSSO: 0.04Bi^{3+}, *y*Eu^{3+} samples	182
6.10	PL spectra of LYSSO: 0.04Bi^{3+}, *y*Eu^{3+} samples	182
6.11	CIE diagram of LYSSO: 0.04Bi^{3+}, *y*Eu^{3+} samples	184
6.12	Lifetime decay curves of LYSSO: 0.04Bi^{3+}, *y*Eu^{3+} samples	184

ABBREVATIONS

CCT	: Correlated Color Temperature
CIE	: Commission Internationale de I' Eclairage
CN	: Coordination Number
CRI	: Color Rendering Index
CT	: Charge Transfer
ED	: Electric Dipole
EDS	: Energy Dispersive Spectroscopy
FWHM	: Full Width Half Maximum
ISO	: International Organization for Standardisation
JCPDS	: Joint Committee on Powder Diffraction Standards
LED	: Light Emitting Diode
LMCT	: Ligand to Metal Charge Transfer
Ln	: Lanthanide
MD	: Magnetic Dipole
NIR	: Near Infrared
pc-WLED	: Phosphor Converted White Light Emitting Diode
PL	: Photoluminescence
RE	: Rare Earth
SEM	: Scanning Electron Microscopy
SSL	: Solid State Lighting
UV-vis	: Ultraviolet Visible
XRD	: X-ray Diffraction

PREFACE

The existing energy demands require low power consuming durable energy sources for building up a sustainable energy management system all over the world. In lighting industry White light emitting diodes, the green lighting sources of modern era is astonishing the industry with their warm light, long lifetime, light stability, energy saving and environmental friendly characteristics. Many efforts are going on to develop suitable and advanced sources of lighting. Every effort to bring in advancements in its characteristics needs careful engineering of the material properties. The crystal phase engineering or selection of crystal structure plays a vital role in the whole task. Weberite type systems have already gained attention in the field of luminescence due to their high chemical as well thermal stability. We have conducted a study on a series of weberite type systems of general formula A3BO7 by varying the A site cations and modified the cationic ratios by doping with Bismuth ions into A site. Bismuth ions are gaining more attention nowadays as dopants in inorganic luminescence related researches owing to their host dependent luminescence behavior which aids the desired results very much. Luminescence of Bismuth ions is based on the electron transitions between the 6s2 ground states and the 6s6p excited states.

Currently many reports on the development of single phase phosphors are drawing our attention. Among the reported studies on single phase phosphors, development of phosphor by utilizing energy transfer mechanism is getting more wide recognition. The energy transfer between activators may be radiative or non- radiative. The non-radiative energy transfer is also classified into resonance-energy transfer, spin-coupling energy exchange, and non-resonance energy transfer. Resonance energy transfer occurs between a sensitizer and an activator with the same radiative frequency, and the mechanism could be of exchange interaction or electric multi-polar interaction. The electric dipole - dipole interactions and dipole - quadrupole interactions can result in energy transfer in solids and both these interactions can take place over metal ion – metal ion distances which are observed in solids. Interactions between electric quadrupoles are not expected to play an important role in solids in view of the very short interaction range. There are reports on electric multi-polar interactions existing between Bi3+/Eu3+ ions. By using Van Uitert's

multi- polar energy transfer - mechanism it is possible to identify the energy transfer mechanism existing phosphor materials.

The present research work is organized into seven chapters. Introduction chapter discusses about the basic concepts of solid state lighting technology and different methods for white light generation with their advantages and practical challenges. The importance of Bi^{3+} as well as Eu^{3+} ions in the development of rare earth phosphors is discussed. Importance of weberite type phosphors is also mentioned here. The need and relevance of developing single phase phosphors for WLED applications is emphasized in first chapter. In second chapter different characterization techniques including powder X-ray diffraction, Scanning Electron microscope, Energy dispersion spectroscopy, X-ray dot mapping, UV-visible absorption spectroscopy and luminescence spectroscopy are explained in detail.

Third chapter discuss about the variation in structural and photoluminescence properties of different weberite system with cationic modification with different rare-earth ions in the *A* site of the system of general formula A_3MO_7(A= La,Gd,Y,Lu). Better luminescence properties were observed for Lanthanum system, hence the rest of the chapter discuss the luminescence tuning in this particular system by suitable doping of Bi^{3+} and Eu^{3+} co-doping. The variation in the luminescence intensity with various Bi^{3+} and Eu^{3+} concentrations in the La_3SbO_7 host lattice was also studied to calculate the optimum doping concentration. The energy transfer mechanism in this phosphor was also studied by statistical analysis of the experimental data.

The influence of various d block elements in the M site of La_3MO_7 (M= Sb,Ta,Nb) system is discussed in the fourth and fifth chapters. In these chapters also we are discussing about direct white light emitting single phase phosphors by co-doping of Eu^{3+} ions along with Bi^{3+} ions. Luminescence intensity variation as well as shift in emission range was occurred due to different M site substitutions. The influence of partial occupancy of Sb ions along with Ta and Nb ions was also studied in these chapters. These phosphors exhibit strong absorptions at near UV and blue wavelength regions and emit intense multiband emissions due to $^1S_0 - ^1P_1$, $^3P_1$ transitions of Bi^{3+} and $^5D_0 - ^7F_{0,\,1,\,2}$ transitions of Eu^{3+}.

Inn the fifth chapter we discuss the luminescence behavior of monoclinic lanthanum system $LaGaGe_2O_7$. Here we have substituted Cerium along with Bismuth ions and then Europium was co-doped with Bismuth ions. Variation in luminescence behavior was studied. Variation in emission for different excitations were studied for Bismuth alone doped system and then Bismuth concentrations were optimized and Europium was co-doped into the matrix. Luminescence emission spectrum covers the whole visible region with multiple emission peaks in the blue and red regions.

Based on the studies described in the chapters three and four we further tried to enhance the photoluminescence properties by compositional variation. With a view to increase the polarizability around the Bi^{3+} ion and for improving the ordering in the host lattice we introduced some compositional variations. In the sixth chapter we studied the luminescence properties and energy transfer mechanism in Bi^{3+} and Eu^{3+} doped stannate pyrochlore system $Ln_2Y_{0.66}Sn_{0.66}Sb_{0.66}O_7$. Broad nature of excitation and emission spectra in this phosphor is found to be very suitable for WLED applications. Structural dependent energy quenching is discussed in this chapter.

Conclusions drawn from the studies on the structural aspects and the Bi^{3+} and Eu^{3+} photoluminescence properties in these closely related host structures which will help in the design of efficient single phase full color emitting phosphors for pc-WLED applications are presented in the Chapter seven.

Chapter 1

PHOSPHORS –INDRODUCTORY FACTS

It was a long journey from the fire candles to the invention of LEDs. Solid state lighting technology can be traced as far back as 1962 to the first laser announced by Hall. The advancements in this field have added many benefits to the lighting industry, as these light sources have superior efficiency, lifetime, reliability which make it more energy saving and environmental friendly for less thermal radiation and no mercury. The first commercially available white light emitting diodes was produced by Nichia corporation in 1996 after the invention of InGaN/GaN blue LED chips by Shuji Nakamura in 1993. To date phosphor converted WLEDs are energy saving devices. The research efforts of developing white emitting single phase phosphors with Bi^{3+} doped phosphors and basics of solid state lighting are included in this chapter. An overview of the ongoing research works in this field and challenges facing to achieving the research goal is also discussed in this chapter.

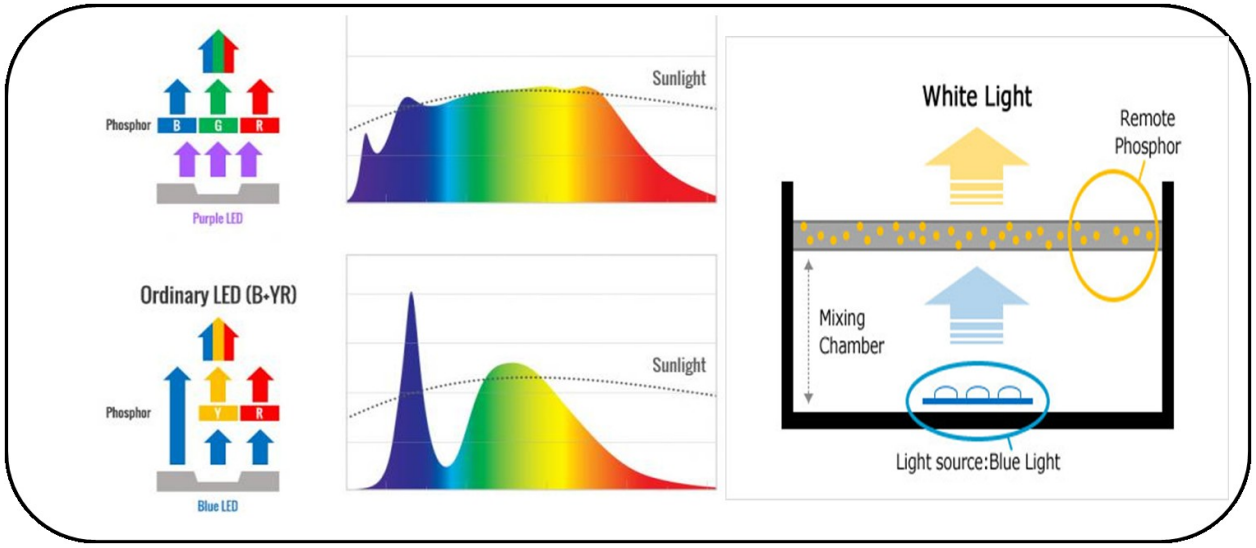

1.1 Introduction

The role of Rare earth ions in the technologies that support our modern society is inevitable from the beginning of the latter half of the 20th century. The unique properties exhibited by rare earths have enhanced the capabilities of established technologies and enabled innovations that affect many aspects of our lives. There are various applications for this rare earth elements ranging from television to telecommunications, materials processing to information processing, medical science to environmental science. Furthermore, research on rare-earth materials continues to stimulate advances in both fundamental and applied science, providing the basis for tomorrow's technological breakthroughs. The creation and manipulation of light is one of the most scientifically exciting and economically significant applications of rare earths. During the last three decades there was a revolution in luminescence technology driven by the use of rare-earth-activated materials in a variety of practical applications. This has led to rare-earth materials becoming an essential component in today's solid-state lasers, fluorescent lights, and information displays. As the next generation of luminescence technology is developed, rare-earth-activated materials will undoubtedly continue to play a leading role.

1.2 Luminescence

The term luminescence comes from the Latin (*lumen* = light) and was first introduced as *luminescenz* by the physicist and historian of science, Eilhardt Wiedemann in 1888. Acording to him "all those phenomena of light which are not solely conditioned by the rise in temperature", as opposed to

incandescence (B. Valeur et al. 2001). Luminescence is cold light whereas incandescence is hot light. Luminescence is the phenomena of emission of light caused by the absorption of energy. And depending on the kind of energy absorbed luminescence is classified. Some of the commonly observed luminescence are

a. *Electroluminescence* is produced by the passage of an electric current through an ionized gas. Example: a gas discharge lamp.

b. Radioluminescence obtains its energy from the high energy particles released via radioactive decay. Example: a luminous radium watch dial.

c. Triboluminescence is derived from the Greek word tribo meaning to rub. It is emitted when certain crystals are stressed, crushed, or broken. Example: certain types of sugar crystals.

d. Sonoluminescence is produced in liquids exposed to intense sound (compression) waves.

e. Chemiluminescence derives its energy from chemical reactions. It is the breaking of chemical bonds that supplies the energy.

f. Bioluminescence can be considered a subdivision of chemiluminescence. It occurs when chemiluminescent reactions take place in living systems and usually involves a ATP reaction. Example: light emitted by fireflies and glow-worms.

g. Cathodoluminescence is light that is generated from the exposure of substances to cathode rays.

h. Photoluminescence derives its energy from the absorption of light energy (most commonly in the wavelength ranges of infrared, ultraviolet, or visible light). Photoluminescence is further divided into the categories of fluorescence, delayed fluorescence, and phosphorescence. Today they are defined via the emission based quantum mechanical mechanism for the orbital angular momentum multiplicity of the emitted electron (i.e. the singlet or triplet excited state). However, before the advent of quantum theory photoluminescence was defined solely on the basis of empirical evaluation of the duration of emissive lifetime.

Fluorescence is defined as a photoluminescent emission that arises from the singlet electronic state. To the human eye fluorescence is observed only when the exciting light source shines on the radiator. Phosphorescence is defined as a photoluminescent process that originates from the triplet electronic state. Emissions from the triplet state are from 10 to 10,000 times longer than fluorescence; therefore, to the eye these radiators appear to emit after the excitation radiation is removed. Delayed fluorescence is a rare phenomenon whereby the electron responsible for the emission starts out in the singlet state, crosses over to the triplet state, but eventually returns to the singlet state prior to emission. The result is a singlet state emission of much longer lifetime than normal. In excited singlet

states, the electron in the excited orbital is paired (of opposite spin) to the second electron in the ground-state orbital. Consequently, return to the ground state is spin-allowed and occurs rapidly by emission of a photon. The emission rates of fluorescence are typically 10-8 s, so that a typical fluorescence lifetime is near 10 ns. Phosphorescence is emission of light from triplet-excited states, in which the electron in the excited orbital has the same spin orientation as the ground-state electron. Transitions to the ground state are forbidden and the emission rates are slow (10 – 100 s), so that phosphorescence lifetimes are typically milliseconds to seconds. Earlier literature refers to phosphorescence for emissions with lifetime > 10-3 s, whereas recent literature suggests lifetime > 10-8 s. Luminescence is an all encompassing term that refers to emission of light from any substance and occurs from electronically excited states. Therefore, luminescence will be used to describe any radiative transition that cannot be defined as either fluorescence or phosphorescence.

1.3 Principles of Lanthanide Luminescence

The 4f electrons of the lanthanides are well shielded from the Environment. Hence the spectroscopic and magnetic properties like electronic spectra and crystal-field splitting of these ions are largely independent of environment like solvent, coordinated ligands, etc. The number (N) of configurations for $\boldsymbol{n}$ electrons rapidly increases with the number of 4f electrons:

$$N = \frac{14!}{n!\,(14-n)!},\ 1 \le \boldsymbol{n} \le 13$$

The lowest energy term for each ion consistent with the predictions of Hund's first and second rules [23, 24]. Since all configurations have different energies, the lanthanides tend to exhibit rich and complex energy level structure. Due to the insignificant dependence of the Ln emission wavelength on the host material one can compile quite universal energy level scheme as "Dieke diagram for the description of the essential absorption and emission bands of such ions. (G.H. Dieke et al. 1963)

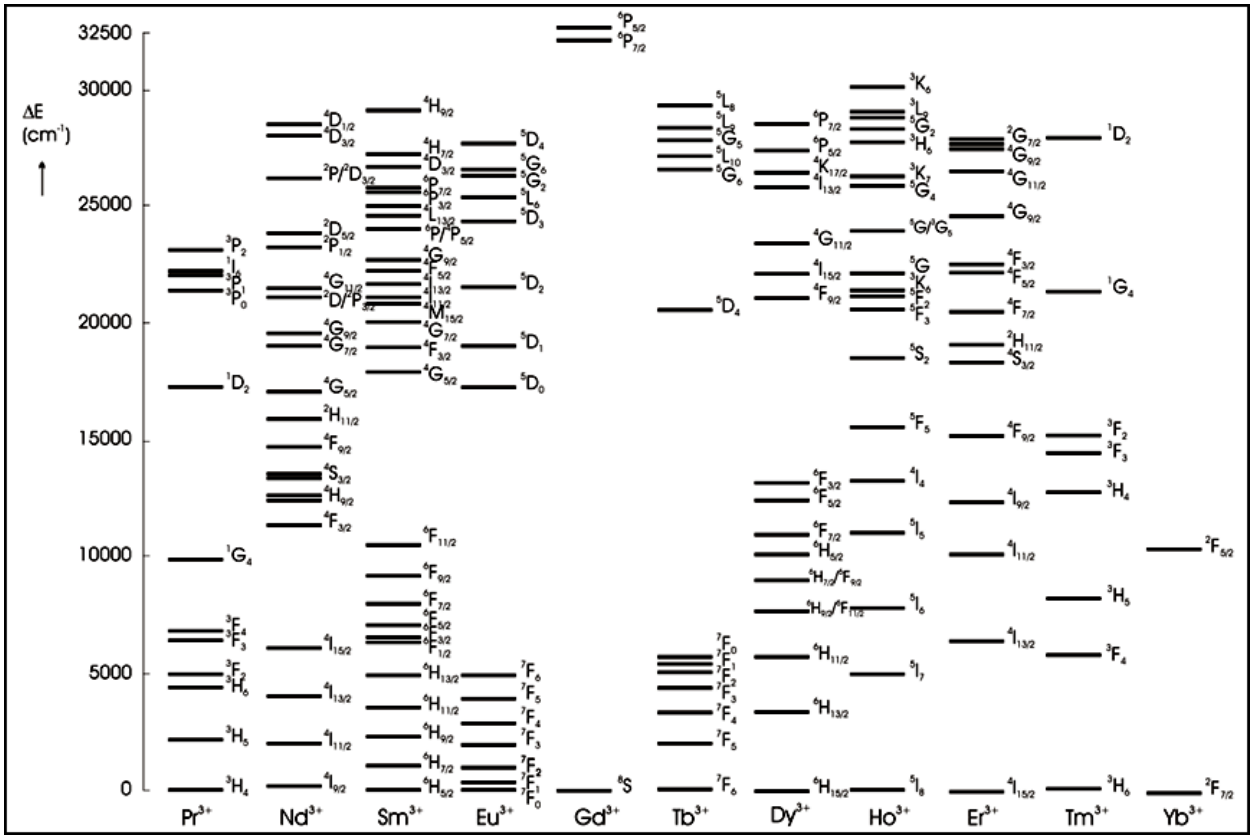

Fig.1 Energy level diagrams of the lanthanide ions.

The energies of the terms are determined by a combination of interelectronic repulsion, spin-orbit coupling and, in a coordination environment, the ligand field. The first perturbation is the electron repulsi*on* within the 4f orbitals. This Columbic interaction yields terms with a separation in the order of 104 cm-1 (N. Sabbatini et al.1993). These terms are in turn split into several ***J***-levels by a second perturbation, the spin-orbital coupling, which is relatively large (103 cm-1) because of the heavy lanthanide nucleus (W.T. Carnall et al.1979). These levels, in turn, can be split again into what are termed Stark sublevels due to ligand field effects from the coordination sphere around the lanthanide; Stark sublevel splitting is on the order of 102 cm-1. When a lanthanide is surrounded by a coordinating environment, with inorganic or organic ligands, all the electrons of the system, other than those of the lanthanide ion itself, destroy the spherical symmetry of the free ion. Usually, this effect is called the crystal-field perturbation.

When the lanthanide is placed in a magnetic field, there is an additional perturbation: the Zeeman perturbation. All remaining degeneracy is destroyed. This results in the overall emission peak position remaining largely unchanged as the f electrons remain shielded, but the emission profile of a lanthanide can vary greatly depending on modulation of these influences (J.C.G. Bünzli et al. 1989, J. Holsa et al. 2005). The number of Stark sublevels depends on the site symmetry of the lanthanide ion, and these can be thermally populated at room temperature, yielding emission spectra that are more complex.

For electronic configurations with even number of equivalent electrons, the ***J*** state degeneracy can be removed completely and the number of the states is $2\boldsymbol{J} + 1$. Based on this it is expected that the luminescence spectra of **Ln** ions can be used as probes for local crystal field symmetry at the impurity centre. Due to spin-orbit coupling, the excited states of the lanthanides are well separated from the ground state manifold. Thus, the excited states are thermally inaccessible and ideal for electronic transitions. With the exceptions of the $4f^0$ and $4f^{14}$ species (La^{3+} and Lu^{3+}), all lanthanide ions absorb electromagnetic radiation, primarily in the visible region, which is manifested in f-electrons from the partially filled 4f subshell being excited from the ground state to an excited state. 4f-4f transitions are forbidden by the Laporte selection, which means transition cannot occur between the same shells ($\Delta L \neq 0$). In other words, the parity of final and initial state should be changed to obtain the allowed transition. However observation of these transitions is explained through simple configuration mixing caused by a non-centro-symmetric crystal field, allowing opposite–parity excited configuration to become slightly mixed into $4f^n$ by the Judd and Ofelt theory (B.R. Judd et al.1962, G.S. Ofelt et al.1962). Thus, when the on is located at a site without inversion symmetry, the electric dipole transition may become allowed by the admixture of states from opposite-parity configuration into 4f wave functions, due to the odd-parity crystal field (G.S. Ofelt et al.1963). The transitions are derived, in most cases, due to forced electrical dipole transitions. In some cases, considerable contribution can also be made by magnetic dipole transitions. However, electric dipole transitions are much weaker in lanthanides [S. Cotton.2006]. Electronic transitions must involve promotion of an electron without a change in its spin ($\Delta S = 0$) and with a variation of either the total angular momentum and the total angular quantum number of one unit at most ($\Delta L = 0, \pm 1$; $\Delta J = 0, \pm 1$). Though absorption of radiation can in

theory promote the lanthanide ion to any energetically accessible state, emission normally occurs only from the lowest lying spectroscopic level of the first excited term due to rapid internal conversion (G. Blasse et al.1994). In cases of low symmetry or vibronic coupling, the f-f transitions can gain intensity through f- and d-state mixing with higher electronic states of opposite parity (R. Jaaniso et al.1991). Broad $4f^n \rightarrow 4f^n15d^1$ transitions can also be seen in the infrared region for some lanthanides. These transitions can be attributed to another class of important spectroscopic features emerging from lanthanide ions. The 5d states differ from 4f states by their remarkably stronger coupling to crystal lattice vibrations and less localized nature. Furthermore, inter-configurational transitions from $4f^n$–$15d^1$state are parity allowed resulting in 104 times higher absorption cross section compared to f-f transitions. Due to the latter and relatively high energy needed for the excitation, these transitions are becoming popular in UV lasers and scintillator applications (P. Mikhail et al.1999).

1.4 Solid State Lighting

Lighting applications that use light emitting diodes, organic light emitting diodes or light-emitting polymers are commonly referred to as Solid State Lighting. This method has many

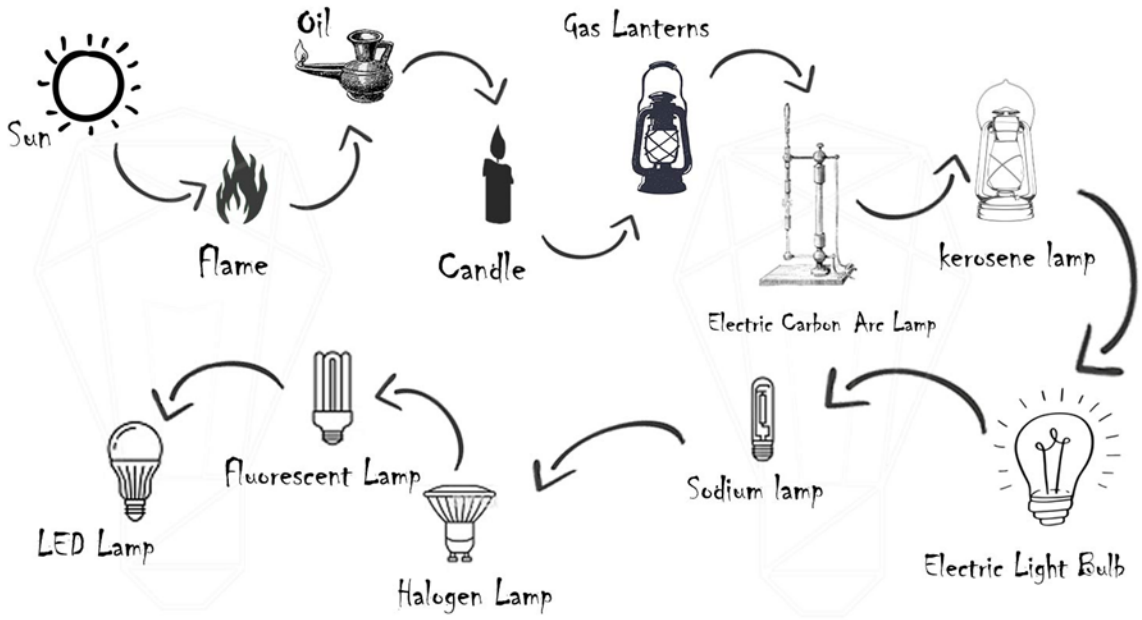

Fig.2 History of lighting

advantages over other methods of lighting. It is more economical and environmental friendly. The high luminous efficiency and Better color tunable property is exhibited in this method. Low power consumption and Long life span are other advantages. The advent of bright-blue LEDs in the 1990s were followed by the development of candela-class high-brightness, blue (In, Ga)N double - hetero structure devices by Nakamura and others was a landmark achievement in solid-state lighting. The availability of bright radiation at the high-energy end of the visible spectrum provided a simple and cost-effective means of generating white light by the process of using phosphors to partially down convert some of the blue emission to longer wavelengths corresponding to colors such as green, yellow, and red. This process results in a device that is driven like a simple LED, i.e., with a dc input into two terminals, that produces white light efficiently. Such white-lighting devices are proliferating all over the world and are increasingly replacing incandescent, halogen, xenon, and fluorescent light sources. In general, they offer greater efficiency, significantly longer working lives, and a complete absence of toxic elements in their constituent parts. In addition, they are, in principle, dimmable and instant-on, both huge advantages over compact fluorescent lamps, which are of comparable efficiency but are mercury hazards and have much shorter life spans.

Energy Efficiency & Energy Costs				
Technology	**Incandescent**	**Compact Flourescent (CFL)**	**SMD style LED**	**Filament style LED**
Average Life Span	1,500 hours / 6 months	8,000 hours / 5 years	25,000 hours / 17 years	50,000 / 34 years
Watts used	60W	15W	9W	5W
Annual power usage (8 hours per day)	176KWh	44KWh	26KWh	14KWh
Power usage for whole house (20 bulbs)	3520KWh	880KWh	520KWh	280KWh

Fig.3 Comparison of different light sources

1.5 Phosphor introducing facts

A phosphor or luminescent material is by definition is a solid that "converts certain types of energy into electromagnetic radiation over and above thermal radiation" (G. Blasse et al. 1994). Phosphors can take a number of forms usually consisting of a host material/matrix doped with activator atoms. The added activator atoms are usually rare-earth (lanthanides) ions or transition metals. Other luminescence centers include actinides, heavy metals, electron hole centers and ZnS-type semiconductors. In some cases when the optical absorption of the activator is weak a sensitizer is also added along with the activator. The host lattice is a combination of optically inert cations and anions. The activator will be an optically active cation so that the phosphor can exhibit luminescence. Such solids can be found among the transition metal compounds and the rare earth compounds of different types. A large variety of phosphors for diverse technological applications is known. The scientific models can explain the optical properties of the phosphors. The energy level of the activator can be denoted using spin- angular momentum (S), orbital angular momentum (L) and spin-orbit angular momentum (J) as $^{2S+1}L_J$. The allowed transitions are governed by the selection rules $L = \pm 1$, $S = 0$, $J = 0, \pm 1$. But no $J = 0$ to $J = 0$ transition is allowed.

1.6 Basic Terminology

The indicators which define the quality of an illuminating source for sophisticated applications like indoor lighting are warm white light with an excellent color rendering index, high luminous efficacy and good output color purity. Basic terms associated with lighting sources specifically pc-WLEDs are briefly given below.

1.6a. Correlated Color Temperature (CCT)

Color temperature is the absolute temperature in Kelvin scale at which a blackbody radiator must be operated to have a chromaticity equal to that of the light source. For an incandescent bulb its color temperature is the temperature of the filament because light of an incandescent bulb is thermal radiation and the bulb is very close to an ideal black body radiator. Color temperature values associated with light sources other than incandescent lamps are correlated color temperature (CCT) and not true color temperatures. Correlated color temperature is the temperature of a blackbody whose chromaticity most nearly resembles that of a light source (Kaufman J. E *et al* 1972). Light sources with a higher CCT are said to be "cool" in appearance, while those with lower CCT are characterized as "warm".

1.6b CIE chromaticity coordinates

CIE color coordinate diagram as introduced by Commission Internationale de l'Eclairage in 1931 represents all of the chromaticities visible to the average person on a scale of *x* and *y* (W.R. Stevens et al. 1969, Q.Y. Zhang et al.2002). A color space is a three dimensional space specified by a set of three numbers (tristimulus values X, Y and Z) which determine the color and brightness of a particular homogeneous visual stimulus. A chromaticity is a color projected into a two dimensional space that ignores brightness. The standard CIE XYZ color space projects directly to the corresponding chromaticity space specified by the two chromaticity coordinates known as x and y which shown in figure1.4. All colors of visible light have chromaticities represented by points inside the region bounded by the horseshoe. According to the chromaticity diagram, the primary colors red, blue and green

are represented as (0.67, 0.33), (0.14, 0.08), (0.21, 0.71) respectively. The CIE color coordinate of pure white is (0.33, 0.33).

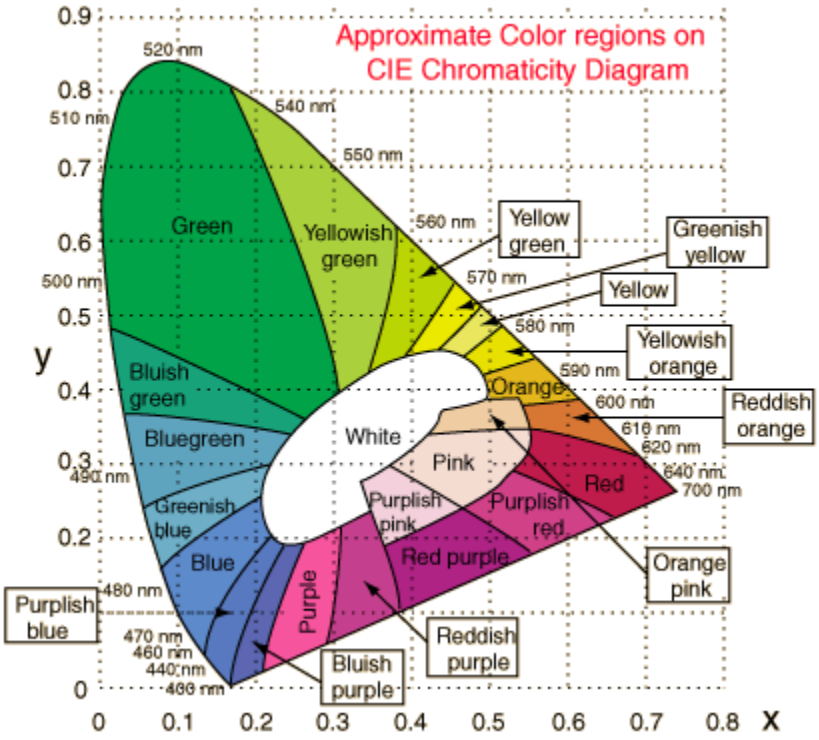

Fig.4.CIE chromaticity coordinate diagram

1.6c Color Rendering Index (CRI)

It is a figure of merit, on a scale of 0 to 100, which gives a quantitative measure of the ability of a light source to reproduce the colors of various objects faithfully in comparison with an ideal or natural light source. CRI is a measure of the degree to which the perceived colors of objects illuminated by the source conform to those of the same objects illuminated by a reference source for specified conditions (Kaufman J. E *et al* 1972). It indicates how well a light source renders colors on a scale of 0 - 100, compared to a reference light source. The test procedure established by the International Commission on Illumination (CIE) involves measuring the extent to which a series of eight standardized color samples differ in appearance when illuminated under a given light source, relative to the reference source. The average shift in those eight color samples is reported as Ra or CRI. In addition to the eight color samples used by convention, some lighting manufacturers report an R9 score, which indicates how well the light source renders a saturated deep red color. A CRI

of 100 would represent that all color samples illuminated by a light source in question would appear to have the same color as those same samples illuminated by a reference source.

Fig.5 Example for color rendition(Franz Mark "Blue horse"(1911))

1.6d Luminous Efficacy

The luminous efficacy of a light source is defined as the ratio of the total luminous flux (lumens) to the power (watts or equivalent) (Kaufman J. E *et al* 1972), ie; how much energy is converted to light by the source, and how well the emitted radiation is detected by the human eye. Here lumen is defined as 1/683 W of monochromatic green light at a frequency of 540 x 1012 Hz which corresponding to a wavelength of about 555 nm where the human eye is most sensitive. Thus theoretically attainable maximum value assuming complete conversion of energy at 555 nm would be 683 lm/W. The luminous efficacy of current light sources still remain far below this ideal value. The luminous efficacy is always in contradiction with CRI, because a high CRI value requires proper spectral dispersion over all the visible range which would make the luminous efficacy far below 683 lm/W. Thus balanced values of these two parameters are adopted for different lighting occasions.

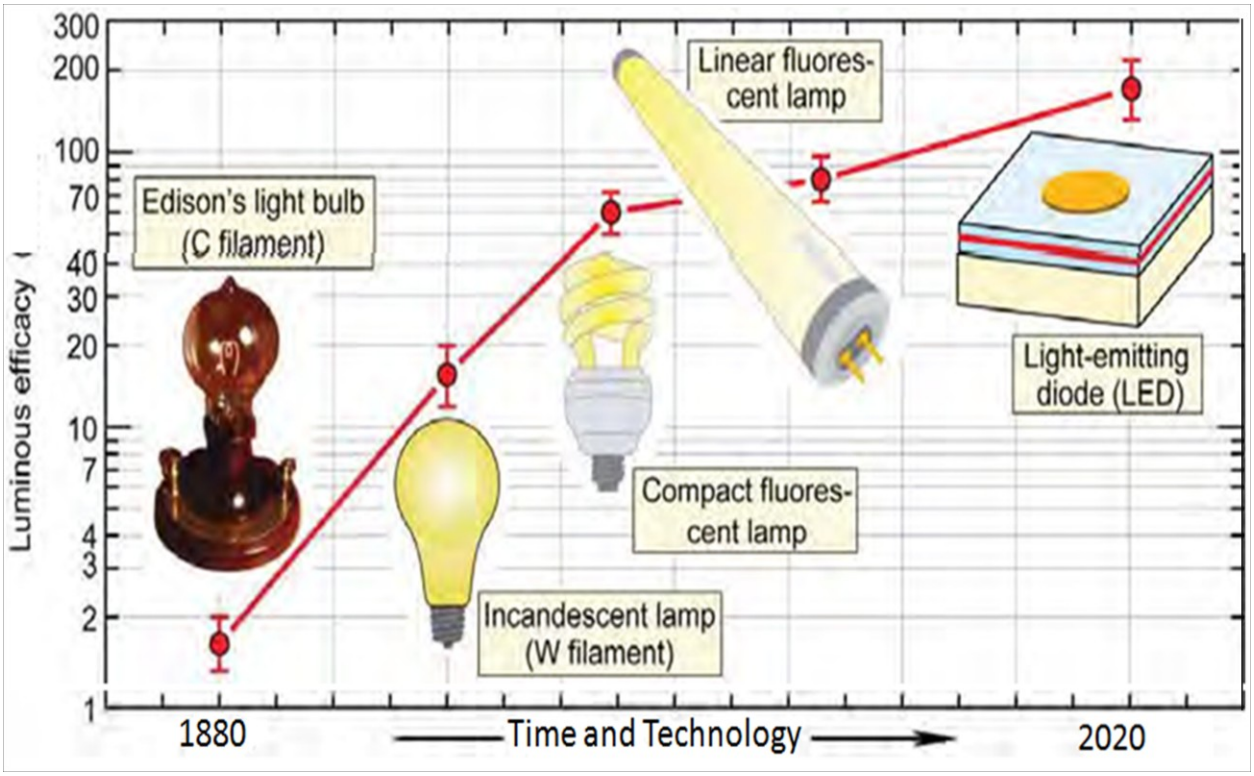

Fig. 6. Luminous efficacy timeline of different light sources

1.5 Different Strategies for White Light Generation

There are three principle strategies for white light generation. The first method is by combining the light emitted from tricolor LEDs, ie., blue, green and red LEDs. This method is the best one because there is no energy lost occur due to stoke shift as in the case of pc-WLEDs. Also the color temperature is tunable by varying the power of the individual LED components. However it needs additional circuitry which will increase cost and complexity. Another drawback is poor color rendering, associated with the white light comprising relatively narrow radiation components thus it will results in low CRI value, around 70s. Furthermore, LED chips that emit at different wavelengths have a different intensity response to changes in voltage. Thus dimming such a device is very challenging. Also differential aging and responses to temperature of the differently colored diodes would also necessitate additional electronic circuitry.

The remaining two mechanisms use LED with down converting phosphors, ie., either combining tri color phosphors with UV LEDs or by combining blue LED with yellow

phosphor. For that purpose LEDs with longer wavelength is more suitable to minimize the energy lose due to stoke shift. And it should be opted suitably to balance the CRI values of the device. ie., for residential purpose warm white light is desired. A device with UV LED and multiple phosphors can cover a broad range of emission wavelengths, giving good color rendering and stable emission color. However, multiple phosphors can reabsorb the emission of other phosphors, adding a loss mechanism and decreasing the efficiency of the system.

Thus the method adopted for white light generation in industry is by combining the blue LED with single yellow phosphor. This method is superior to the other two due to the long life time and high efficiency despite the limitation of relatively poor color rendering (CRI < 80) and high color temperatures (>4,000 K).

1.6 Challenges of existing technology

The major challenges of currently existing technology of white light generation is poor color rendering properties , high color temperature due to the lack of red emitting component, low efficacy, phosphor aging, low color purity and thermal quenching of luminescence. Also self absorption among phosphor materials and varying lifetime of different LEDs are hot issues. It results in color variation that comes from different tolerance of different phosphors to the LED chip temperature and color imbalance, white light distortion and low luminescence efficiency. To overcome these persisting issues an alternative approach for white light generation is proposed ie., single phase phosphors. While developing a single phase phosphor for WLED application the different issues described above are considered for clarification. But the crucial part in the development of a phosphor material for WLED application is balancing the CRI (color rendering index), efficacy and CCT(Color correlation temperature) values at the same time. Because there is always a tug of war between the CRI, efficacy and CCT values of a light device. When the CRI value goes to higher end the efficacy also goes beyond the expected values. Hence very careful approaches are needed to develop a good phosphor material for WLED application that tally the CRI, efficacy and CCT values to ideal level.

1.7 Single Phase Phosphor for WLED, prerequisites, need and relevance

For a phosphor material to be suitable for WLED applications it should satisfy certain pre-requisites. They are it should have an emission spectrum that, in combination with the emission of the other components (LED, other phosphors), leads to a pure white emission with a specific color rendering and color temperature. Also the excitation spectrum should show good overlap with the pumping LED. It must have broad absorption strength. The emission spectrum, excitation spectrum and the quantum efficiency must remain unchanged at elevated temperature. High quantum efficiency is essential. An excellent chemical and temperature stability is another factor. Also it should be compatible with LED production process.

Single phase phosphors are expected to satisfy these needs and they have better CRI, CCT and CIE values compared to the existing phosphors. And single phase phosphors can overcome the issue of re-absorption existing in RGB phosphors. White light can be obtained from single phase phosphor by doping a single or combination of multiple rare earth ions into a suitable single phase host material. Also white light can be generated by co-doping ion pairs like Ce^{3+} - Eu^{2+};Ce^{3+} - Tb^{3+}; Eu^{2+} - Mn^{2+}; Ce^{3+} - Mn^{2+} etc. based on energy transfer mechanism. Defect-related luminescent materials can also emit white light by controlling the concentration of the defect and reaction conditions.

1.8 Energy transfer mechanism

Energy transfer is the process in which excitation of certain ion migrate to another ion. The energy transfer mechanism between activators can be classified in to two as radiative and non-radiative. Radiative transfer occurs when an emission transition of one activator ion overlaps in energy and absorption transition of a second activator ion. The first activator absorbs enough energy and get excited which is followed by emission of photons. And these photons will be captured by the second activator, which is separated by

a few unit cells from the first ion. As a result of photon capturing the second activator ion also get excited. The non- radiative energy transfer can be a resonance energy transfer, spin coupling energy exchange and non-resonance energy transfer.

Resonance energy transfer occurs between a sensitizer and an activator with same radiative frequency. This can occur by exchange interaction, electric multi polar interaction or phonon assisted energy transfer. The exchange interaction occurs when the donor and acceptor are located so close that their electronic wave functions overlaps and the transfer is due to the quantum mechanical interactions. Exchange interactions occur for a very short range. It can be super exchange, ie; exchange between cations by way of one or two anion intermediaries; or by direct overlap of the cation wave functions. Phonon assisted energy transfer occurs when there is difference between the transition energies of donor and acceptor and is compensated by either phonon emission or absorption. The multi polar interactions can occur by multi polar resonance, multi polar transfer or non- resonant transfer. Multi polar transfer is a reversible energy transfer mechanism between two same energy levels. Here effective life times of all levels involved are long compared to the time required to transfer energy between the ions. But multi polar transfer is non reversible energy transfer process. Here effective lifetime of the terminal level of first ion is short compared to transfer time. Non resonant transfer has very small probability to occur. It is a non reversible process. From higher lying of one ion to lower lying level of second by transition that are not matched in energy. And it requires the simultaneous transfer of the difference in energy to a third ion.

By using Dexter's energy transfer formula for exchange and multipolar interactions and Reisfeld's approximation we can say $\ln(\eta_o/\eta) \alpha C$ for exchange interaction, and $\eta_o/\eta \alpha C^{n/3}$ with n = 6, 8, 10 are related to dipole-dipole, dipole- quadrupole and quadrupole-quadrupole interactions respectively. Where, C is the total concentration of Bi^{3+} and Eu^{3+} ions. The value of η_o/η is approximately calculated by the ratio of relative luminescence intensities, ie; (I_{so}/I_s).

The spin coupling energy exchange occurs between two adjacent activators which re no further than two to three lattice sites apart. This is usually observed in activators, which

can absorb infra red radiation and which is then converted to visible light. Hence it is also called anti - Stoke process.

The successful occurrence of energy transfer is said to be occur only when there is an overlapping between a sensitizer and activator in steady state spectra and shortening of decay rate of sensitizer with increasing activator content.

Importance of Ln3MO7 structures

The host lattice plays a vital role in the performance of a phosphor material. Because the liand ion charge transfer mechanisms as well as the electro negativity, ionic nature , covalency of the ligand cations can play key role in determining the emission and excitation properties of the phosphor. The excitation and emission process become successful only when the doped activators and sensitizers are suitably incorporated into the host lattice.

Thus the crystal structure of the host lattice, symmetry and coordination of the doping site, ordering of the host lattice etc. should be studied in detail. Activator doping concentration, uniformity in the activator distribution and various other factors also depend on the host lattice. Weberite type Ln_3MO_7 structure was studied extensively for their structural magnetic as well as luminescence properties (T. Linda Francis et al.2016, Jing Wang et al.2014, K. P. F. Siqueira et al 2013, Y. Hinatsu et al. 2009). Ln_3MO_7 structure can be classified as a class of typical weberite structure of general formula $A_2B_2X_7$. Where, A and B are cations and X an anion, O or F. It is an anion deficient fluorite related superstructure. Compared to fluorites reduction in the number of anions leads to decrease in the coordination number of B cations (VI coordination) with respect to A cations (VIII coordination). Thus it allows accommodation of diverse cations. Hence weberites have broad range of chemical and physical properties and great technological potential. Here the A ions have two different coordination environments A1 and A2. A1 cations lie in a highly distorted cube and are edge shared to form a series of chains in [100] direction. A2 cations are located within bi-hexagonal pyramids in which anions are spaced at three different distances from central cations. Each pyramid is corner shared with two other pyramids and edge shared with four A_1X_8 cubes. A1 and A2 ions occupy in 4d and 4a Wyckoff sites respectively. B ions are located in 4b and 4c Wyckoff positions and have coordination number six. Weberites are network of corner shared BX_6 octahedra with a penetration of A

cations. Anions have three Wyckoff positions 8h, 16j, and 4e. The general A2B2O7 can be rearranged with three lanthanoid cations, one transiton metal cation and oxygen anions to get Ln_3MO_7(Lu Cai et al.2009). Various compounds possess similar stoichiometry but fall under different crystal structures due to the difference in the cations and anions occupied. However, all these compounds of this stoichiometry could be explained as a superstructure of fluorite (AO2 or A4O8) structure. Crystal structure of these compounds varies from defect fluorite or pyrochlore type cubic to weberite type orthorhombic with increasing ionic radius of the Ln^{3+} ion (H.J. Rossell et al.1979). Weberite structure also shows a wide variety of modifications including monoclinic and trigonal structures. The preferential coordination and the number of anions are dependent on the size and the valency of the cation with respect to the anionic radius. In Ln3MO7, four tetravalent metal ions in the A site are replaced by three trivalent (Ln) and one pentavalent (M) ions forming one oxide vacancy per fluorite cell [M.A.subramanian et al. 1983]. This reduction in the number of anions from eight to seven leads to a decrease in the coordination number of B cations (VI coordination) with respect to the A cations (VIII coordination) and introduces a variation in the cation coordination to keep the compound neutral. However, the compounds with smaller Ln cation (ionic radius within the tolerance limit) could occupy to form a stable and anion deficient defect fluorite structures.

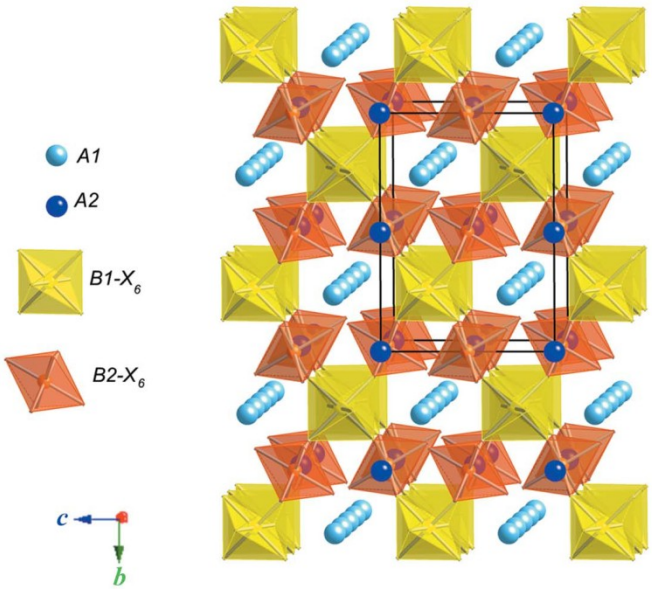

Fig.7. Representation of Weberite structure

Pyrochlore structure (*Fd*-3*m*) can be considered as an ordered, defective fluorite solid solution derived by ordering the cation sublattice and creating ordered oxygen vacancies in such a way that coordination of A atoms remains cubic, as in fluorite, but coordination of B cations decreases to octahedral thereby doubling the unit cell with respect to thefluorite. In cubic pyrochlore, about 1/8th of the oxygen (anion) atoms are orderly replaced (L.Cai et al. 2010) C-type or bixbyite structures is another modification of fluorite formed by removing 1/4th of the oxygen atoms in an orderly manner. The M5+ ion iscoordinated with six oxygen ions, forming an MO6 octahedron. These octahedra share corners forming one dimensional chains which are oriented along the c-axis. One third of the La cations are 8 – coordinated and lie in (001) rows which alternate with parallel rows of corner linked MO, coordination octahedra within slabs parallel to (100). The remaining Ln cations lie in between these slabs in seven – fold coordination. Ln_3MO_7 orthorhombic crystal can possess a variety of space groups like Pnma, Cmcm, C2221, Ccmm, P212121 etc. with difference in the symmetry elements. Crystal structure of a typical weberite is given in figure 1.9. Fluorite and weberite lattices are compared in figure 1.10. Polymorphic modifications in these crystallographic structures are produced as the processing conditions changes.

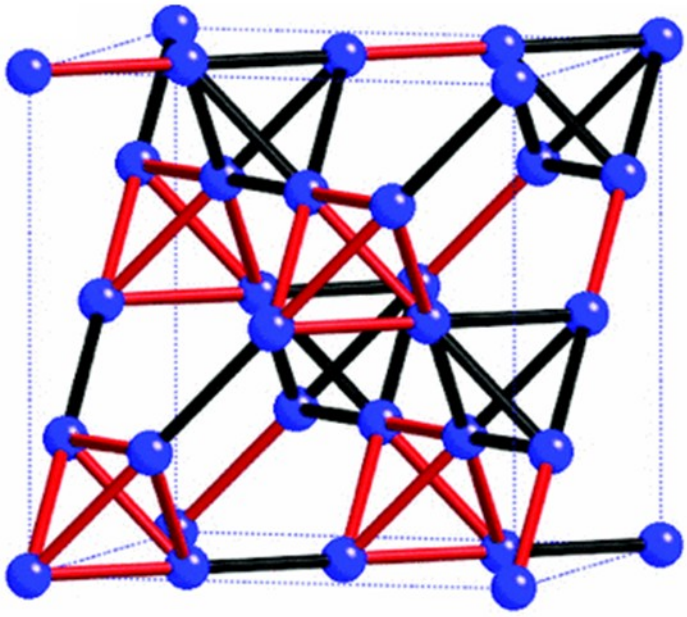

Fig.8. Representation of Pyrochlore structure

Rossell has reported study on La3NbO7 which is found to be one of the earlier work in this system(H.J. Rossell et al.1973). His studies revealed the structure as an orthorhombic superstructure of cubic fluorite type with space group Cmcm bearing three distinct cation sites with one distorted cubic Ln3+, one distorted pentagonal bipyramidal Ln3+ site and one octahedral M5+ site. Studies on the structural transitions of this kind of system were reported many times. With different combination of Ln and trivalent M elements various systems were reported on this structure. The magnetic properties of this system were extensively stuied in the earlier years (K.P.F. Siqueria et al. 2013, 2014). Greedan et al. (1997) studied the electronic and thermal properties of La_3MoO_7 by magnetic susceptibility, electric resistivity and neutron diffraction measurements. Luminescence properties of this structure with different cationic modifications were reported by Yanyan et al. (2013) and Wang et al(2014). The wideness of these studies indicates the importance of the structure.

1.9 Luminescence Properties of Bi^{3+}

The Bi^{3+} ions are the most thoroughly investigated main group element in the field of photo luminescence. It is a magical element in the 15^{th} group of periodic table owing to the easy involvement n chemical combinations for the electrons in its p orbital; they possess very peculiar characteristics such as host dependent luminescence, variety of oxidation states such as 0, +1, +2, +3, +5, characterized by multi-type electronic structures, a profound propensity to form clusters, which widely exist in molten Lewis acids, molecular crystals or porous zeolitic solids. Also Bismuth shows strong spin–orbit coupling effect. These peculiarities allow them to behave as smart optically active centers in diverse host materials. Unlike the ions like Eu^{3+}, the Bi^{3+} ions are capable of exhibiting different luminescence outputs by varying the host lattice. The luminescence properties of Bi^{3+} ions arise due to the transition from $^1S_0$ ground state to $^1P_1$ and $^3P_1$ excited states. The excited states of Bi^{3+} ion consist of $^3P_0$, $^3P_1$ and $^3P_2$ triplet states and $^1P_1$ singlet state. The transitions between these levels are termed as A, B, C and D bands. A band is the transition from $^1S_0$ to $^3P_1$ and it is allowed due to spin orbit coupling. The B band transition, $^1S_0$ to $^3P_2$ is forbidden, but it can occur if it is coupled with unsymmetrical lattice vibration modes. The next band C band, which is $^1S_0$ to $^1P_1$ transition, is allowed. But the $^1S_0$ to $^3P_0$ transitions

are strongly forbidden. The D band is somewhat different from A, B, and C bands. It is the charge transfer bands which have high energy than C bands.[1] The A band lies in the UV region and C band in vacuum UV region, which constitute the broad absorption band of Bi^{3+} ions.

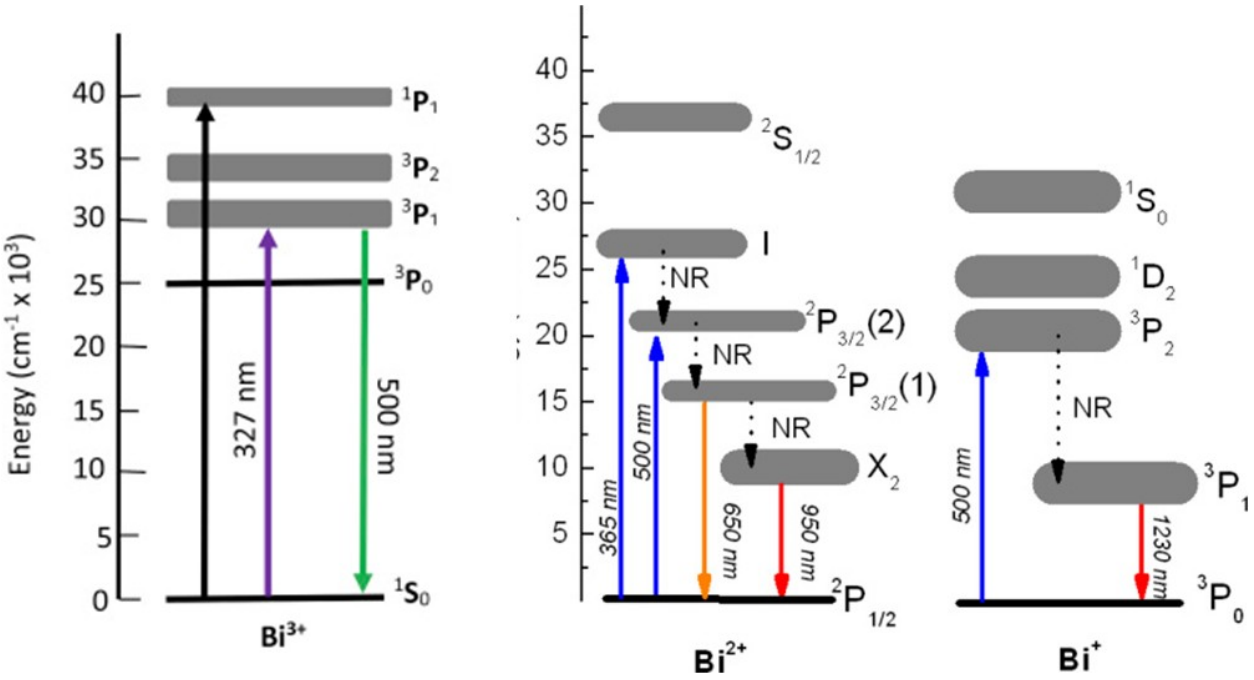

Fig.9 Energy level Diagram of Bismuth ions

The very notable feature of Bi^{3+} luminescence is its broad nature of emission and excitation spectra, which make it a suitable candidate for full color emitting phosphors. In some host lattices with ns^2 ground state the emission spectra comprises an uncharacteristic peak of ns^2 ions incorporated. It is attributed due to the photo ionization process arises du to the interaction between the host lattice conduction band and the excited states of ns^2 ions. In this process the excited state inject an electron into the host lattice conduction band. Thus an impurity trapped exciton – like state is created with the hole in the luminescent centre and electron in the delocalized surrounding cations. These excitons may relax to ground state radiatively or non-radiatively. When there occur a non – radiative decay it affect the emission efficiency adversely.[3] as it is already pointed out the Bi^{3+} luminescence is influenced by the host lattice a lot. Especially ions with $nd^{10}ns^0$ electronic configuration have very strong influence on ns^2 ion luminescence. The ions like Ga^{3+}, Sb^{5+}, In^{3+} …etc have strong influence on Bi^{3+} ions give emission in the yellow spectral region – when Sb^{5+} ion are

octahedrally coordinated as in weberites. Whereas Ga^{3+} ions are capable of blue emissions in association with Bi^{3+} ions.[2, 4]

1.10 Literature review

Many research groups are reporting ongoing studies on phosphor materials. Nowadays Bismuth doped systems are more widely studied owing to their peculiar optical properties. Recently many reports are concentrated on single phase phosphors and energy transfer mechanism in ion pairs co-doped systems. A. M. Srivastava has reported the nature of Bi^{3+} luminescence in pyrochlore type systems in the temperature range 15 -300 K. It is reported that Bi^{3+} has characteristic emission in UV region, especially with pyrochlore systems. Emission in visible region due to the presence of Bi^{3+} clusters is also explained. Bi^{3+} luminescence in three different hosts were discussed in this paper. Thus the host dependent luminescence nature of Bi^{3+} ions is discussed in very detail.

Tunable and White Light Emission of a Single-Phased $Ba_2Y(BO_3)_2Cl:Bi^{3+},Eu^{3+}$ Phosphor by Energy Transfer for Ultraviolet Converted White LEDs were reported by Anjun Huang et al. they have reported the presence of three various Bi^{3+} sites occupied by the host material.Eu^{3+} co-doping in this system results in dipole-dipole energy transfer mechanism in this phosphor and which helps the color tuning of the phosphor. Both Eu^{3+} concentration as well as excitation wavelength determine the color tunability of the reported phosphor. LED was constructed with the prepared phosphor and white light emission is illustrated in the paper.

Electronic structure and photoluminescence properties of a novel single - phased color tunable phosphor $KAlGeO_4:Bi^{3+}$, Eu^{3+} for WLEDs was reported by Wenzhi Sun et.al. Color tunability from blue to orange – red region by adjusting the Bi^{3+} - Eu^{3+} mole ratio is reported in this system. Structural analysis was studied on the basis of reitveld analysis. Under 320 nm excitation blue emission of Bismuth and red emission of Europium were obtained. Combination of these two emission produce white light in appropriate circuitry. Further the energy transfer mechanism in this phosphor was analyzed through statistical analysis of data. Dipole – dipole energy transfer mechanism is reported in this phosphor.

Lei Wang *et.al* reported Tunable luminescence of the full-color-emitting $LiGd_5P_2O_{13}:Bi^{3+}$, Eu^{3+} phosphor based on energy transfers. The samples were prepared by conventional solid state reaction method. This phosphor produces bluish green emission of Bismuth ions and red emission of Europium ions. They have reported white light emission under 290 nm excitation with CRI and CCT 4250 K. They have reported energy transfer from Bismuth to Europium and the statistical analysis of the data reveals the existence of dipole-dipole type energy transfer in the system.

Design, luminescence and energy transfer of single-phase color-tunable YNbO4: Bi^{3+}, Eu^{3+} phosphor for UV pumped white light-emitting diodes was reported by Ziqiang Jiang *et.al.* This single phase white light emitting phosphor was also prepared by conventional solid state reaction method. By varying the Bi^{3+} / Eu^{3+} ratio they have produced various emission hue ranging from (0.16, 0.18) to (0.33, 0.24) and then to (0.62, 0.33). They have investigated the energy transfer mechanism in detail.

1.11 Goals & Objectives of the Work

From the literature review, the overwhelming need for an alternative method for white light generation is understood. The research works all over the world on this particular problem is now concentrated on developing a single phase phosphor for WLED application based on various host and activator materials. The primary aim of this research work is to develop novel and potential single phase phosphor candidates to be used in pc-WLEDs. Understanding various factors affecting the luminescence behavior of the phosphor material ie., structural as well as morphological factors is an objective of this study. Exploring the possibilities of Bi^{3+} luminescence in various single phase host materials and detailed analysis of the energy transfer mechanism in the developed phosphors were the core objective of our study.

Chapter 2

Studies on photoluminescence properties of weberite type phosphors with different cationic modifications

The influence of various rare earth substitutions (La, Y, Gd, Lu) and metal element substitutions (Sb, Nb, Ta) in the A and B site of Weberite type systems with of general formula A_3BO_7 is investigated on local structure and associated photoluminescence properties. These substitutions produce distinct effects on structure, absorption and luminescence. La in the A site produce better optical tuning properties compared to other rare earths. Thus La was fixed in A site and B site was varied with Tantalum, Antimony and Niobium. Tantalum and Antimony in B site with Lanthanum in A site produce broad excitation spectrum in the UV region and emission spectra covering the visible spectra up to 600 nm only. But the Niobium based samples show emission spectra covering the whole visible region. The CIE values of Niobium based samples are very close to ideal values.

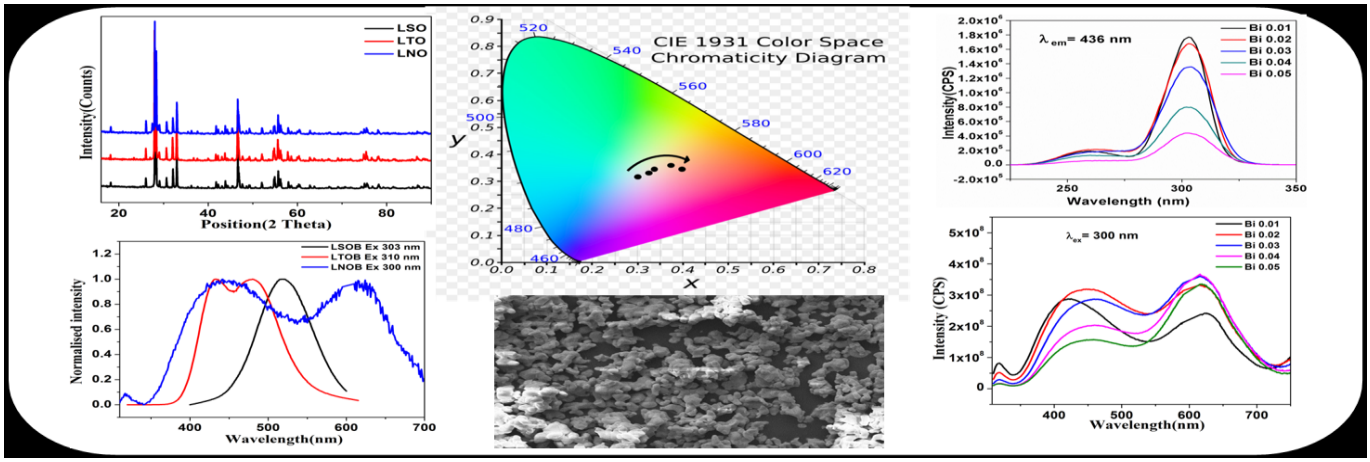

2.1 Introduction

The modern optical materials in industry have to satisfy the demand for enhanced performance. Especially in the field of phosphors diverse modifications are enrolled to overcome the existing issues of environmental friendliness and energy saving at the same time economical also. Phosphor finds different applications and the core area is phosphor converted white LEDs. The current technology utilizes different methods mainly three for white light generation from Phosphors. The currently using technology of combining YAG yellow phosphor with UV/ blue LEDs or by combining tricolor phosphors with UV LEDs is facing drawbacks such as poor color rendition due to spectral gap in green region, high correlated color temperature, color re-absorption among different phosphors, phosphor aging etc. To improve the quality of light generated each of these aspect should be considered carefully. The issue of spectral gap in green region faced by YAG phosphor can be rectified by considering a suitable substitution or co- doping into the host matrix. It will subsequently improve the color rendering issues. Also the issue of color re-absorption among different components can be clarified by using a single phase phosphor instead of tricolor phosphors. The idea of single phase phosphor is very fruitful as it reduces the total cost as well as the drawback of color absorption and phosphor aging. Combining the emission from a single phase phosphor with UV LED will produce white light. Color rendering index of the light source is another matter of concern. The ideal light source The Sun produces light with CRI value of 100. The research efforts are going on to bring phosphor converted LEDs with high color rendering index, as the reported cases and currently using technology just cross around 80. While controlling the CRI value another factor for concern is the correlated color temperature. There is always a tug of war between CRI and CCT. Balancing both these is a curious job to researchers.

Currently many reports are there on single phase phosphors. Oxides, phosphates, Silicates etc are reported as host material for the purpose of single phase phosphors. The weberite type oxides are extensively studied for magnetic application purpose in the past decades. These systems are very special due to their chemical and physical stability features. Studies on Europium based luminescence in these systems also reported with good results. In our

present study we consider Weberite systems for Bismuth based luminescence studies. Weberites are anion deficient fluorite related super structures with general formula $A_3B_3O_7$. Compared to fluorites reduction in the number of anions leads to decrease in the coordination number of B cations (VI coordination) with respect to A cations (VIII). Thus it allows accommodation of diverse cations. Hence weberites have broad range of chemical and physical properties and great technological potential.

The present study includes Bismuth based luminescence in weberites. Bismuth shows variety of oxidation states including 0, +1, +2, +3, and +5 characterized by multi type electronic structures. Among different ionic forms Bi^{3+} is the most common and stable ionic form. Bi^{3+} doped materials usually display broad absorption bands in the UV region. As their electrons in 6p, 6s, 5d orbital are sensitive to their coordination environments they exhibit host dependent luminescence. There are reports on blue, green and yellow emission Bismuth doped phosphors. The luminescence of Bi^{3+} arise due to $1S_0$, $1S_1$ singlet and $3P_1$ singlet transitions.

Here a series of samples with general formula A_3BO_7 was prepared by varying the *A* site with different rare earth ions La, Gd, Y and Lu with Sb in the B site. Then *A* part was fixed with La and B site was varied. Similar work was reported by Jing Wang et al. (2014) in Eu^{3+} luminescence. It is reported that this kind of structure allows wide variety of chemical substitutions at A and B site with mixed valences such as 3+ and 4+ or 2+ and 5+ together with oxygen vacancies. These type of compounds have fluorite like structure with four tetra valent metal ions replaced by three trivalent ions and one pentavalent ion and one oxygen vacancy per fluorite cell in the general formula $M_4^{4+}O_8$ (A. Kahn-Harari et al. 1995). In this structure cation ordering occurs on metal sites and oxide –vacancy ordering on the anion sites due to significant difference in ionic radii of A and B ions.

Experimental

The weberite phosphors were synthesized by the conventional solid state reaction method using La_2O_3, Gd_2O_3, Lu_2O_3, Y_2O_3, Sb_2O_5, Ta_2O_5, Nb_2O_5 and Bi_2O_3 (99.9% purity; Sigma-Aldrich, Steinheim, Germany) as the starting materials. The required stoichiometric

amounts of these materials were weighed and then thoroughly wet mixed in an agate mortar with acetone as the wetting medium. The mixing is followed by drying in an air oven at a temperature of 100°C. This process of mixing and drying was repeated thrice to obtain a homogeneous product. The obtained mixture was calcined at 1400°C twice for 6h in an alumina plate in an air atmosphere furnace each time. The calcined product was then ground into a fine powder for carrying further characterization.

The crystalline structure and the phase purity of the samples were analyzed by recording the X-ray powder diffraction (XRD) pattern using a PANalytical X'Pert Pro diffractometer having a Ni filtered Cu-Kα radiation with an X-ray tube operating at 40 kV, 30 mA and 2θ varying from 10 to 90° in 0.016 steps. The morphology of powder particles was studied using a scanning electron microscope (Carl Zeiss EVO 18) operated at 20 kV. The X-ray microchemical analysis and elemental mapping of the samples were carried out using a Silicon Drift Detector-X-MaxN attached with the SEM. The selected-area electron diffraction (SAED) patterns and high-resolution electron microscopy of the samples were taken using a TECNAI 30G2 S-TWIN transmission electron microscope (FEI, The Netherlands) operating at 300 kV. Absorbance studies of the samples were carried out using a Shimadzu UV-3600 UV-Vis spectrophotometer in the 200-500 nm wavelength range using barium sulfate as a reference. The photoluminescence spectra of the prepared samples were obtained using a Spex-Fluorolog DM3000F spectrofluorimeter with a 450 W xenon flash lamp as the exciting source. The luminescence lifetime of the phosphors was recorded using the phosphorimeter attached to a Fluorolog®3 spectrofluorimeter. All the measurements were carried out at room temperature.

2.3 Results and discussion

2.3.1Powder X-ray diffraction studies

The powder XRD patterns of weberite samples with different rare earth substitution in the A site is depicted in figure 1. Phase purity of all the samples is confirmed. Gd_3SbO_7 matched well with orthorhombic weberite type structure with space group $C222_1$ and is matched with ICDD No.00-038-1409. La_3SbO_7 crystallized into orthorhombic structure with space group Cmcm (63)

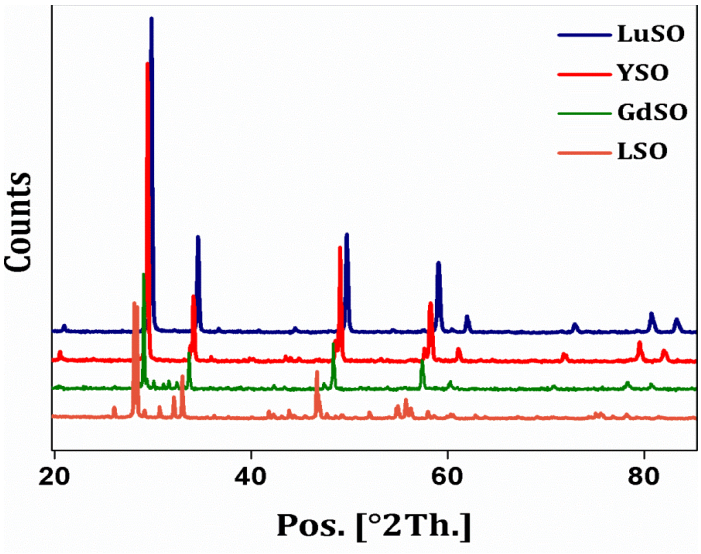

Fig.1 Powder X-ray diffraction patterns of A_3SbO_7 (A = Y, La, Lu, Gd) samples

and is well matched with ICDD No. 01-073-8085. Y_3SbO_7 (cubic, Fd-3m) and Lu_3SbO_7 forms cubic defect flourite structure with space group Fm-3m and ICDD No. is 00-024-069. The Ln^{3+} substitution induces variation of crystalline structure from defect fluorite to weberite types with increased ordering of the cations from Lu to La. As the ionic radius increases more super structure peaks are formed in XRD pattern and crystal structure changes from cubic to orthorhombic

2.3. Morphological studies

The SEM images of A_3SbO_7 samples are shown in figure 2. Better spherical morphology is obtained for La_3SbO_7 samples. Agglomeration is also less in the case of La_3SbO_7 compared to the other three results. Decreasing trend in particle size is observed from La to Lu. Other three samples except Lanthanum are crystallized with irregular particles. The average size of particles estimated from the micrograph is about 1 – 2 μm.

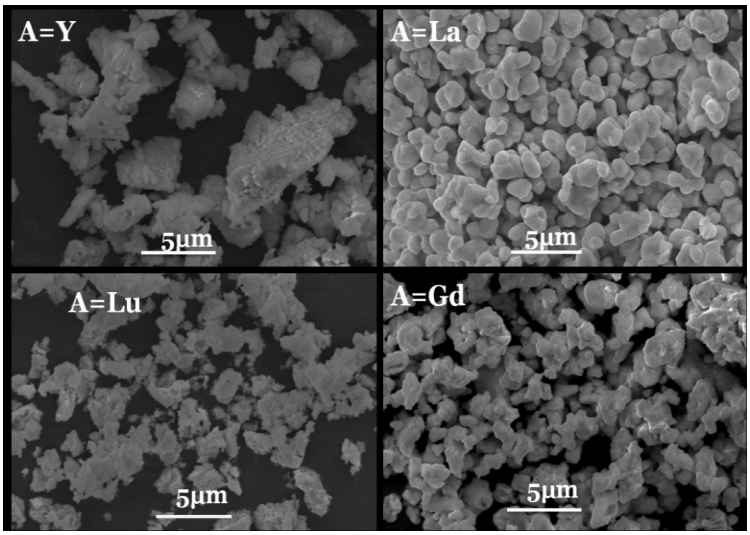

Fig.2 SEM images of A_3SbO_7 (A = Y, La, Lu, Gd) samples

2.3.3Photoluminescence studies

Figure 3 and figure 4 represent the photoluminescence excitation and emission spectrum of A_3SbO_7 samples. For all the samples both excitation and emission spectra are broad in nature. But there is overall red shift in the spectra with variation in *A* site cations. Bigger ion Lanthanum exhibits higher degree of red shift. Yttrium, Gadolinium and Lutetium samples produce emission in the blue region of electromagnetic spectra. But the La_3SbO_7 samples covers the visible spectra from 450 nm to 600 nm, it is much broad compared to other three samples. Hence it is found to be a more suitable host for further studies for full color emission phosphors applications. Thus Lanthanum was fixed in the *A* site and *B* site was varied with different metal elements Antimony, Tantalum and Niobium.

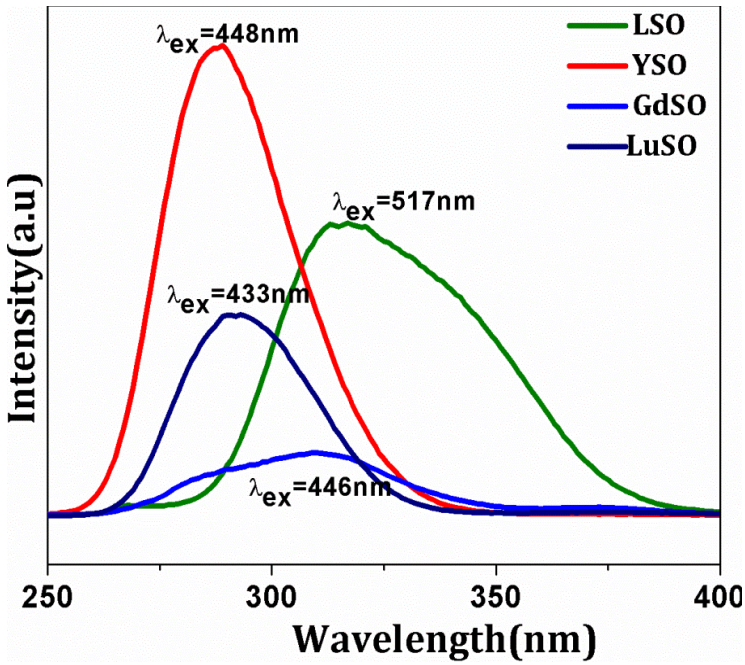

Fig.3 PLE spectra A_3SbO_7 (A = Y, La, Lu, Gd) samples

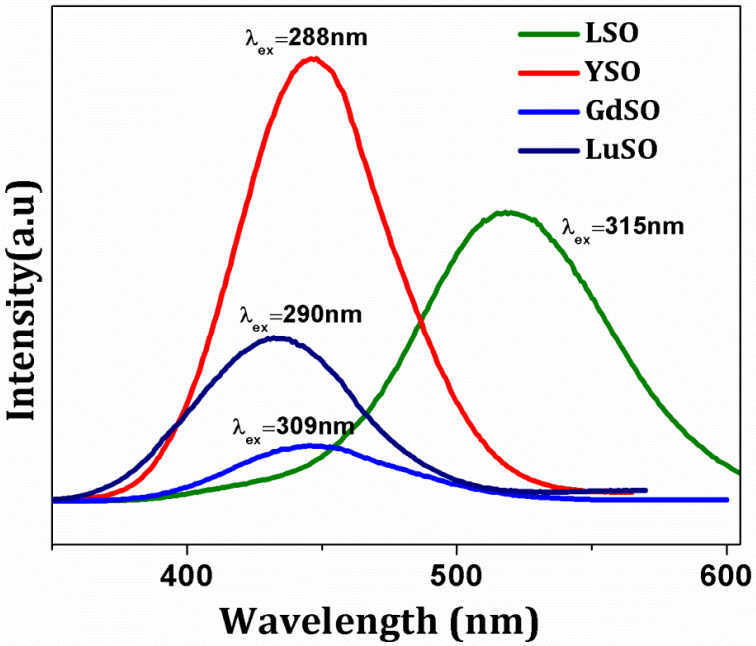

Fig.4 PL spectra A_3SbO_7 (*A* = Y, La, Lu, Gd) samples

2.3.2 Variation in B site cations

2.3.2.1 Powder X-ray diffraction studies

The XRD patterns of La_3BO_7 (*B*= Sb, Ta and Nb) samples and La_3BO_7: Bi^{3+} (*B*= Sb, Ta and Nb) samples are depicted in figure 5 and figure 6. Phase purity of the samples is confirmed from XRD studies. There is a right shift in main peaks with variation in *B* site cation. Comparatively smaller Antimony shows higher right shift. The Bismuth doped samples do not introduce any additional peak in the powder XRD pattern. It means Bismuth is successfully doped into the host matrix. And thus there are no secondary peaks in the XRD patterns. The average crystallite size calculated (in nm scale) using Debye - Scherrer equation, $\Delta d = 0.91\lambda/\beta Cos\theta$, where λ is the wavelength of X-ray used, β and θ are the half width of the X-ray diffraction lines and half diffraction angle 2θ respectively, is tabulated in table 1. The calculated values show a decreasing trend from Antimony to Tantalum to Niobium. Niobium based sample has the lowest crystallite size.

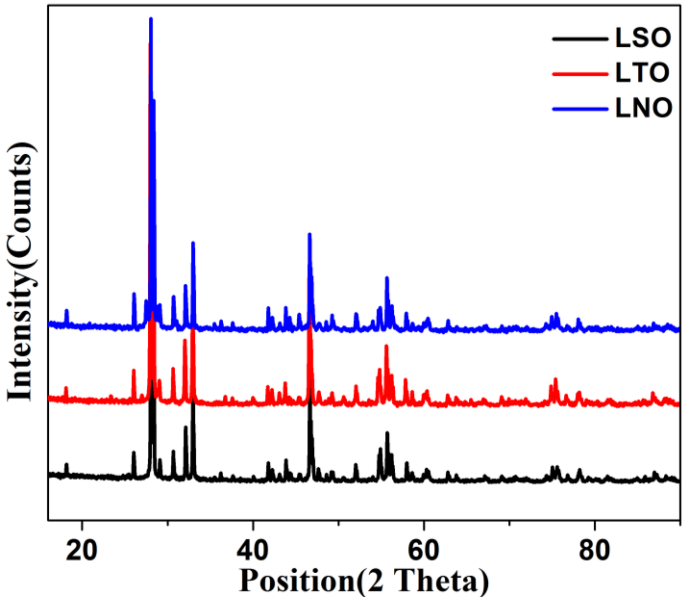

Fig.5 Powder X-ray diffraction patterns of La_3BO_7 (*B*= Sb, Ta and Nb) samples

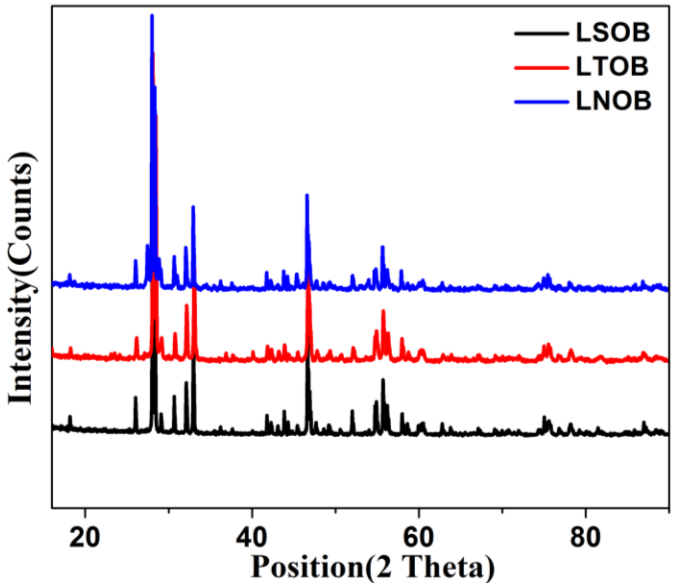

Fig.6 Powder X-ray diffraction patterns of La_3BO_7: Bi^{3+}(*B*= Sb, Ta and Nb) samples

Table 1. Average crystallite size of L*B*O compounds

Composition	β	θ	Cos θ	λ (Å)	Average crystallite size (nm)
LSO	0.12	14	0.9702	1.5406	69
LTO	0.14	14	0.9702	1.5406	59
LNO	0.15	14	0.9702	1.5406	55

2.4.2Absorption

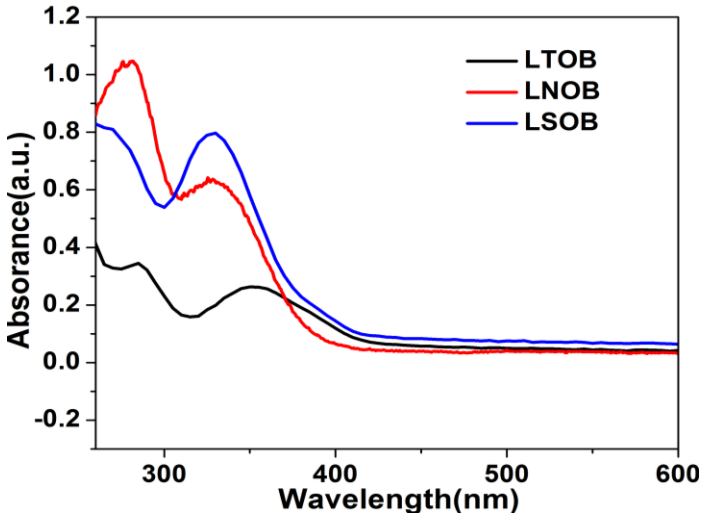

Fig.7 Absorption spectra La_3BO_7: Bi^{3+} (*B* = Sb, Ta and Nb) samples

All the three samples have absorption peaks in n-UV region. Comparing the absorption spectra of the three samples it is seen that Antimony substituted samples exhibit stronger absorption in n-UV region. The peak below 300 nm is due to the O^{2-} to Sb^{5+} charge transfer (Renping Cao et al. 2016). The Niobium substituted samples shows higher absorption around 290 nm along with a shoulder peak at 350 nm. Peak around 290 nm is attributed due to the host absorption and peak around 350 nm can be assigned due to optical absorption of Bi^{3+} ions owing to $1S_0$ to $3P_1$ transitions of Bi^{3+}. For tantalates the absorption intensity is comparatively less but the peaks are broader comparatively. Here the absorption peak due to the $1S_0$ to $3P_1$ transitions of Bi^{3+} has a red shift. The charge transfer transitions from oxygen ligands to the central Ta atom in TaO6 group give rise to the peaks below 300 nm.

2.4.3 Photoluminescence

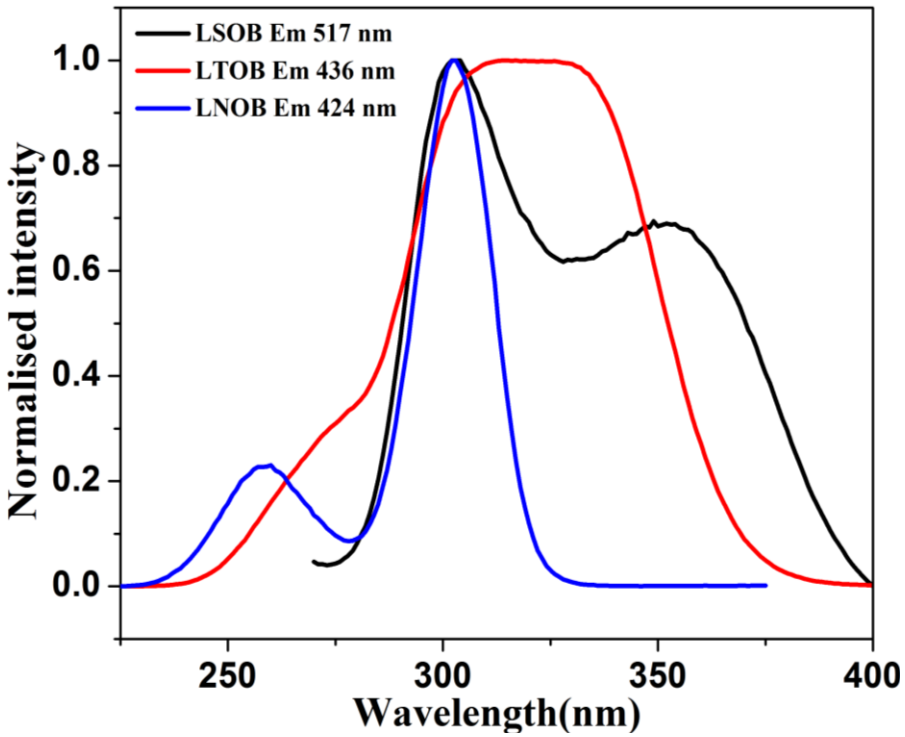

Fig.8 Photoluminescence Excitation spectra of La_3MO_7: Bi^{3+}(M = Sb, Ta and Nb) samples

Figure 8 represents the PLE spectra of La_3MO_7: Bi^{3+}(M = Sb, Ta and Nb)samples. Here also double peaked spectrum was obtained for all the three samples as in absorption spectra. These double peaks are attributed to ligand transitions and Bismuth ion transitions as discussed in the case of absorption. Antimonate and Tantalate peaks are broader than Niobate. They are more red shifted compared to Niobate. The emission spectra in figure 9 shows that Niobium sample covers the whole visible region whereas Tantalum and Antimony samples produce emission only up to 600 nm. This type of emission property exhibited by Niobate is very exciting and interesting, because whole emission was produced with a single dopant. Due to this peculiar emission property exhibited by Niobate sample a series of Niobium samples were prepared and their detailed analysis was done with different characterizations.

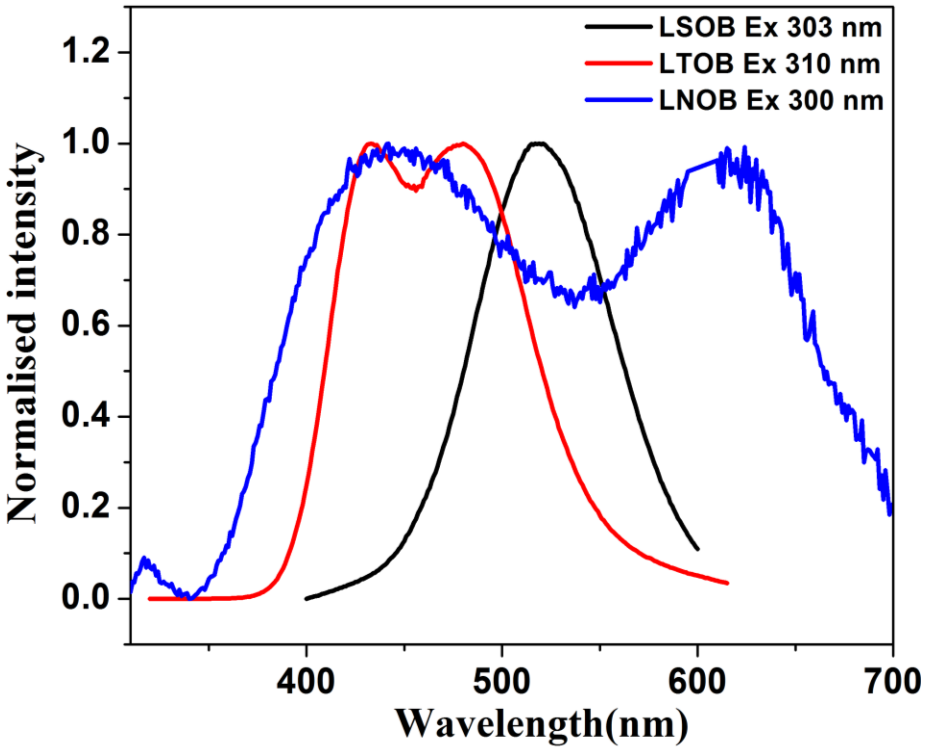

Fig.9 Photoluminescence emission spectra of La_3MO_7: Bi^{3+}(M = Sb, Ta and Nb) samples

2.4.1 La3NbO7: Bi3+

2.4.1.1 Morphological studies

Figure 10 shows the SEM images of La_3NbO_7: xBi^{3+}. The particles are almost spherical natured. Agglomeration is also very less. The average particle size estimated from SEM image is around 1 µm. Particles are uniformly distributed also. The EDS spectrum in the figure 11 is a clear evidence of the presence of all elements in the matrix. Experimental data of atomic weight percentage is in accordance with the calculated values. X-ray dot mapping images of representative sample is shown in figure 12. Uniform distribution of elements in the matrix is understood from these images.

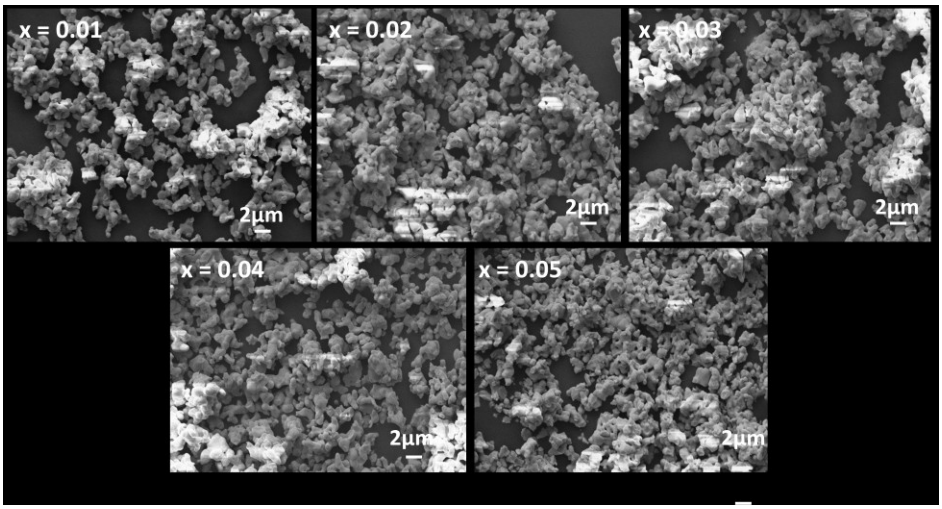

Fig.10 SEM images of LNO: xBi^{3+} (x = 0.01, 0.02, 0.03, 0.04, 0.05)

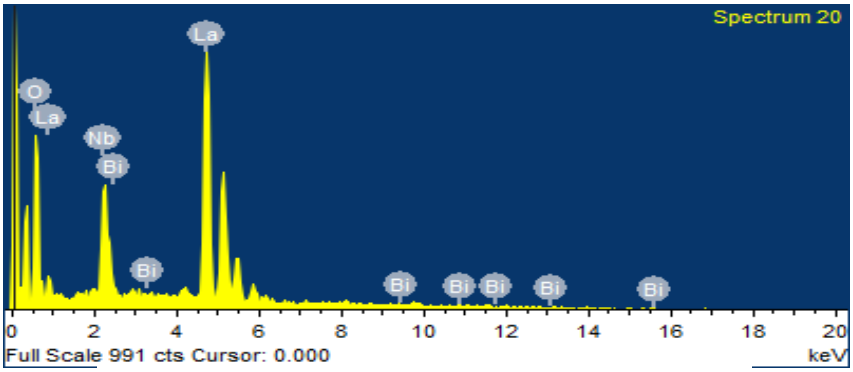

Element	Weight%	Atomic%
O K	21.15	68.08
Nb L	15.02	8.33
La L	63.25	23.45
Bi M	0.59	0.15
Totals	100.00	

Fig.11 EDS spectra of LNO:Bi^{3+} sample

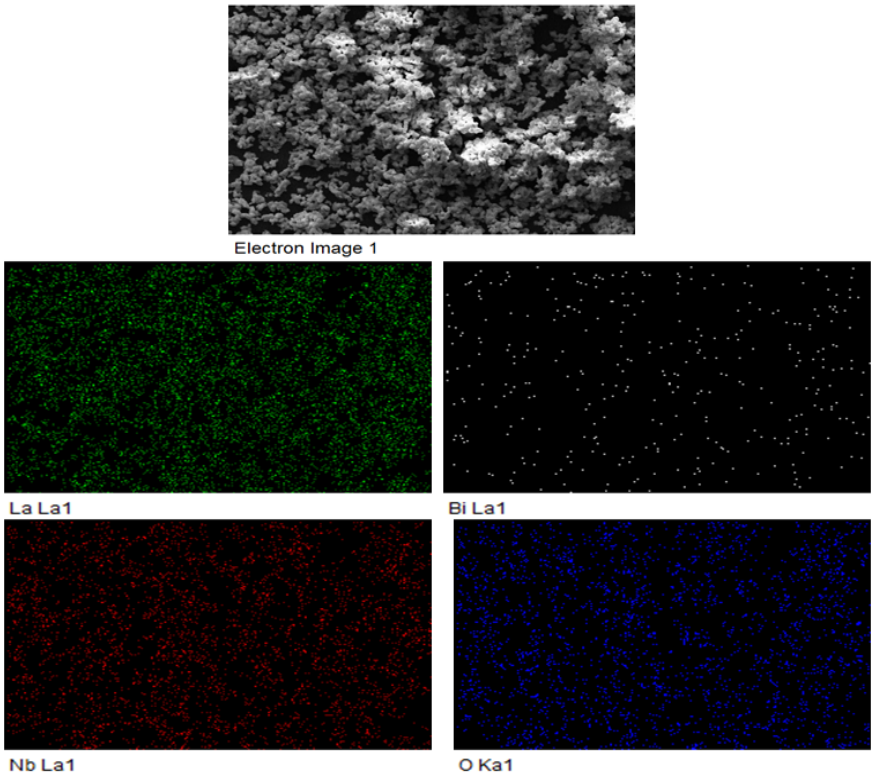

Fig.12 X-ray dot mapping images of LNO: Bi^{3+}

Absorption studies

The absorption spectra of LNO: Bi^{3+} samples are depicted in figure 13. And the band gap values calculated by Shapiro's method is tabulated in the Table 1. The absorption spectrum consist of a broad band in the UV region with peaks around 290 nm and 310 nm. Peak around 290 nm is attributed to host absorption and a peak around 310 nm can be assigned due to optical absorption of Bi^{3+} ions owing to the $1S_0$ to $3P_1$ transitions of Bi^{3+} ions. Absorption of Bismuth peaks is maximum for x = 0.04. The calculated band gap values exhibit a reduction trend.nas the electronegativity of Bi^{3+} ions are slightly greater compared to the La^{3+} ions. Thus the average electronegativity around La^{3+} ions may increase with increasing Bi^{3+} content. This increase in electronegativity may affect the covalency and charge transfer mechanism of ligand ions.

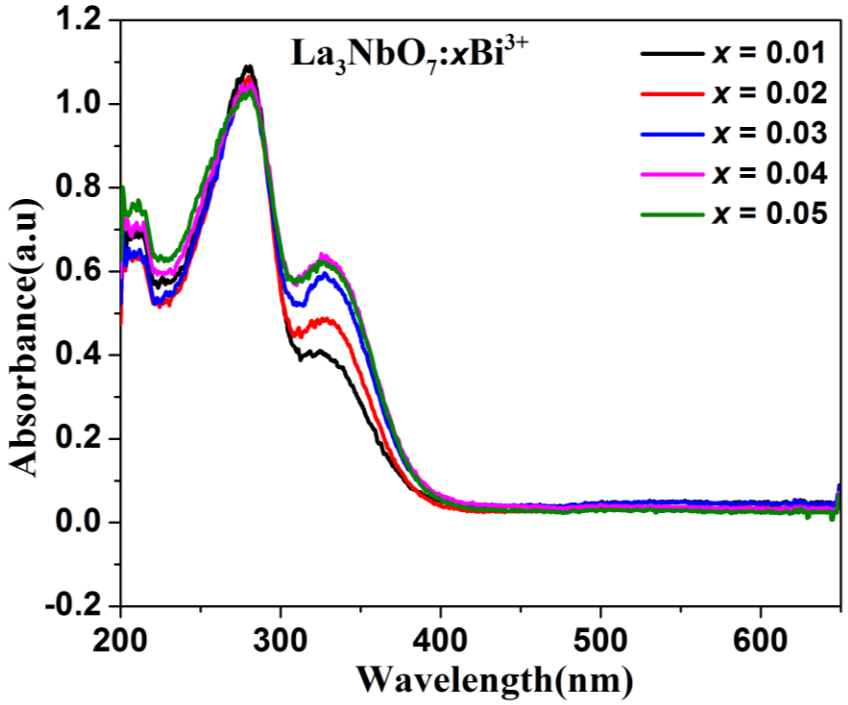

Fig.13 Absorption spectra La_3NbO_7: Bi^{3+} samples

Table.2 Band gap values of La_3NbO_7: Bi^{3+} samples

Composition	Band gap E_g *(eV)*
0.01	**3.18**
0.02	**3.09**
0.03	**3.04**
0.04	**2.98**
0.05	**2.91**

Photoluminescence studies

Photoluminescence excitation and emission spectra for the series of La_3NbO_7: xBi^{3+} samples are represented in figure 14 and figure 15 respectively. Excitation spectrum was monitored for emission wavelength 436 nm. Major excitation peaks falls around 300 nm. The emission spectra cover the whole visible region with double peaks around 450 nm and 600 nm. This kind of Broad nature of emission peaks is very suitable for WLED applications. Since the emission spectra covers the whole visible region with a single dopant there is no need of co-doping in these samples.

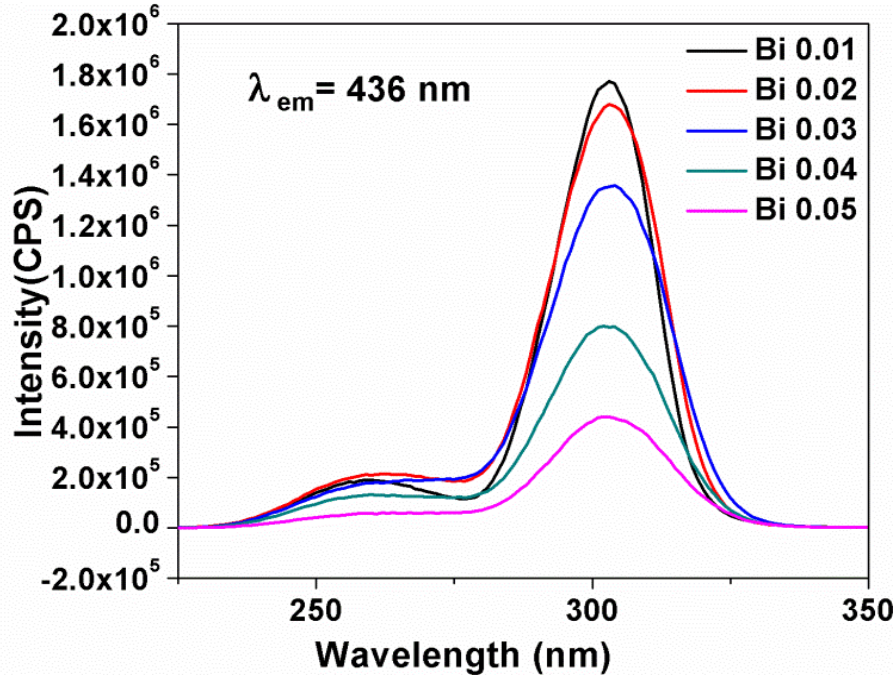

Fig.14 Photoluminescence excitation spectra of La_3NbO_7: xBi^{3+} samples

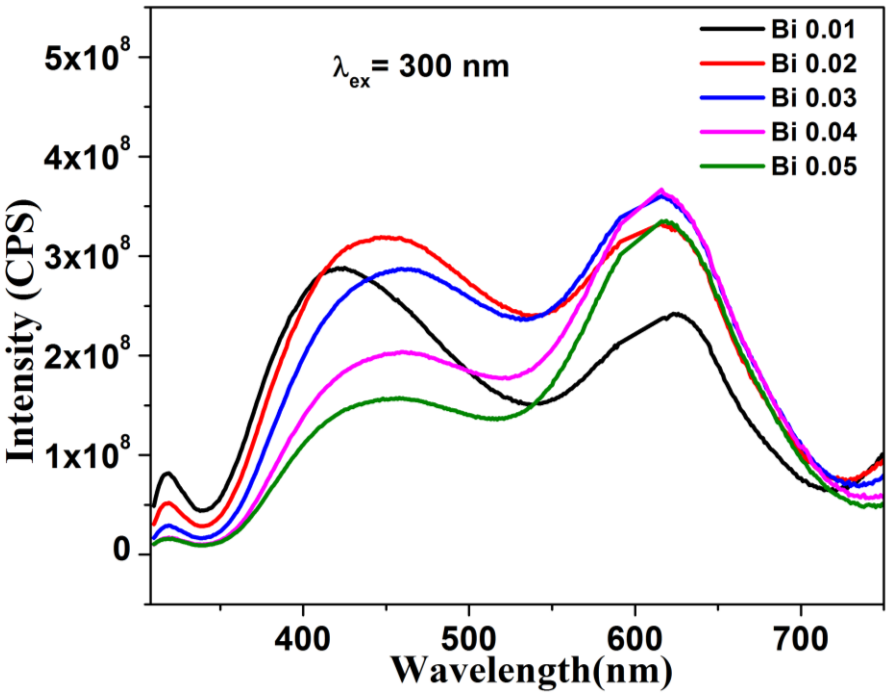

Fig.15 Photoluminescence emission spectra of La_3NbO_7: xBi^{3+} samples

The CIE values of the series of samples were calculated and marked in the CIE diagram in figure 16. Also the values are tabulated in table 3. From the table it is inferred that the CIE values of the prepared sample are very close to ideal value (0.33, 0.33).

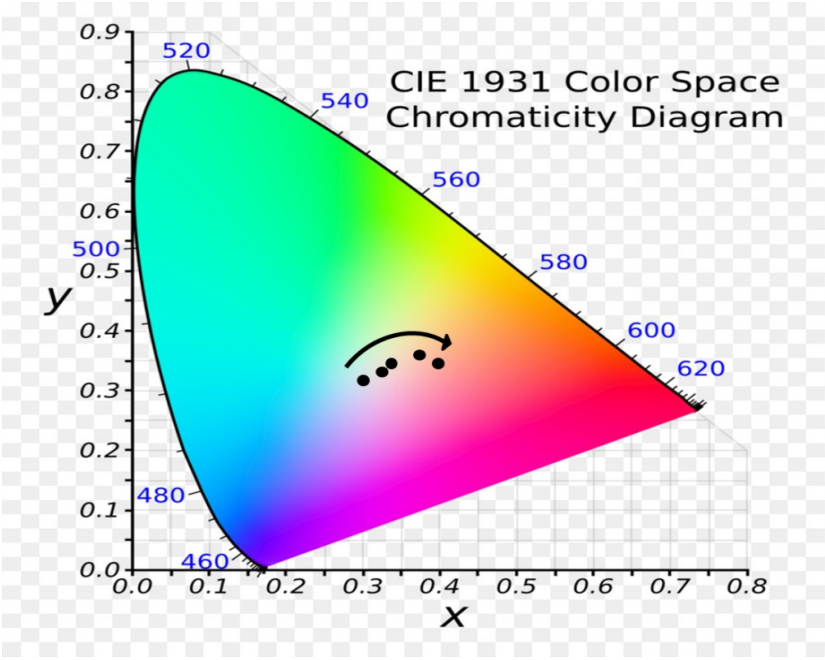

Fig.16 CIE Diagram of La_3NbO_7: Bi^{3+} samples

Table 3. CIE values of La_3NbO_7: Bi^{3+} samples

x	Color Coordinates
0.01	**(0.30,0.28)**
0.02	**(0.33,0.31)**
0.03	**(0.34,0.32)**
0.04	**(0.38,0.34)**
0.05	**(0.40,0.33)**

Conclusions

A series of weberite type samples were prepared via conventional solid state reaction method. Phase purity of the samples were ensured from powder X-ray diffraction patterns. The effect of *A* site variations in weberite type system A_3SbO_7 were studied and better structural and optical properties were confirmed for Lanthanum based systems. Hence further studies were carried out by fixing the Lanthanum in the *A* site.By fixing Lanthanum in the *A* site, *B* site was varied with different penta-valent elements ie; Nb, Ta and Sb. Tantalum and Antimony samples have emission spectra covering the visible spectra up to 600 nm. But the Niobium based samples is showing an emission spectrum covering the whole visible region. Hence the Niobium based samples were subjected for further characterizations. Niobium based samples have good absorption strength in the n-UV region and emission spectra covers the whole visible region. There exist concentration quenching after 3 mol%. The calculated CIE values fall around ideal value of white light.

Chapter 3

Color - Tunable Phosphors in Weberite Type System, $La_3SbO_7:Bi^{3+}$, Eu^{3+} for Near-UV LED Applications

The $La_3SbO_7:Bi^{3+}$ phosphors crystallize into a phase pure weberite type structure with good particle morphology. Upon UV light excitation at 315 nm, these phosphors show broad band emission in the blue green region centered near 517 nm owing to the $3P_1$-$1S_0$ transitions of the Bi^{3+} activator. Critical emission quenching of $La_3SbO_7:xBi^{3+}$ samples was observed at x = 0.04. Eu^{3+} is co-doped with $La_3SbO_7:0.04Bi^{3+}$ blue green phosphor to incorporate the red component to make a full color emission phosphor. The effective energy transfer from Bi^{3+} to Eu^{3+} ions has been assessed using Dexter's theory indicating resonance type through dipole-quadrupole interaction. Further the decreasing trends in lifetime measurements confirm the existence of energy transfer process from Bi^{3+} to Eu^{3+}. The near white light emitting phosphor $La_3SbO_7:xBi^{3+}, yEu^{3+}$ can be realized by adjusting the concentrations of the Bi^{3+} and Eu^{3+} with chromaticity coordinates: (0.30, 0.48).

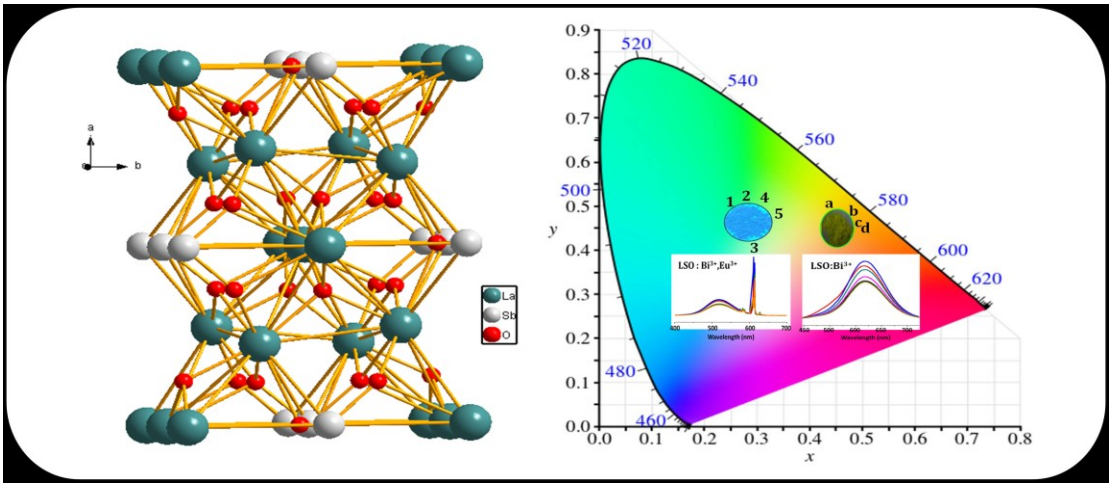

Introduction

Lighting applications that use light emitting diodes, organic light emitting diodes / light-emitting polymers are commonly referred to as Solid State Lighting (SSL). The history of SSL technology can be traced as far back as 1962 to the first semiconductor laser announced by Hall and later it was a mile stone in the lighting industry when Shuji Nakamura announced his invention of InG/GaN blue light emitting diode (LED) chips for the first time in 1993. And the first commercially available white light emitting diodes was produced by Nichia Corporation in 1996.

Currently in pc-WLEDs down-converting phosphors are clubbed with blue or n-UV LEDs to generate white light. In pc-WLEDs two methods used to obtain white light are as by combining emission from red, green, blue phosphors with n-UV chips or by using a yellow emitting phosphor with a blue LED. The multi-phased phosphors show low efficiency due to the strong re-absorption emission of blue or green phosphors by yellow or red emitting phosphors. In the second method it commonly uses 460nm blue InGaN LED chip with cerium doped yttrium aluminum garnet. But due to the lack of red component it shows low color rendering index (CRI) values in the range 70 - 80 and high correlated color temperature (CCT) temperature of 4000-7500K. Here comes the need for a single phase tunable emission phosphor for UV-chip WLEDs. A single phase phosphor contains a microcrystalline host doped with suitable activator ions and sensitizer ions, and it should be capable to emit more than one spectral color simultaneously. In this light, efforts are going on to develop direct white emitting novel phosphors for LED application. And nowadays there are many reports about direct white emitting phosphors with different activators combinations such as Bi^{3+}- Eu^{3+}, Dy^{3+}- Eu^{3+}, Eu^{2+}- Mn^{2+}, Ce^{3+}- Mn^{2+}/Dy^{3+}, etc. *Fengwen Kang et al.(2015)* have reported white light emission from Bi^{3+} and Eu^{3+} co-doped yttrium silicates, *Yaomiao Feng et al.(2015)* have reported $Sr_5(PO_4)_3F:Eu^{2+},Mn^{2+}$ white emitting phosphors and recently *Xiong et al.(2016)* have reported white light emission from host sensitized single phase $Y_2WO_6:Ln^{3+}$ (Ln^{3+}= Eu^{3+},Dy^{3+}) phosphor.

The properties of a single phase phosphor depend on the nature of host material as well as the activator and sensitizers used along with it. The crystal structure of host lattice, symmetry and coordination of doping site, activator doping concentration, uniformity of activator distribution…etc plays a vital role in the performance of WLEDs. Thus careful analysis should

be taken while selecting a host material and dopants. Orthorhombic systems with a general formula Ln_3MO_7 have already got wide recognition for their amusing luminescent properties. It is a class of typical weberite structure with three lanthanide cations, one transition metal cations and oxygen anions. Crystal structure of Ln_3SbO_7(Ln = La - Dy) and magnetic properties of ternary Ln_3SbO_7(Ln=Rare earths) were reported by *Siqueira et al.(2011)* and *Hinatsu et al. (2009)* respectively.La_3SbO_7 is having ordered defective fluorite type structure. It crystallizes into orthorhombic structure with Cmcm space group. According to *Hinatsu et al*. the unit cell for oxides have the general formula $M_4^{4+}O_8$ in which four tetravalent ions are replaced by three trivalent ions (Ln) and one pentavalent ion (M). Thus it creates one oxygen vacancy per fluorite cell. Here cation ordering occurs at the metal site and the oxide-vacancy occurs at anion site, because of the significant difference in ionic radii of Ln^{3+} and M^{5+} cation. Photoluminescence properties of Eu^{3+} doped R_3SbO_7(R = La, Gd ,Y) and Sm^{3+} doped La_3SbO_7 were studied by *Jing Wang etal*.(2014) and *Zeng-Mei Li et al.(2016)* respectively. It is reported that this compound has high chemical and thermal stability as well as lattice stiffness. The SbO_6 octahedron and La_2O_8 cube in La_3SbO_7 system is found to be more regular compared to other rare earth systems of R_3SbO_7 series.

The selection of activators is as important as the selection of host material. The same activator can produce different emission with different host lattice. Of the different activators, used such as Eu^{3+}, Ce^{3+}, Dy^{3+}...etc. Bi^{3+} luminescence is getting more importance nowadays. Exploring the luminescence properties of Bi^{3+} ions is a curious job due to its wonderful emission properties. A lot of studies have been conducting across the world in the Bi^{3+} luminescence. The Bi^{3+} attains much attention because of the fact that it shows wide variety of optoelectronic properties and the presence of large number of its valence states enable its potential application. The ground state of Bi^{3+} is $6S^2$ electronic configuration. The excited states coming from nsnp configuration are $^3P_0$, $^3P_1$, $^3P_2$ and $^1P_1$ states. Transitions from $^1S_0$ to $^3P_0$ and $^3P_2$ are completely spin forbidden, if no other configurations are taken into account. The two energy states $^3P_1$ and $^1P_1$ are mixed by spin-orbit coupling. Therefore, only two transitions are expected to have reasonable absorption strength. Transitions from $^1S_0$ to $^3P_1$, $^1S_0$ to $^3P_2$, $^1S_0$ to $^1P_1$ are termed as A band, B band and C band respectively. Charge transfer bands which have high energy than C band are coined as D band. Emission properties of Bi^{3+} ions vary with host lattice. *Rambabu et al.(2013)* have reported the greenish-yellow luminescence of Bi^{3+} ions in lanthanide vanadate

phosphors. Whereas red luminescence in scandium vanadates and blue emission in calcium antimonates were reported by *Fengwen Kang et al*. (2014) and *Shiyue Yao et al.* (2016) respectively. The Bi^{3+} ions are usually used as sensitizers along with Ln activators (Eu^{3+}, Sm^{3+}, Er^{3+}). The resonance type energy transfer from Bi^{3+} ions to Ln ions could result in highly enhanced emissions of the Ln ions in Bi^{3+}/Ln co-doped materials.

If come to the case of Eu^{3+}, it is a potential candidate as an activator for red phosphor but it shows very weak absorption peak at 400 nm due to the forbidden 4f - 4f absorption transitions due to parity selection rules. And it is also reported that its optical oscillator strength is small and its narrow FWHM make it intolerant to the tiny emission wavelength shift of UV LED chips.

In this study we attempt to develop single phase white phosphors from Eu^{3+}co-doped yellow phosphor La_3SbO_7:Bi^{3+} by calcination at 1400°C/6h. Here we have carried out structural, optical as well as morphological studies for different concentrations of Bi^{3+} (x = 0.025, 0.04, 0.05, 0.06, 0.075). Then by keeping Bi^{3+} concentration constant we have varied the Eu^{3+} concentration and the effect of Eu^{3+} substitution is studied. According to the previous reports when Bi^{3+} ions are co-doped with Eu^{3+} ions emission spectra shows no Bi^{3+} emissions but only Eu^{3+} emission. Here in our case we got simultaneous emissions from Bi^{3+} and Eu^{3+}. Furthermore energy transfer between Bi^{3+} and Eu^{3+} ions have been discussed on the basis of the life time decay curves. To the best of our knowledge, there are no reports on the PL properties of Eu^{3+} co-doped La_3SbO_7:Bi^{3+} antimonate phosphors.

Experimental section

The samples, La_3SbO_7:$x$$Bi^{3+}$ (x = 0.025, 0.04, 0.05, 0.06, 0.075) and La_3SbO_7:*0.04*Bi^{3+}, $y$$Eu^{3+}$ (y = 0.005, 0.01, 0.02, 0.03, 0.04) were prepared by the conventional solid state method. The starting materials (La_2O_3, Sb_2O_5, Bi_2O_3, Eu_2O_3) were weighed according to stoichiometry and mixed thoroughly in an agate mortar in acetone media. The mixed samples were dried in an air oven at 100°C for one hour. This process of mixing and drying was repeated three times for obtaining homogeneity. After intermittent mixing and drying the samples obtained were homogeneous in nature, and which was calcined twice at 1400°C/6h by keeping it at an intermediate temperature of 900°C for 30 minutes. The structural studies were carried out using an X-ray diffractometer (X'Pet Pro PANalytical) which is operated at40 kV/30mA, making use

of Cu Kα radiation of wavelength 1.54 Å and the patterns were recorded in the range from 10°-90°. Rietveld analysis was performed to refine the structure using X'pert Highscore Plus software. Absorbance study of the samples were carried out using a Shimadzu, UV-2450 UV–Vis spectrophotometer in the 200-800nm wavelength range using Barium Sulfate as a reference. Photoluminescence spectra were recorded on a Fluorolog HORIBA fluorescence spectrophotometer with a Xe lamp (450 W) as the excitation source. Luminescence life time of the phosphors was recorded by the phosphorimeter attached to Fluorolog_3 spectrofluorimeter. Morphological homogeneity of the samples was confirmed using a scanning electron microscope (JEOL, JSM-5600LV) operated at 15 kV.

Results and discussion

XRD refinement and crystal structure

Structural studies of La_3SbO_7:$x$$Bi^{3+}$ (x = 0.025,0.04,0.05,0.06,0.075) and La_3SbO_7:$x$$Bi^{3+}$,$y$$Eu^{3+}$ (x = 0.04, y = 0.005,0.01,0.02,0.03,0.04) (LSO:$x$$Bi^{3+}$, $y$$Eu^{3+}$) were carried out. And the crystal structure of La_3SbO_7 host is shown in Figure 1. The crystal structure of the weberite type compounds of the formula, Ln_3MO_7 (Ln = La-Lu, Y; M = Nb, Ta, Sb) is formed by an arrangement of Ln_1O_8 cubes and MO_6 octahedra in layers. Further, a layer of VII coordinated Ln_2 cation lies in between the layers of MO_6 - LnO_8. In La_3SbO_7 system the SbO6 octahedra share one oxygen ion O(3) and forms infinite one dimensional zigzag chain parallel to [001] direction. La1 ions are coordinated by eight oxygen ions and distorted La2-O7 form a one dimensional chain by sharing their edges. The SbO6 and La1-O8 chains lie alternately parallel to [100] plane and La2-O7 slab consists of these chains. In an eight coordinated system the ionic radii of Bi^{3+} and La^{3+} ions are 1.17 Å and 1.16 Å respectively and that of Eu^{3+} is 1.066 Å.

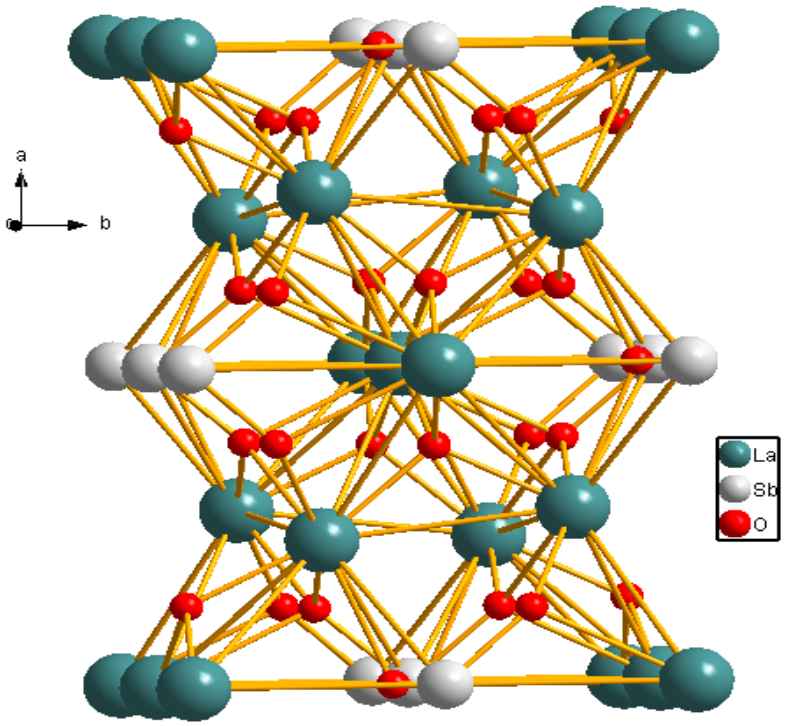

Figure1. Crystal structure of La_3SbO_7.

Since La^{3+} has two coordinated sites VII and VIII in the lattice, the substitution of larger ion like Bi^{3+} and relatively smaller ion Eu^{3+} has lead to preferential occupation of these ions in the lattice. The site preference of cations on substitution is mainly based on the ionic size and covalent nature of the ion. In the present case Bi^{3+} is relatively big and more ionic character compared to Eu^{3+}, owing to this it can be assumed that Bi^{3+} prefers to occupy the La-VIII coordinated site, on the other hand Eu^{3+} takes the VII coordinated site. Rietveld analysis on these assumptions of preferential occupations of cations also indicates increasing of bond distances in the VIII coordinated site and decreasing trend in the VII coordinated site on substitution of Bi^{3+} and Eu^{3+} in the system. Further the Eu^{3+} luminescence which is discussed in the later part of the text also shows the behavior of VII coordinated occupancy. This type of preferential occupation has been reported in this system. All these results confirm the preferential occupation of Bi^{3+} and Eu^{3+} in the Lanthanum sites.

Figure 2 shows the powder XRD patterns of Bi^{3+} doped LSO samples and host sample. It is inferred that the samples are crystallized into a orthorhombic crystal system with Cmcm space group and are in well agreement with JCPDS file No. 01-073-8085. Absence of any additional peaks ensures the phase purity of the samples and thus formation of a single phase phosphor is confirmed.

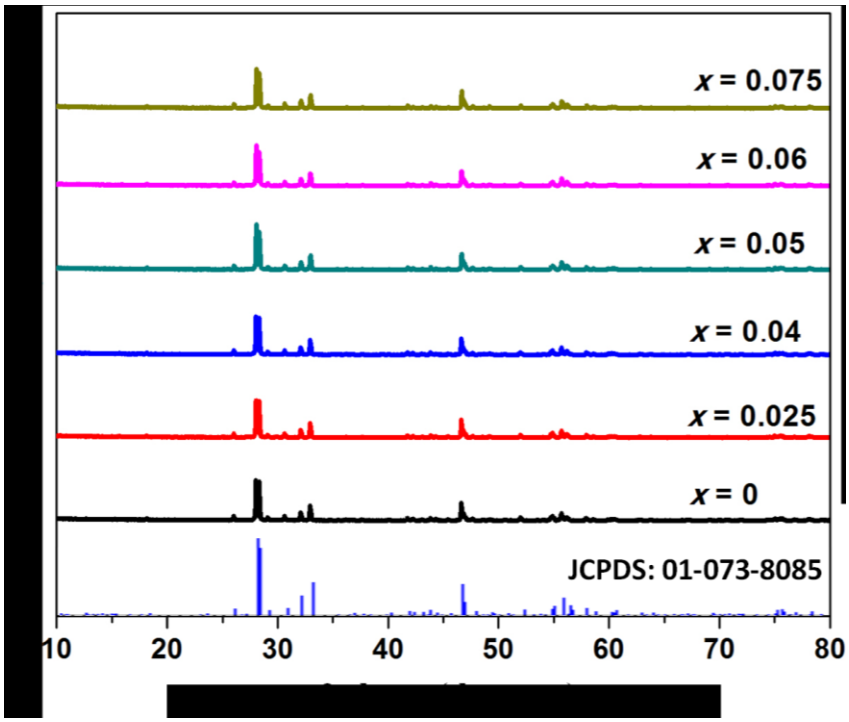

Figure 2. Powder XRD patterns of LSO:xBi^{3+}(x = 0, 0.025, 0.04, 0.05, 0.06, 0.075).

Figure 3 shows the XRD patterns of LSO: xBi^{3+}, yEu^{3+} (x = 0.04, y = 0.005, 0.01, 0.02, 0.03, 0.04). It is also in agreement with the JCPDS file No. 01-073-8085. Absence of impurity peaks ensures the phase pure nature of the samples. XRD studies reveal that the structure of La_3SbO_7 host remains unchanged on the doping of Bi^{3+} or co-doping of Eu^{3+}. In Eu^{3+} co-doped samples we can see a slight right shift in the reflection peaks and the inset illustrates more prominently in the enlarged 2θ range around 30-34°. It is attributed due to the smaller ionic radius of Eu^{3+} ions compared to that of La^{3+}. A kind of lattice shrinkage is expected and which is evident from the right shift of XRD patterns.

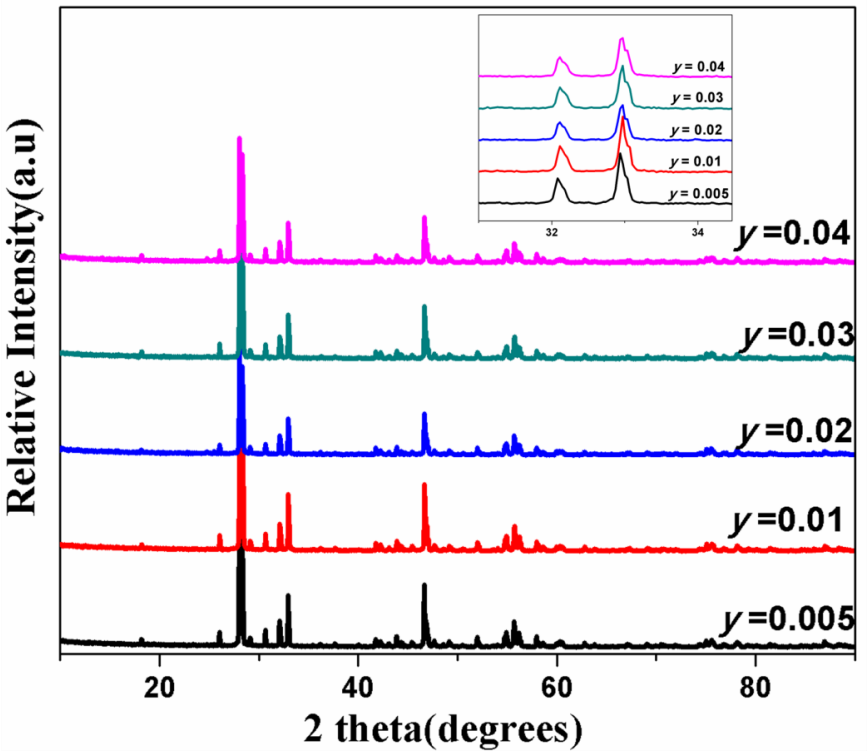

Figure 3. Powder XRD patterns of LSO: $0.04Bi^{3+}$, yEu^{3+}(y = 0.005, 0.01,0.02, 0.03, 0.04) samples, the inset illustrates the enlarged 2θ range around 30- 34°.

Rietveld refinement of all the samples was carried out to understand the details of lattice parameter. Starting model for the refinement of the phases was taken from the reported crystal structure of La_3SbO_7 and it is shown in Table 1. Table 2 shows the refined parameters obtained from Rietveld analysis. It shows the variations in lattice parameters with Eu^{3+} co-doping.

Table 1. Starting structure model of $La_{2.93}SbO_7$:0.04 Bi^{3+}, 0.03Eu^{3+}

Element	Wyckoff	*x*	*y*	*Z*	SOF
La1	4a	0	0	0	1
La2	8g	0.22727	0.29716	0.25	0.976
Bi	8g	0.22727	0.29716	0.25	0.013
Eu	8g	0.22727	0.29716	0.25	0.01
Sb	4b	0	0.5	0	1
O1	4c	0	0.442	0.25	1
O2	16h	0.1283	0.3157	-0.0348	1
O3	8g	0.1207	0.0219	0.25	1

Table 2. Refined parameters obtained from Rietveld analysis of LSO: *x*Bi^{3+}, *y*Eu^{3+}

	a (Å)	*b* (Å)	*c* (Å)	*V* ($Å^3$)	R_{exp} (%)	R_p (%)	W_{Rp} (%)	*GOF*
$x = 0,\ y = 0$	11.1559	7.6347	7.7468	659.8231	14.7	12.0	16.0	1.17
$x = 0.025,\ y = 0$	11.1549	7.6332	7.7459	659.5397	14.9	12.7	16.9	1.28
$x = 0.04,\ y = 0$	11.1555	7.6329	7.7457	659.5332	14.8	12.1	16.2	1.19
$x = 0.05,\ y = 0$	11.1544	7.6335	7.7458	659.5250	14.6	11.6	15.5	1.13
$x = 0.06,\ y = 0$	11.1537	7.6341	7.7460	659.5571	14.9	11.9	15.8	1.13
$x = 0.075,\ y = 0$	11.1542	7.6335	7.7455	659.5092	15.0	12.3	16.2	1.15
$x = 0.04,\ y = 0.005$	11.1547	7.6333	7.7456	659.5171	14.4	12.1	15.7	1.18
$x = 0.04,\ y = 0.01$	11.1540	7.6334	7.7458	659.4946	14.4	12.6	16.3	1.28
$x = 0.04,\ y = 0.02$	11.1536	7.6336	7.7460	659.5052	15.6	13.5	17.7	1.28
$x = 0.04,\ y = 0.03$	11.1525	7.6344	7.7460	659.5161	15.0	13.3	17.0	1.27
$x = 0.04,\ y = 0.04$	11.1536	7.6342	7.7458	659.5386	15.0	13.3	17.3	1.32

Morphological studies

Morphological studies of both set of samples were taken. SEM images of La_3SbO_7 host and LSO: xBi^{3+} (x=0.04) are shown in Figure 4. It shows that with Bi^{3+} doping the morphology is improving and the average particle size falls in the range 1-2 μm. Nature of agglomeration is also less in these samples. The SEM images of Eu^{3+} co-doped LSO:0.04Bi^{3+} samples were also studied (Figure 5). It is seen that morphology is getting improved on addition of Eu^{3+} addition ie; particles attained more spherical shape and uniform nature. Agglomeration is also very less. The average particle size is found to be less than that of singly Bi^{3+} doped samples but as the Eu^{3+} concentration increases it is increasing and it falls in the range of 1 μm. These modifications in morphology due to Eu^{3+} co-doping assist the enhanced luminescence behavior of Eu^{3+} co-doped LSO: xBi^{3+}.

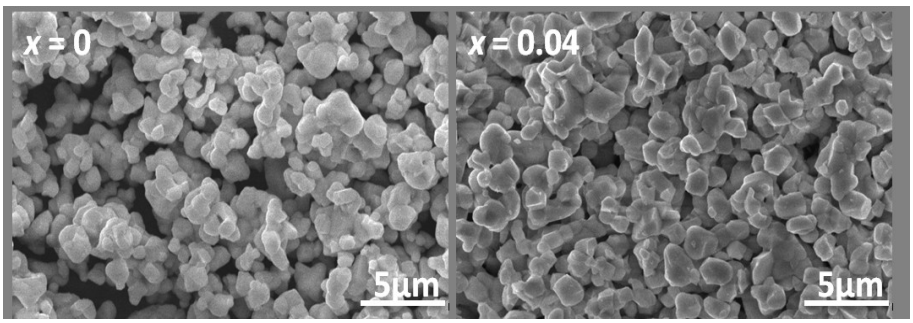

Figure 4.SEM images of LSO:xBi^{3+}(x=0,0.04)

EDS spectra of LSO:0.04Bi^{3+} and LSO:0.04Bi^{3+}, 0.03Eu^{3+} are shown in Figure 6 and Figure 7. The EDS analysis confirms the presence of all the expected elements. Further stoichiometry of the samples obtained from EDS analysis are matched with the theoretically calculated values.

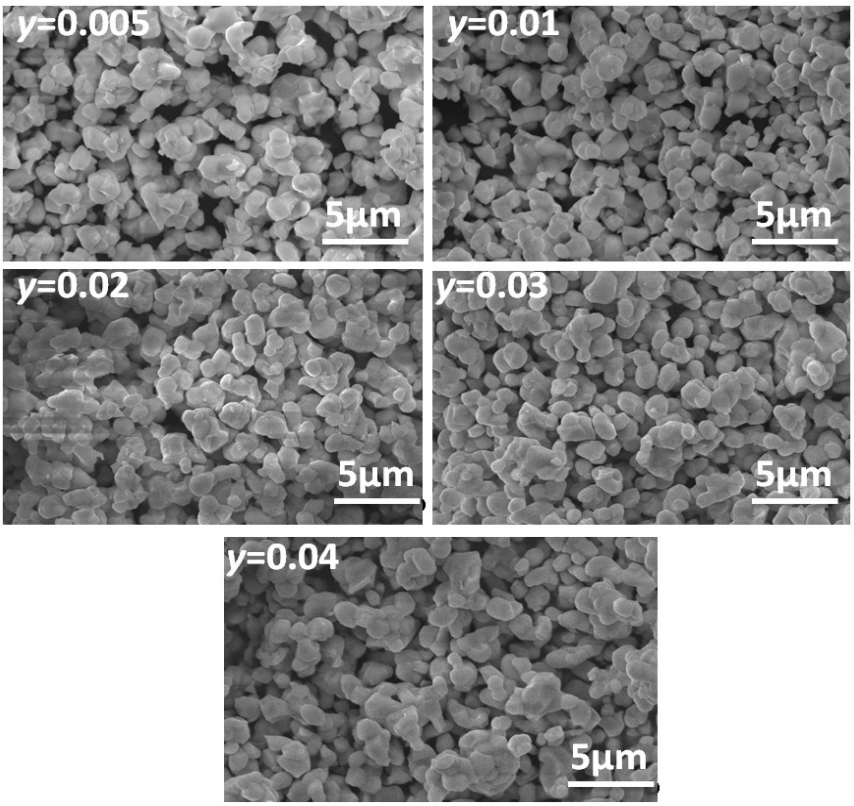

Figure 5. SEM images of LSO: xBi^{3+}, yEu^{3+} (x = 0.04, y = 0.005, 0.01, 0.02, 0.03, 0.04)

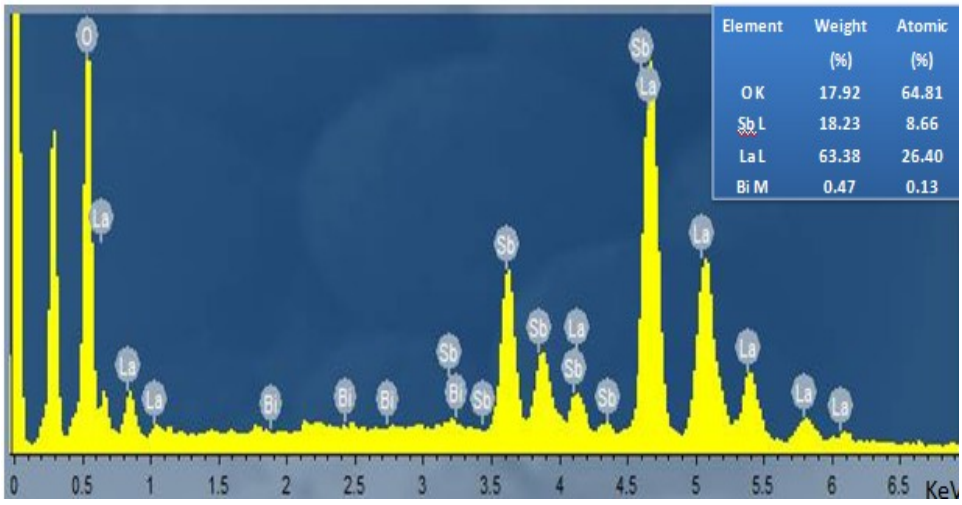

Figure 6.EDS spectra of LSO:xBi^{3+}(x=0,0.04)

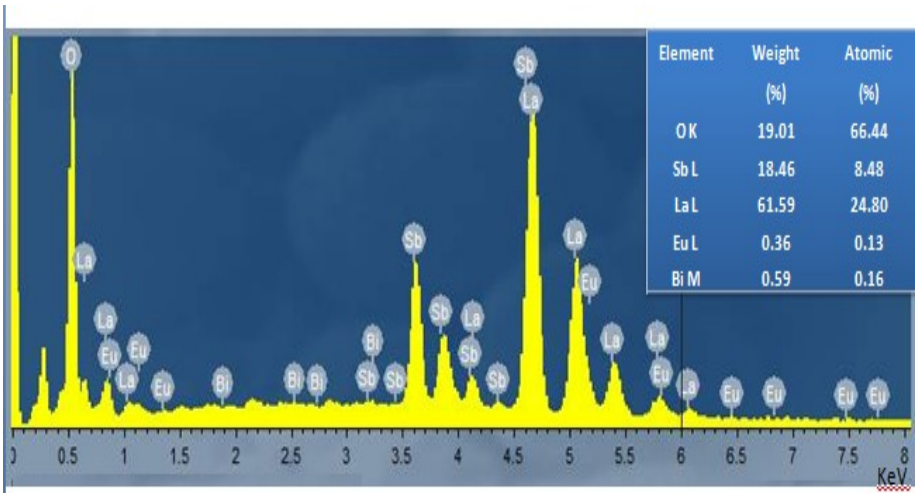

Fig. 7. EDS spectra of LSO: $0.04Bi^{3+}$, $0.03Eu^{3+}$

Absorbance

Figure 8(a) and 8(b) shows the UV-Vis absorption spectra of LSO: xBi^{3+} and LSO: xBi^{3+}, yEu^{3+}respectively. Careful analysis of absorption spectra enables us to understand about the possible transitions of electrons and distribution of energy states. Here in both cases we can observe strong absorption peaks below 400 nm, and it is desirable for WLED applications. In Bismuth alone doped samples the absorption peak shows maxima at 325 nm. And Eu^{3+} co-doped samples also show similar results.

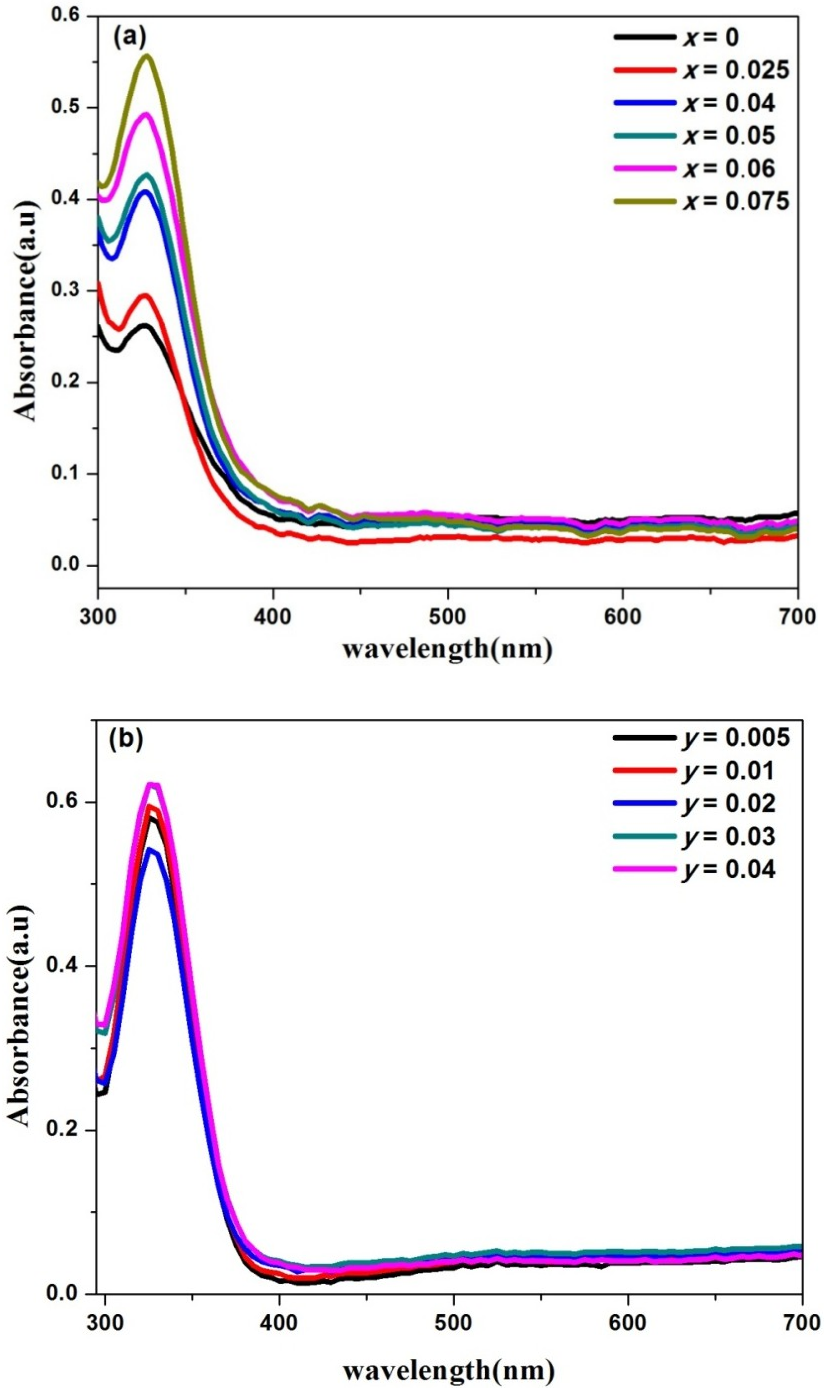

Figure 8. Absorption spectra of (a) LSO: xBi^{3+} and (b) LSO: 0.04Bi^{3+}, yEu^{3+}

Table 3. Band gap energy of
LSO: $0.04Bi^{3+}$, yEu^{3+}(y = 0.005, 0.01, 0.02, 0.03, 0.04)

y	***Band gap energy E_g(eV)***
0.005	3.22
0.01	3.20
0.02	3.14
0.03	3.13
0.04	3.11

The fundamental absorption which manifests itself by a rapid rise in the absorption spectra can be used to determine the energy gap. The band gap calculated using Shapiro's method by extrapolating the onset of absorption curve to wavelength axis is listed below in Table 3. It shows a decreasing trend with increasing Eu^{3+} concentration. As the Eu^{3+} concentration increases it steadily decreases from 3.22 eV to 3.11 eV. It shows that band gap energy can be flexibly adjusted by controlling cationic ratios. This reduction in band gap may be due to the difference in the electronegativity of Bi^{3+} ions and Eu^{3+} ions ie; Bi^{3+} ions are highly electronegative than Eu^{3+} ions. Hence the average electronegativity reduces with increased Eu^{3+} content. Thus covalency increases and it will affect the charge transfer mechanism of ligand ions.

Photoluminescence properties, energy transfer and chromaticity

Metal ions like Bi^{3+} having ns^2configuration have great importance in luminescence. Bi^{3+} have $6s^2$ electronic configuration and its luminescence properties strongly depends on the composition and crystal structure of host lattice. Due to the spin selection rule only two transitions are expected to take place in Bi^{3+} ie; $^1S_0$ to$^3P_1$ and $^1S_0$ to $^1P_1$(Y.Feng, 2015). All other transitions are strictly spin forbidden. At room temperature the emission and absorption bands in Bi^{3+} doped phosphors are attributed to the $^3P_1$ to $^1S_0$ and $^1S_0$ to $^3P_1$ transitions respectively. Due to the presence of ns^2 electronic configuration the emission and absorption spectra of Bi^{3+}

ions are expected to be broad, which depends on the covalence, coordination number, bond volume polarisability and present charge. Photoluminescence and stoke shift strongly depends on the coordination characteristics of Bi^{3+} (Zhou, 2015).

The excitation spectra corresponding to emission wavelengths of 517 nm, 560 nm and 570 nm of LSO: $0.04Bi^{3+}$ is shown in Figure 9. As expected we got broad excitation peaks in the n-UV region, which is very much desirable for WLED application. It is evident from the Figure 9 that though the emission wavelength increases we get excitation in the same wavelength region but the intensity of excitation spectrum is decreasing with increasing wavelength and the intensity is maximum for an emission wavelength 517 nm. As we get excitation in the same wavelength region for different emission wavelengths we can confirm that there exist only a single Bi^{3+} site, and it is assumed to be occupying the La^{3+} site owing to their well matched ionic radii, and this excitation peak can be attributed to the $^1S_0$ to $^3P_1$ transition of Bi^{3+} ions. Whereas, Anjun Huang *et al.(2017)* have reported the presence of more than one Bi^{3+} sites.

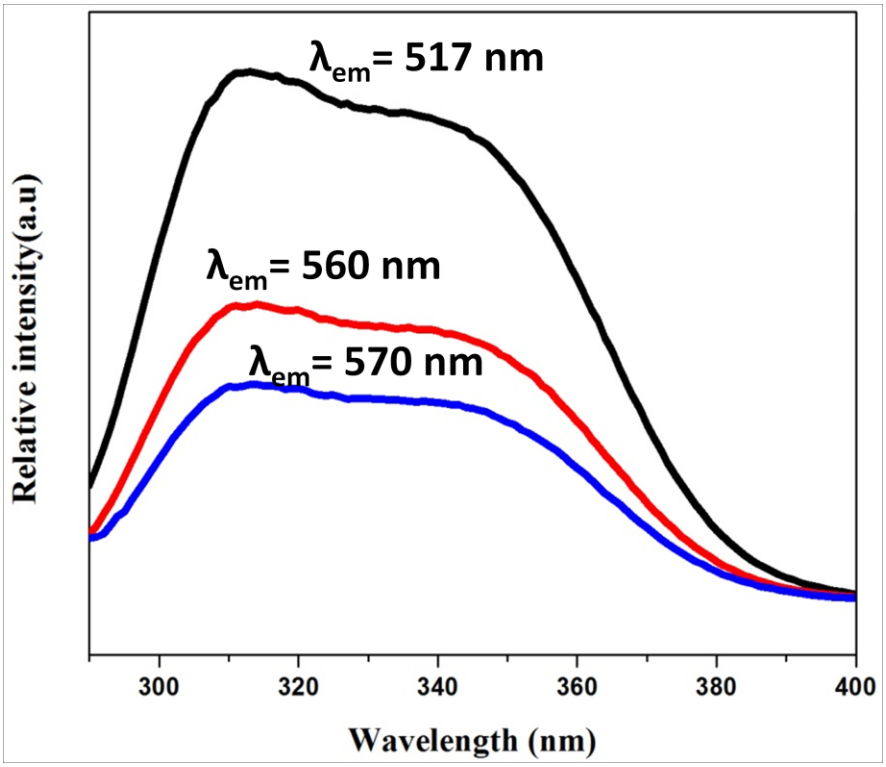

Fig.9. PLE spectra of LSO: $0.04Bi^{3+}$ under λ_{em} = 517 nm, 560 nm, 570 nm

Also the excitation spectra have double peak nature, which is peaked around 310 nm and 340 nm. It is known that the excitation of Bi^{3+} could present as two bands due to the electron

transitions from $^1S_0$ to $^3P_1$ and $^1P_1$ states. But this case would less likely ascribed to that because the energy difference between the two bands is too small, as a result, the two bands present as deeply overlapped but not distinctly separated. Thus, the two bands could be reasonably ascribed to the Bi^{3+} occupying distinct crystallographic sites (Z.Jiang et al. 2015).

Since we got a broad, double peaked excitation spectra, emission spectra corresponding to different excitation wavelength in the range 300 nm to 370 nm were observed, and it is shown in Figure 10. It is seen that as the excitation wavelength increases from 303 nm there is a steady increase in emission intensity up to 315 nm, and then it starts decreasing. Hence the maximum emission intensity is obtained for an excitation at 315 nm. Hence emission spectra for the series Bi^{3+} doped samples were monitored at 315 nm excitation wavelength. The excitation and emission spectra for a series of LSO samples with different Bi^{3+} concentrations are shown in Figure 11 and Figure 12 respectively. It is observed that as the Bi^{3+} ions were doped into the sample we got an additional peak around 345 nm along with host excitation peak around 310 nm. The peaks around 310 nm can be attributed to the charge transfer bands of antimony ions and the peaks around 345 nm is due to the emission from Bi^{3+} centers. The broad nature of emission and

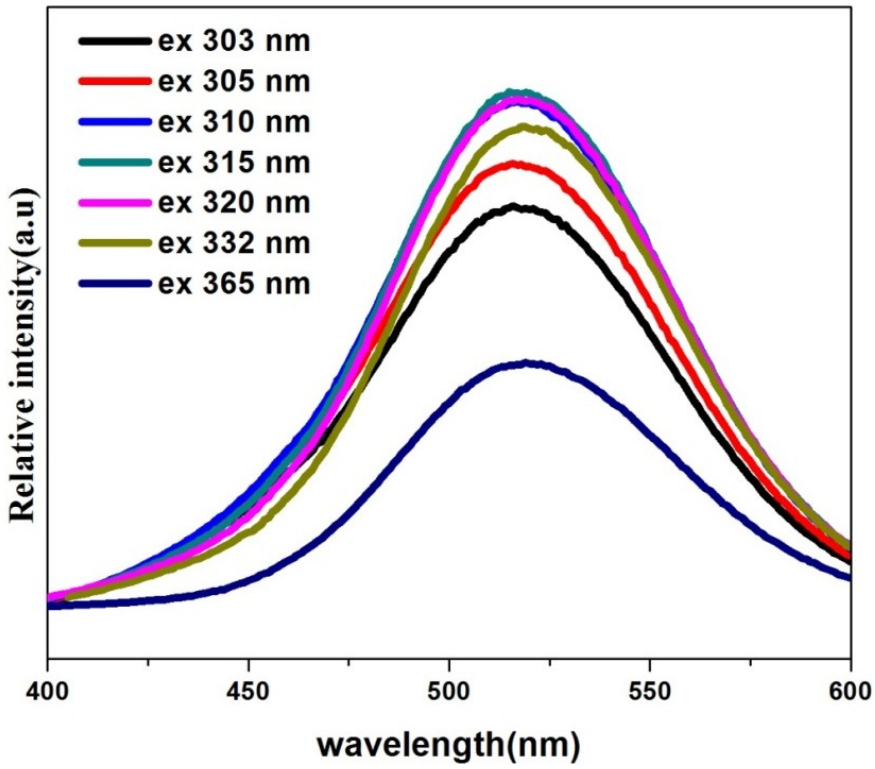

Fig.10. PL spectra of LSO: $0.04Bi^{3+}$ under different excitations

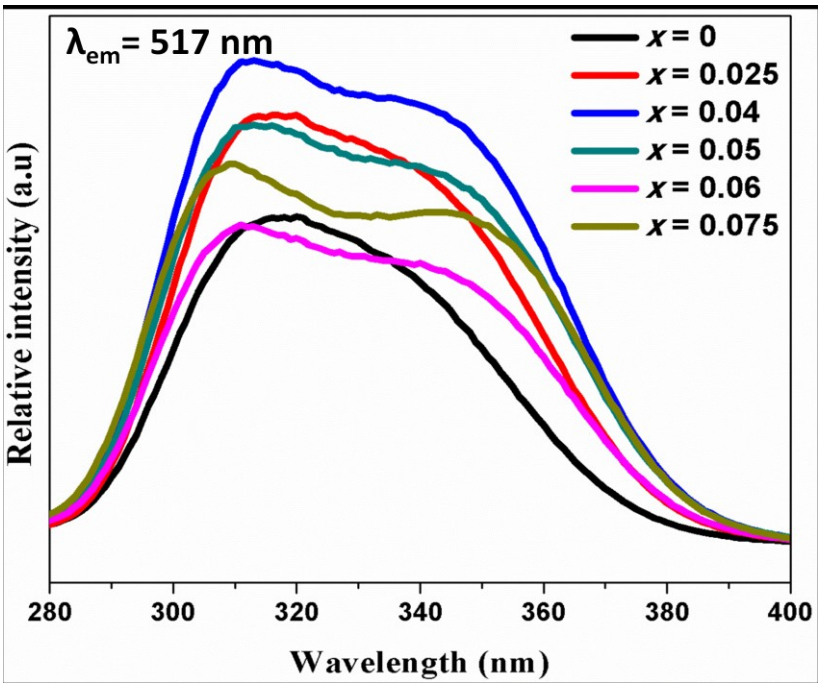

Fig. 11.PLE spectra of LSO: xBi^{3} for λ_{em} = 517 nm

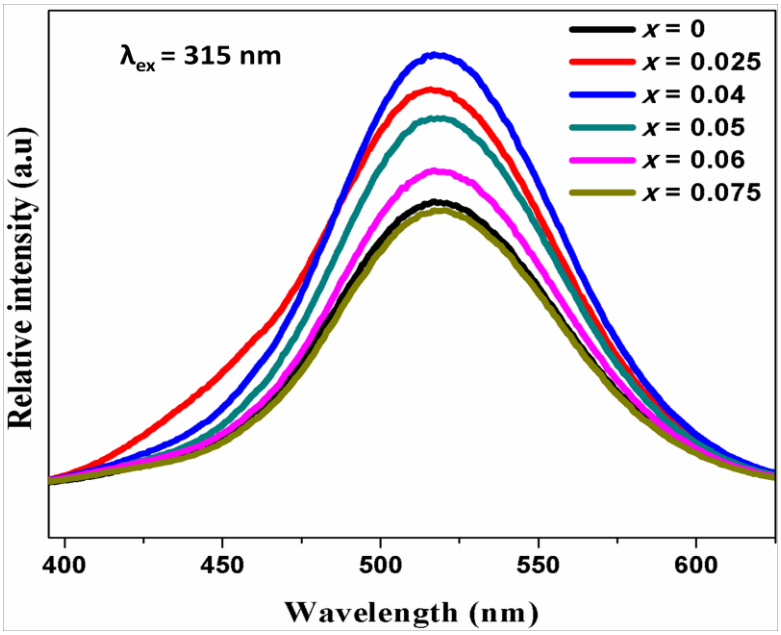

Fig.12. PL spectra of LSO: xBi^{3+}(x = 0, 0.025, 0.04, 0.05, 0.06, 0.075) under λ_{ex} = 315 nm

excitation spectra is due to the fact that in most hosts A band lies in UV region and C band in vacuum UV region, which constitute broad absorption band of Bi^{3+} ion(L.Wang.2012). According to *Hong Tao Sun et al.(2014)* the absorption and emission bands of Bi^{+}, Bi^{2+} and Bi^{3+} are much broader than those of f-f transitions of RE^{3+}, owing to the unsheltered outer electrons. The broad, single peaked emission spectra are peaked around 517 nm. These peaks arise due to the $^3P_1$ to $^1S_0$ transitions of Bi^{3+} ions. The emission intensity increases with increase in Bi^{3+} concentration up to 0.04 mol and is found to decrease with further increase in the Bi^{3+} content due to concentration quenching effect . Because as the concentration of Bi^{3+} increases the Bi^{3+}-Bi^{3+} distance reduces and non-radiative energy transfer occurs through cross relaxation. Accordingly, the optimum concentration of Bi^{3+} is found to be 0.04 mol. As the PL luminescence spectra indicate there is absence of red emission component. Hence it is needed further co-doping with suitable rare earth ions in order to obtain emission in red region also. The CIE color coordinates of these samples are listed in Table 4. It also shows that further color tuning is needed so that it will become a potential full color emitting phosphor for WLED applications. Hence we kept the Bi^{3+} concentration constant at $x = 0.04$ and Eu^{3+} was co-doped into La^{3+} site to obtain a full color emitting phosphor by monitoring the energy transfer phenomena between Bi^{3+} and Eu^{3+} ions.

Table 4. Coolor coordinates of
LSO: xBi^{3+}(x = 0, 0.025, 0.04, 0.05, 0.06, 0.075).

x	**Color Coordinates**
0	(0.51,0.47)
0.025	(0.49,0.48)
0.04	(0.51,0.47)
0.05	(0.51,0.47)
0.06	(0.51,0.46)
0.075	(0.51,0.46)

Excitation corresponding to different emission wavelengths of Europium co-doped samples was observed, and the Bismuth excitation is found to be better compared to that of Europium. As it is shown in Figure 9 excitation intensity is maximum for the emission wavelength at 517 nm. It is found that for emission at 517 nm we get a double peaked broad excitation spectra with maxima around 303 nm and 350 nm as observed in the case of singly Bi^{3+} doped samples. While increasing the emission wavelength ie; 575 nm onwards there appears a small sharp peak at 390 nm and the intensity of this sharp peak enhances with increasing emission wavelength. As the emission wavelength become 616 nm intensity of the sharp peak at 390 nm is greater than the peak due to Bi^{3+}. This shifting of the excitation wavelength to longer wavelength is due to the energy transfer between Bi^{3+} and Eu^{3+} ions (A.Huang et al. 2017). The stokes shift corresponding to Bi^{3+} alone doped samples are 19342.85 cm^{-1} and that of Eu^{3+} co-doped sample is 9407.26 cm^{-1}.

The excitation spectra of a series of Eu^{3+} co-doped samples at an emission wavelength 517 nm is shown in Figure 14. The excitation spectra are very broad in the n-UV region. That is desirable for WLED application. Since the excitation spectra are broad, different excitation wavelengths ranging from 280 nm to 400 nm. The best emission was obtained for Bismuth excitations than Europium excitations (Figure 15).

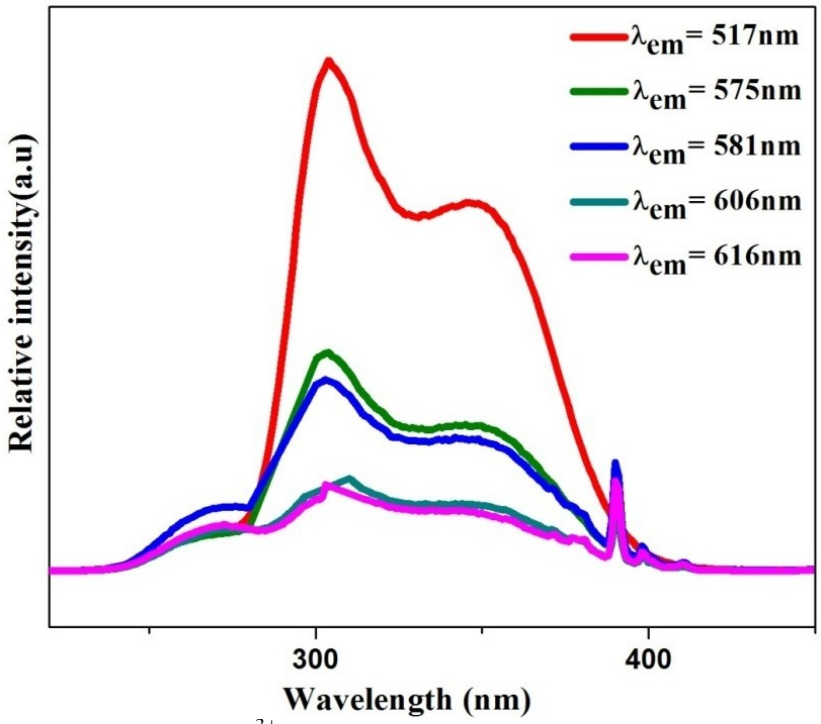

Fig.13. PLE spectra of LSO: 0.04Bi^{3+}, 0.03Eu3+ under λ_{em} = 517 nm, 575 nm, 581 nm, 606 nm, 616 nm

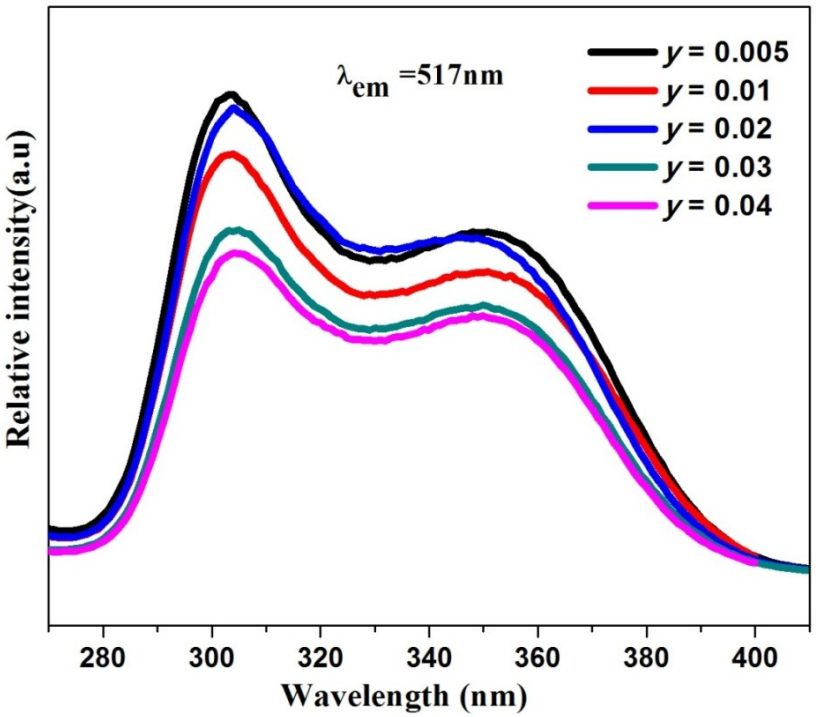

Fig.14. PLE spectra of LSO: Bi^{3+}, Eu^{3+} samples with different Eu^{3+} concentration

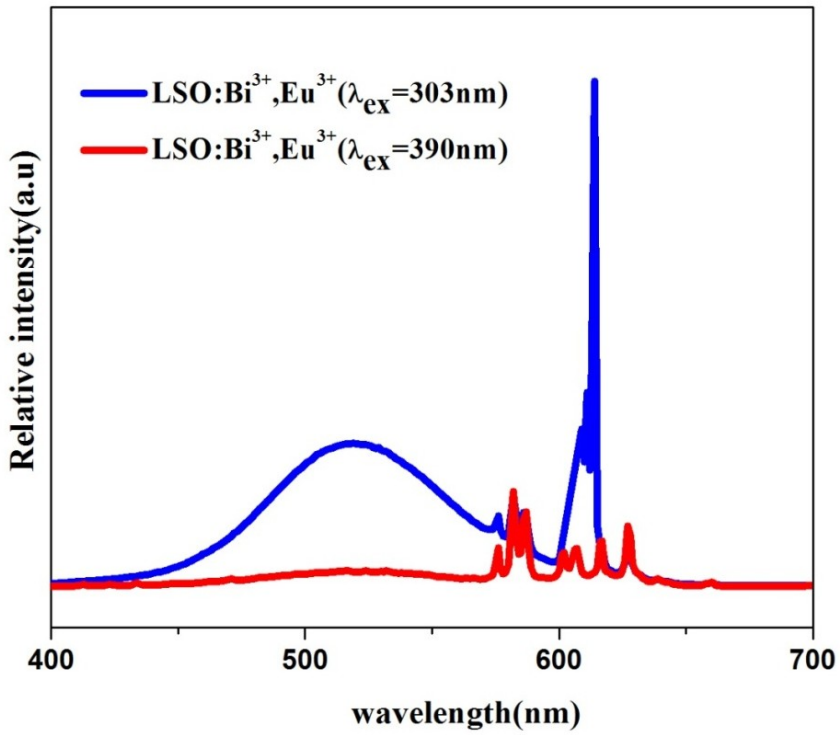

Fig.15. PL spectra of LSO: Bi^{3+}, Eu^{3+} samples under λ_{ex} = 303 nm and 390 nm

Under Bismuth excitations we got broad emission peak of Bi^{3+} covering the blue green region of visible spectrum, and sharp characteristic peaks of Eu^{3+} ions around 600 nm. Similar results were also reported by Ziqiang Jiang et al.(2017) As the excitation wavelength around 300 nm is not an efficient excitation region for Eu^{3+} samples the high intensity emission peaks of Eu^{3+} may be due to the energy transfer between Bi^{3+} and Eu^{3+} ions. For excitation at 303 nm it is observed that there is a steady decrease in intensity of both Bi^{3+} curves and Eu^{3+} curves with increasing Eu^{3+} content except for the concentration of y = 0.02, where both Bi^{3+} and Eu^{3+} peaks are maximum. Again it started to decrease with further increase in the Eu^{3+} content (Figure 16).

Figure 17 shows PL spectra of LSO: Bi^{3+}, Eu^{3+} samples for an excitation wavelength λ_{ex} = 390 nm. Under Eu^{3+} excitation at 390 nm we got broad emission peak in the blue green region along with sharp characteristic peaks of Eu^{3+} at 576 nm, 582 nm, 587 nm, 601 nm, 606 nm, 616 nm, 626 nm. These sharp peaks are attributed to the electric dipole and magnetic dipole transitions in Eu^{3+} ions. And these peaks clearly indicate that Eu^{3+} is sensitized by excited Bi^{3+}. Emission at

616 nm is attributed to the hypersensitive forced electric-dipole $^5D_0$ to $^7F_2$ transitions. The peaks at 582 nm is due to the $^5D_0$ to $^7F_0$ transitions. And the presence of additional peaks around 587 nm is may be due to the split in energy levels due to crystal field splitting.

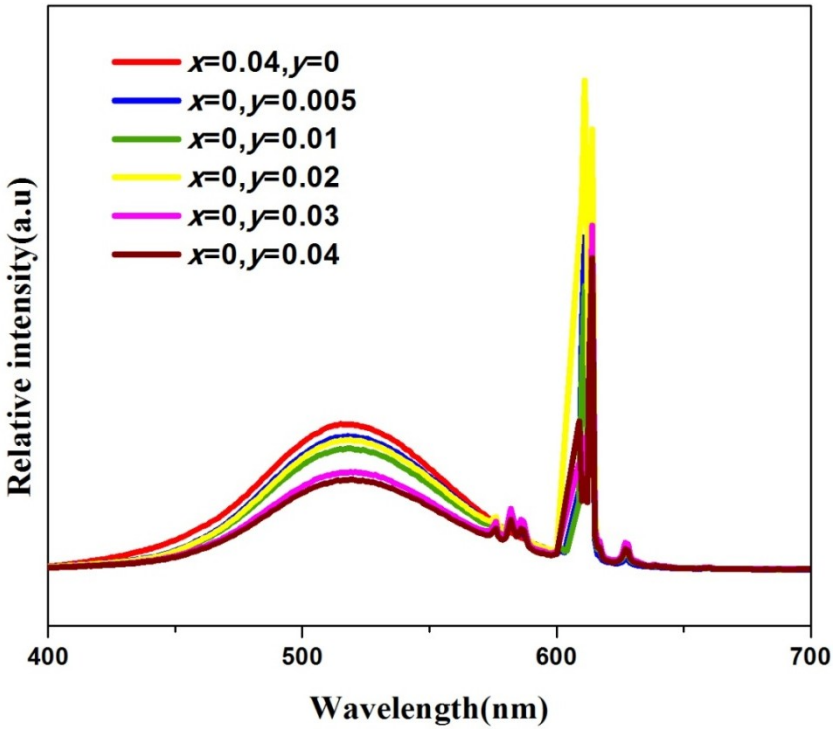

Fig.16. PL spectra of LSO: Bi^{3+}, Eu^{3+} samples under λ_{ex} = 303 nm

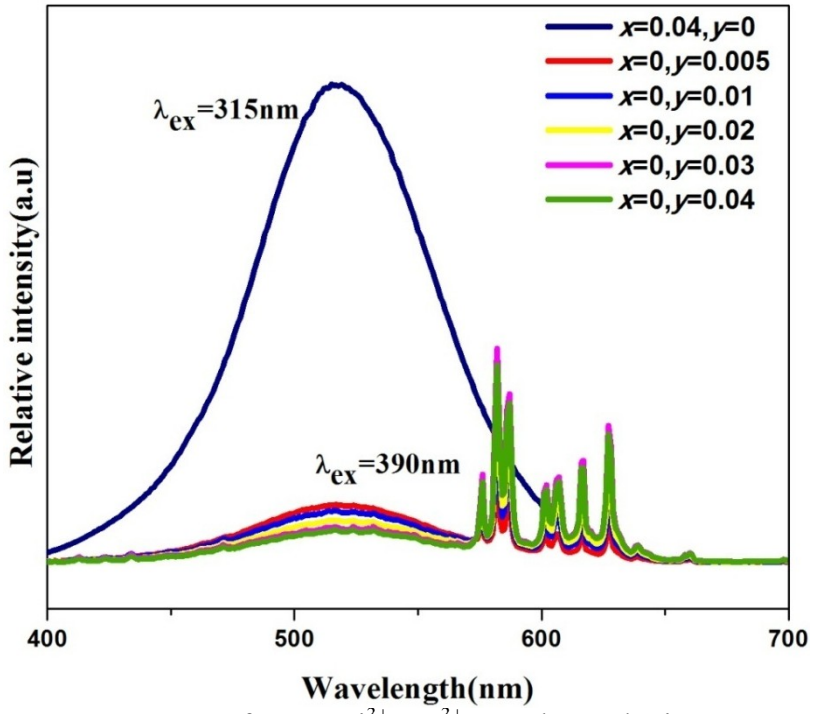

Fig.17. PL spectra of LSO: Bi^{3+}, Eu^{3+} samples under λ_{ex} = 390 nm

found to decrease further due to concentration quenching. This reduction in intensity of Bismuth emissions which is followed by increase in Europium emission is a clear indication of efficient energy transfer taking place between Bi^{3+} and Eu^{3+} ions. The energy transfer mechanism between Bi^{3+} ions and Eu^{3+} ions is depicted in Figure 18.

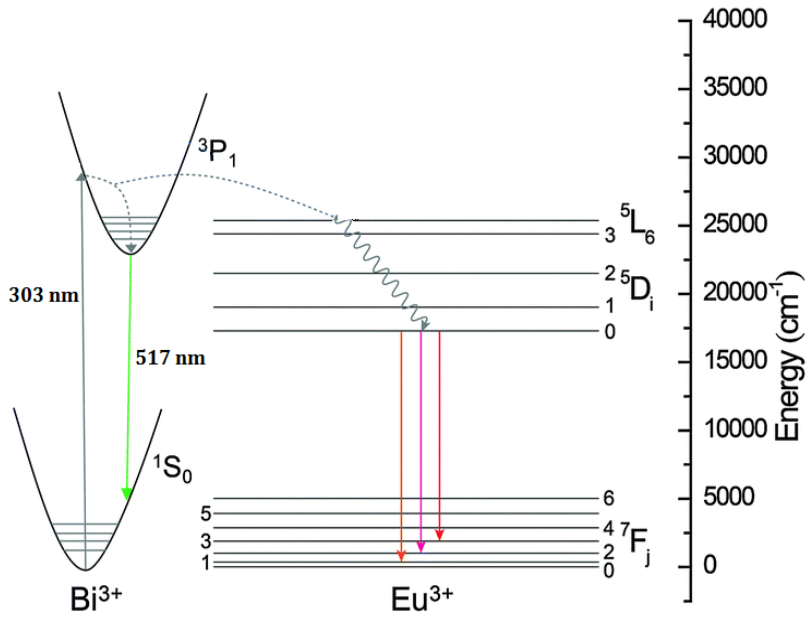

Fig.18. Energy transfer mechanism in LSO: xBi^{3+}, yEu^{3+} samples

Also it is observed that for Europium excitation at 390 nm the Bismuth emission is reducing with increasing Eu^{3+} concentration and Europium emission increases up to y = 0.03, and is In the case of both emission spectra, ie; emission spectra corresponding to excitation wavelength of 303 nm and 390 nm it is seen that the intensity of emission peaks of Eu^{3+} ions are stronger than Bi^{3+} emission. This can be attributed to the fact that as the Eu^{3+} content increases more energy of Bi^{3+} is transferred to Eu^{3+}, and hence Eu^{3+} emit more than Bi^{3+} (Z.Jiang et al. 2017). Resonant type energy mechanism depends on the distance between the activator and the sensitizer. The critical distance for energy transfer from sensitizer to activator was calculated using equation suggested by Blasse(G.Blasse et al.1968, G.Blasse et al.1994)

$$R_c = 2[\frac{3V}{4\pi X_c N}]^{\frac{1}{3}} \qquad \ldots\ldots\ldots\ldots\ldots (1)$$

where R_c is the critical distance, V is the volume of unit cell, X_c is total concentration, N is number of available sites for the dopants in unit cell. For LSO, N = 3 and V = 659.5 Å^3.The critical distance is estimated to be 8.87 Å when X_c is 0.07. For energy transfer from sensitizer to activator by exchange interaction, the critical distance should be less than 5 Å (G.Blasse. 1994). Since our calculated value is greater than 5-8 Å we can neglect the possibility of energy transfer by exchange interaction, and it is assumed to be due to electric multi-polar interactions (Sk. Khaja Hussain et al. 2017). Which can be specified as dipole - dipole, dipole - quadrupole,

quadrupole - quadrupole by studying the relation between energy transfer efficiency and concentration of dopants.

The energy transfer efficiency can be calculated by the formula (P.Chen et al.2016),

$$\eta_T = 1 - \frac{I_s}{I_{so}} \ldots\ldots\ldots\ldots\ldots\ldots \quad (2)$$

Where I_s and I_{so} are the luminescence intensities of the sensitizer in the presence and absence of activator, respectively. It is shown in Figure 19.

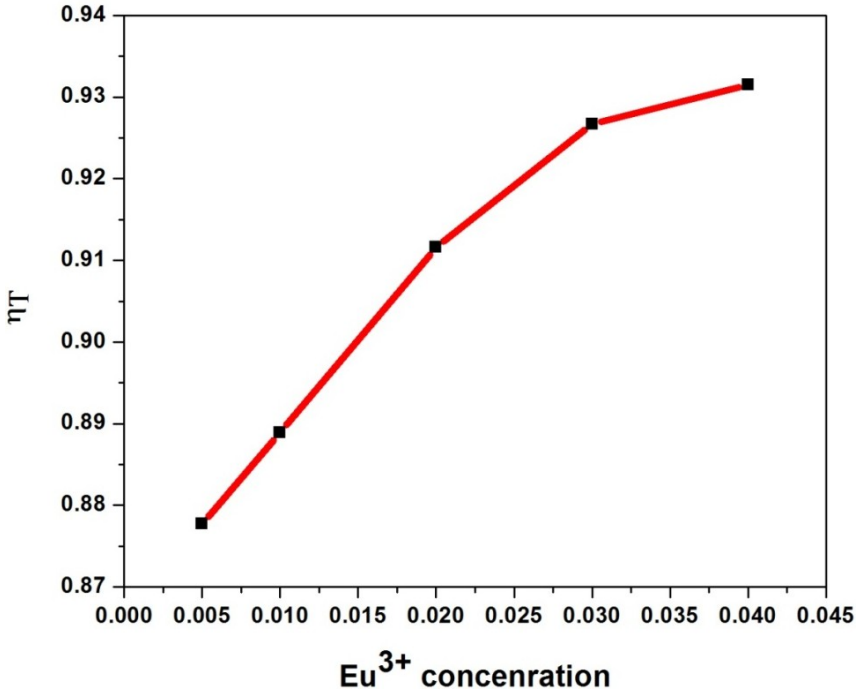

Fig.19. Dependence of η_T on Eu^{3+} concentration

As the figure indicates there is a increasing trend in energy transfer efficiency we can confirm the efficient energy transfer between Bi^{3+} and Eu^{3+} ions. Now by using Dexter's energy transfer formula for exchange and multipolar interactions and Reisfeld's approximation we can say $\ln(\eta_o/\eta) \propto C$ for exchange interaction, and $\eta_o/\eta \propto C^{n/3}$ with n = 6, 8, 10 are related to dipole-dipole, dipole-quadrupole and quadrupole-quadrupole interactions respectively. Where C is the

total concentration of Bi^{3+} and Eu^{3+} ions. The value of η_o/η is approximately calculated by the ratio of relative luminescence intensities, ie;(I_{so}/I_s). Thus the plots of $\ln(I_{so}/I_s) \propto C$ and $I_{so}/I_s \propto C^{n/3}$ are made and are shown in Figure 20. The fitted curves are also shown below (Figure 21). It is noticed that the curve fitting values are least in the case of n = 10. Hence we may neglect the chance for quadrupole-quadrupole energy transfer mechanism. The highest value is obtained for n =8, hence we expect dipole – quadrupole resonant energy transfer mechanism is taking place in our case.

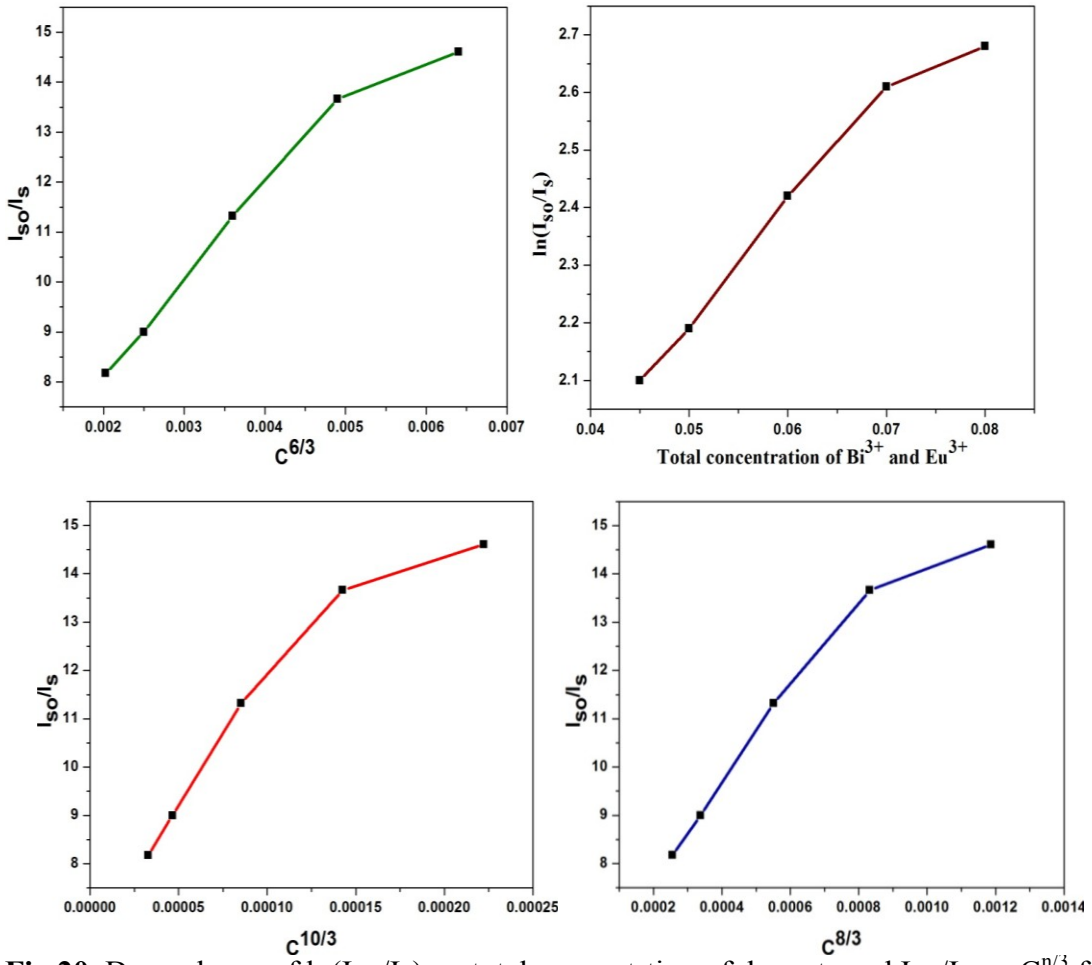

Fig.20. Dependence of ln(Iso/Is) on total concentrtion of dopants and Iso/Is on $C^{n/3}$ for n = 6, 8, 10

Luminescence decay measurements of the samples were conducted to understand more about the energy transfer process between Bi^{3+} and Eu^{3+} ions. While introducing Eu^{3+} ions into La site along with Bi^{3+} the decay curves shows exponential behavior. The decay curve of LSO: $x$$Bi^{3+}$, $y$$Eu^{3+}$ (x = 0.04, y = 0.005, 0.01, 0.02, 0.03, 0.04) phosphor with excitation at 303 nm and

emission at 616 nm is shown in Figure 22. These decay curves were fitted using function I = Aexp(-x/ τ) where I, τ and A are intensity, decay time and fitting parameter respectively.

The energy transfer efficiency can also be calculated using the lifetime values according to the relation

$$\eta_T = 1 - \frac{\tau_{so}}{\tau_s} \ldots\ldots\ldots\ldots\ldots\ldots \quad (3)$$

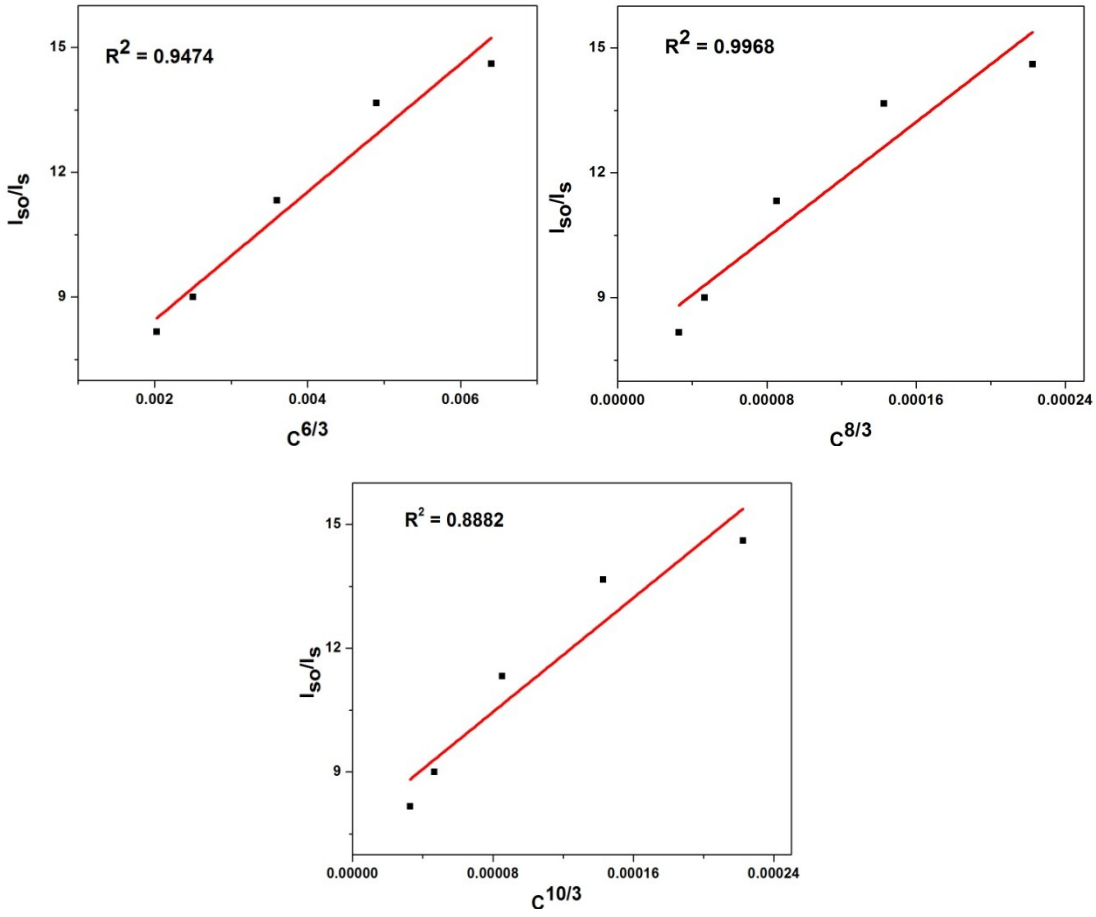

Fig.21. Fitted curves of dependence of Iso/Is on $C^{n/3}$ for n = 6, 8, 10

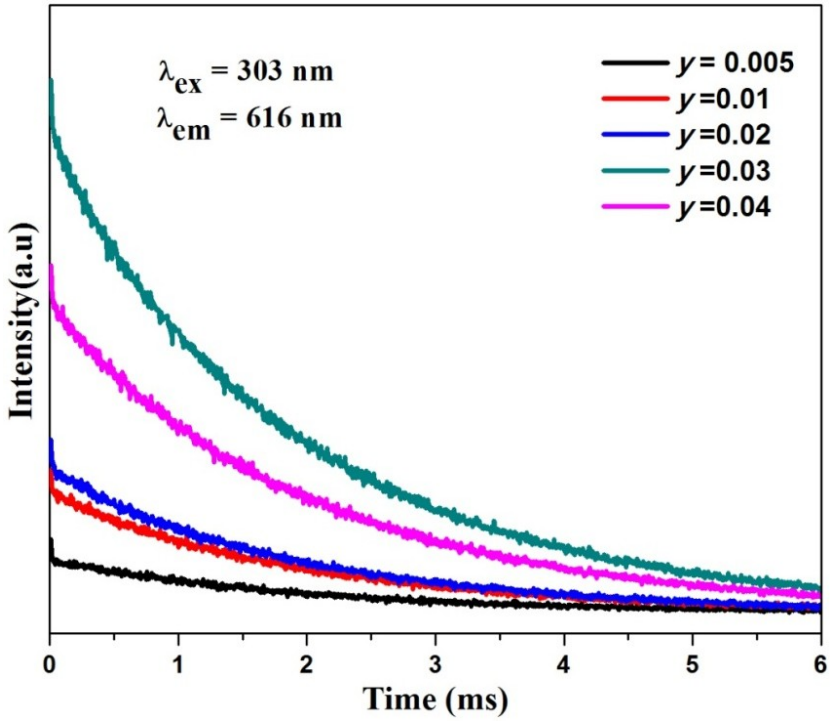

Fig.22. Decay curves of LSO: xBi^{3+}, yEu^{3+}(x = 0.04, y = 0.005, 0.01, 0.02, 0.03, 0.04) at λ_{ex} = 303 nm and λ_{em} = 616 nm

Thus by combining it with equation(2) and Dexter's energy transfer equation we can say $\tau_{so} / \tau_s \propto C^{n/3}$(Blasse et al.1968). In our case we can see a decreasing trend in lifetime values up to y = 0.02 and further it starts to increase with increase in Eu^{3+} content (Figure 16). Hence we can say energy transfer takes place efficiently up to the concentration y = 0.02, and then decreases further. A plot of lifetime values obtained for different Eu^{3+} concentration at an excitation 303 nm and emission 616 nm are shown in figure 23.

As our aim was to obtain direct white emission from single phase Eu^{3+} co-doped LSO: Bi^{3+} samples, and our emission spectra consist peaks covering the blue-green region of visible spectra as well as the red region, we have calculated the x and y values of Commission Internationale de I' ' Eclairage 1931 chromaticity coordinates for the samples under 303 nm excitation as well as 390 nm excitations, and it is shown in the Table 5.

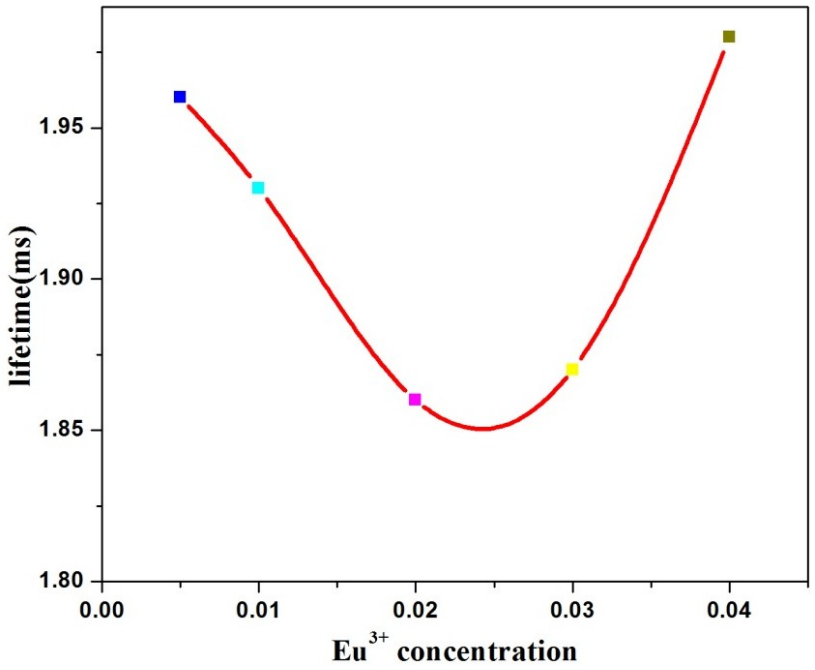

Fig. 23. Plot of lifetime values against Eu^{3+} concentration

Table 5. CIE color coordinates and lifetime values of La_3SbO_7: xBi^{3+}, yEu^{3+}(x = 0.04, y = 0.005, 0.01, 0.02, 0.03, 0.04).

y	τ (ms)	CIE Color Coordinates	
		λ_{303}	λ_{390}
0.005	1.96	(0.28,0.49)	(0.29,0.48)
0.01	1.93	(0.29,0.49)	(0.34,0.47)
0.02	1.86	(0.30,0.48)	(0.39,0.46)
0.03	1.87	(0.30,0.49)	(0.43,0.44)
0.04	1.98	(0.30,0.49)	(0.44,0.44)

The calculated values of chromaticity coordinates are almost approaching the CIE values of white light and hence we can say that by changing the Eu^{3+} concentration we can tune the emission color accordingly.

Conclusions

A series of Eu^{3+} co-doped La_3SbO_7:$x$$Bi^{3+}$ phosphors were synthesized and its structural as well as optical properties were studied in detail. Single Bi^{3+} doped samples gave broad excitation and emission spectra owing to the $^1S_0$ to $^3P_1$ and $^3P_1$ to $^1S_0$ transitions respectively. Maximum luminescence intensity of Bi^{3+} ions in La_3SbO_7:$x$$Bi^{3+}$ samples were found to be at $x = 0.04$. As the Eu^{3+} concentration was increased by keeping the Bi^{3+} at $x = 0.04$ we could obtain full color emission covering the whole visible spectrum, with broad emission peaks in the blue-green region with sharp narrow peaks in the red region. Hence it was inferred that by controlling the concentration of dopants we can ensure the energy transfer mechanism and thereby the color tuning property can be enhanced. As the synthesized phosphors have their excitation wavelength in the n-UV region and the emission spectrum covers the whole visible spectrum, it is proposed to be a potential single phase full color emitting phosphor for WLED applications.

Chapter 4

New full color emitting phosphor through energy transfer in Bi^{3+} and Eu^{3+} co - doped La_3TaO_7 weberite system

The chapter investigates the effect of partial substitution in photoluminescence properties of weberite system La_3TaO_7 and igate the energy transfer mechanism existing in the phosphor. The samples were crystallized into orthorhombic weberite type structure with Cmcm space group. Photoluminescence studies reveal that the Bi^{3+} and Eu^{3+} ions co-doped La_3TaO_7 phosphors show broad excitations in the n-UV region and displays broad bluish-green emission due to the $^1S_0$ to $^3P_1$ and $^1P_1$ transitions of Bi^{3+} and intense orange-red emission due to $^5D_0$ to $^7F_{0-2}$ transitions of Eu^{3+} leading to cover the whole visible spectral region. The lifetime measurements and the overlap of the spectral regions with the variation of Eu^{3+} concentration with Bi^{3+} suggests an effective energy transfer from Bi^{3+} to Eu^{3+}, allowing to fine tune the chromaticity coordinates close to the white point. Further, the energy transfer mechanism existing in this phosphor is established, and it is found to be due to the dipole - quadrupole interaction.

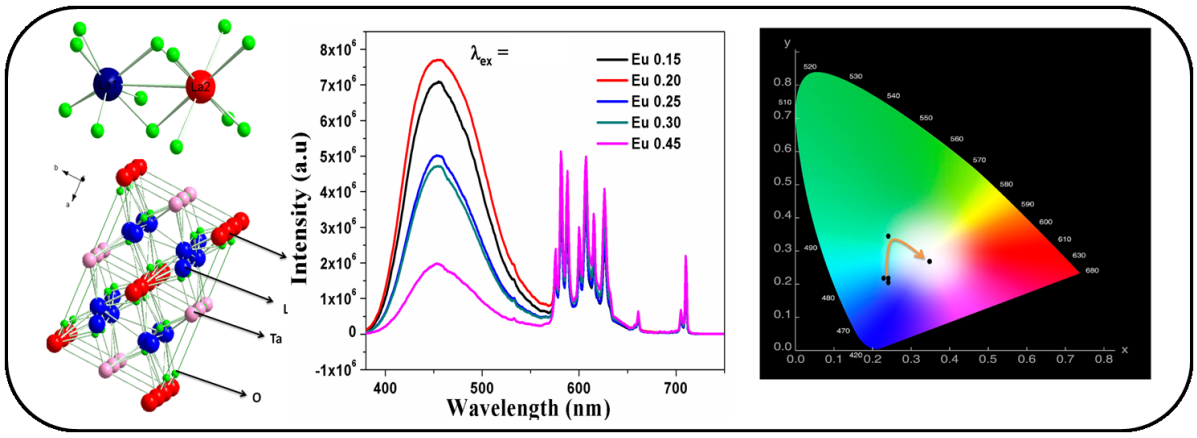

Introduction

Development of inorganic phosphors for lighting application gains worldwide attention as its applications vary from earlier trichromatic phosphors to the current color converters in white light emitting diodes. The efforts to bring up direct white emitting single phase phosphors have added more hope to the lighting industry as it can overcome the existing issues of low CRI and high CCT, re-absorption among phosphor particles etc., at a lower cost and less effort. Large size, short lifetime, low luminescent efficiency and high working temperature make the incandescent and halogen lamps inappropriate for many practical applications, even though they give continuous emission covering from visible to the infrared region (Q.Shao et al. 2018). In such a scenario, direct white emitting single phase phosphors will be a better substitute for currently using technologies for white light generation. As it is a single material which is to be clubbed with n-UV LEDs to generate white light, it should exhibit broad emission spectra covering the whole visible region.

The broad absorption and emission bands in ions like Bi^{3+} can be utilized for the development of single phase phosphors. Bi^{3+} emission centers spread the whole visible spectral region starting from the ultraviolet (UV) to the red spectral range (S.Zhang et al. 2014). The Bismuth emission behavior in the visible spectral region can be modified by altering its chemical surroundings and coordination in different crystal systems. The Bi^{3+} ion has a $6s^2$ a configuration with a ground state ($^1S_0$) and the excited states $^3P_{0,\,1,\,2}$ are raised by electronic transitions from the ground state to $6s^16p^1$ configuration. The process of absorption and emission occurs due to the transitions between these ground state and excited states of Bi^{3+} ions. These transitions from $^1S_0$ to $^3P_1$ and $^1P_1$ are mixed by spin-orbit coupling (L.Wang et al. 2012). The emission band of these phosphors can be designed in the wavelength region from 450 nm to 670 nm, depending on the strength of the crystal field and covalency of the host lattice. Also, the presence of dopants such as Bismuth makes the prepared phosphor material is much environmental friendly due to its low toxicity, even less toxic than table salt and non-carcinogenic (R.Mohan. 2010). And the intra - configurational f - f transitions in Eu^{3+} ions make it a potential candidate for red emitting phosphors. By combining the emission properties of Bi^{3+} and Eu^{3+} ions, it is expected to develop novel white light emitting phosphor for n-UVLED applications via energy transfer

mechanism. The unique nature of luminescent materials based on lanthanide ions, owing to its comparatively small stokes shift and hence higher quenching - temperature, makes it a perfect candidate for LED applications (T.Justel et al. 1998).

Currently many reports on the development of single phase phosphors are drawing our attention, like fabrication of white light emitting LEDs by combining UV LED chip (380 nm) $Ba_2Y(BO_3)_2Cl:Bi^{3+}$, Eu^{3+} phosphors by Huang et al(2017*).* and $Sr_3LuNa(PO_4)_3F$: Eu^{2+}, Mn^{2+} white emitting phosphors by Mengmeng et al(2018) are examples. Among the reported studies on single phase phosphors, the development of phosphor by utilizing energy transfer mechanism is getting more wide recognition. The energy transfer process between activators may be radiative or non- radiative. Further, the non-radiative energy transfer process can be achieved by non-resonance energy transfer, resonance-energy transfer, or by spin-coupling energy exchange (R.C.Ropp et al. 2004). Resonance energy transfer takes place between an activator and a sensitizer at the same radiative frequency, and the mechanism for the same may arise from the exchange interaction or electric multipolar interaction. The electric dipole - dipole interactions and dipole-quadrupole interactions can cause energy transfer in solids and both these interactions can occur for specific metal ion – metal ion distances that are seen in solids. The electric quadrupole interactions cannot play much key role in solids due to the short interaction range. There are reports on electric multipolar interactions existing between Bi^{3+} and Eu^{3+} ions. Recently Wei Xie et a.l(2018*)* have reported a color tuning Phosphor in La_2MgGeO_6: Eu^{3+}, Bi^{3+} through energy transfer with enhanced Eu^{3+} luminescence via the controllable energy transfer. By using Van Uitert's multipolar energy transfer mechanism, they have proposed a dipole – quadrupole energy transfer mechanism existing in this phosphor (W.Xie et al. 2018). From a detailed investigation on the existing phosphor materials published so far, we may infer that still there is a tug of war between the CRI values and CCT values of each phosphor. Our aim is to produce a better combination of these values so as to meet the energy demands as well as the practical applicability. In the current study, the effect of partial substitution and the energy transfer mechanism existing in Bi^{3+}/ Eu^{3+} co-doped La_3TaO_7 phosphors, which was prepared by using a conventional solid state method was studied. Usually, rare earths are acid-soluble, whereas Tantalum is base soluble. Thus it renders wet chemical methods more cumbersome. Hence solid state reaction method is

adapted for the preparation of tantalates (K.P.F.Siqueira et al. 2014). We have studied structural, morphological and photoluminescence properties of partially subsbstituted samples $La_3Sb_{1-x}Ta_xO_7$ and La_3TaO_7 for different mole fractions of Eu^{3+} with fixed Bi^{3+} content. In photoluminescence studies, the emission spectra for different excitation wavelength was recorded and it was found to be showing better results corresponding to an excitation wavelength of 320 nm. At this excitation wavelength, the obtained emission spectrum is broad in nature and it is peaked around 517 nm and characteristics peaks of Eu^{3+} around 616 nm due to $^5D_0$ to $^7F_2$ transitions. Luminescence lifetime measurements evidence the effective energy transfer from Bi^{3+} to Eu^{3+}. The calculated values of CIE color coordinates of the samples fall around (0.33, 0.33), close to the standard CIE coordinates of white light.

The prepared phosphor material is a potential candidate for WLED applications due to its better optical properties and very low temperature conducting nature of La_3TaO_7 structure due to its relatively complex crystal lattice (Z.H. Ming et al. 2017).

2. Experimental section

The compositions of the general formula, La_3TaO_7: $x$$Bi^{3+}$, $y$$Eu^{3+}$ were prepared by a conventional high temperature ceramic method. The starting materials (La_2O_3, Ta_2O_5, Bi_2O_3, Eu_2O_3) were weighed according to the stoichiometry and then mixed the products in an agate mortar in wet media. The mixed samples were dried in an air oven at 100 °C. The above process was repeated thrice for obtaining homogeneity. After intermittent mixing and drying, the samples were made homogeneous mixture, and which was calcined twice at 1400 °C/ 6 h by keeping it at an intermediate temperature of 900 °C for 30 minutes. The structural studies were carried out by powder X-Ray diffractometer (X' Pert Pro PANalytical) operating at 40 kV/30 mA, making use of Cu Kα radiation of a wavelength of 1.54056 Å and powder patterns were recorded in the 2θ scan range from 10°-90°. Morphological homogeneity of the powder samples was confirmed using a scanning electron microscope (JEOL, JSM-5600LV) operated at 15 kV. Absorbance spectra of the phosphor powders were analyzed using a Shimadzu, UV-2450 UV–Vis spectrophotometer in the wavelength range 200 - 800 nm using Barium Sulfate as a

reference. Photoluminescence studies were carried out on a Fluorolog HORIBA fluorescence spectrophotometer with a Xe lamp (450 W) as the excitation source. Luminescence decay curves of the phosphors were measured by the phosphorimeter attached to the Fluorolog_3 spectrofluorimeter.

4. Results and discussion

4.1. Effect of partial substitution

In the previous chapter photoluminescence properties of La_3SbO_7:Bi^{3+}, Eu^{3+} phosphor was reported. As an effort to modify the CIE values obtained for this phosphor modification in the B site of the weberite type system La_3SbO_7 was planned. Tantalum was substituted in the B site along with Antimony. Structural and optical properties of the partially substituted samples were studied and the results were compared with the end results ie., La_3SbO_7 and La_3TaO_7. The final results of these studies are recorded below.

4.1.1. XRD analysis

The XRD patterns of $La_3Sb_xTa_{1-x}O_7$: Bi^{3+}, Eu^{3+} samples are depicted figure 1. La_3SbO_7: Bi^{3+}, Eu^{3+} and La_3TaO_7: Bi^{3+}, Eu^{3+} crystallizes into orthorhombic crystal structure and their peaks are well matched with ICDD file No. 01-073-8085. But in the partially substituted samples $La_3Sb_{1-x}Ta_xO_7$: Bi^{3+}, Eu^{3+} some additional peaks are observed around $2\theta = 40°$. Presence of additional peaks indicates the structural change induced due to partial substitution.

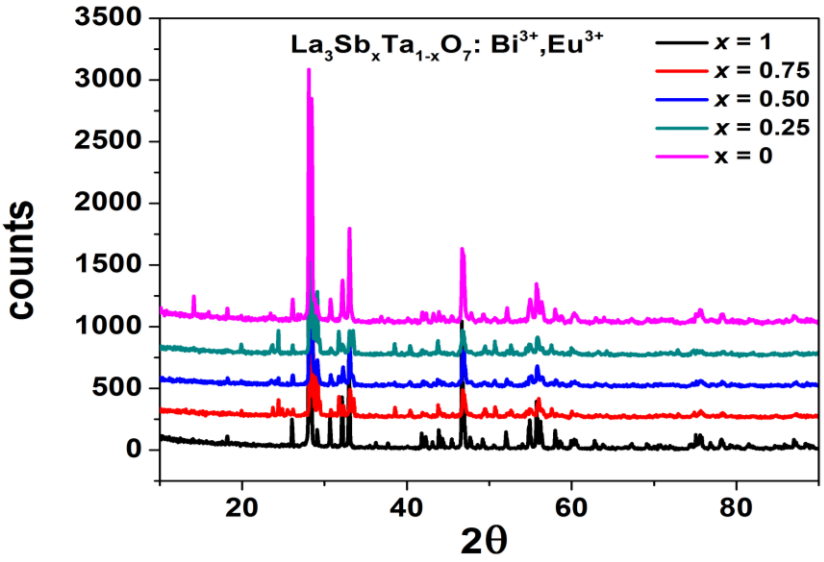

Fig.1 The powder XRD patterns of $La_3Sb_xTa_{1-x}O_7$: Bi^{3+}, Eu^{3+} samples

4.3.1.2. Photoluminescence studies

The ionic radii of Bi^{3+} and Eu^{3+} are well matched with that of La^{3+}. Thus both of them will occupy La site than Sb / Ta site. Also Sb is more electro negative than Ta. Thus there will be more electron cloud pulling towards Sb. Hence lower energy or higher wavelength emissions occur for Antimony and higher energy lower wavelength emissions occurs for Tantalum. By partial substitution the aim was to tune the emission whole visible region of electromagnetic spectrum. PLE spectra of LSTO: Bi^{3+}, Eu^{3+} samples at 582 nm(Europium emission) emission wavelength is shown in figure 2. It is seen that the spectra is broad in nature in the near UV region with characteristic sharp peak of Europium at 390 nm. I is noticed that for partially substituted samples the broad part of the spectrum have two peaks around 254 nm and 320 nm. As the Antimony content reduces there is variation in intensity of the peaks and more intense peak was obtained for La_3TaO_7:Bi^{3+}, Eu^{3+}. The PLE spectrum was also recorded for 456 nm and 517 nm corresponding to Tantalum alone and Antimony alone samples respectively. Though the spectrum shows broad nature for both the wavelengths the intensity of partially substituted samples is better under 456 nm emission wavelength. The emission spectra was also recorded for two wavelength regions 315 nm and 332 nm corresponding to Antimony alone and Tantalum alone based samples. It is seen that for both these excitations the partially substituted samples

produce spectrum covering the whole visible region with a broad peak in the blue region and characteristic Europium peaks in the red region. But the spectral intensity is very poor in the green region and the overall spectral intensity is very less compared to unsubstituted samples. The lifetime decay measures show single exponential decay nature. The lifetime decay time recorded in table does not show any particular trend. The CIE values were calculated and recorded in the table. It shows that the values are scattered around ideal value for partially substituted samples. Comparing the overall results it was found that the unsubstituted $La_3TaO_7:Bi^{3+},Eu^{3+}$ samples have better results compared to partialay substituted samples. Hence the study was further proceeded with $La_3TaO_7:Bi^{3+},Eu^{3+}$ samples.

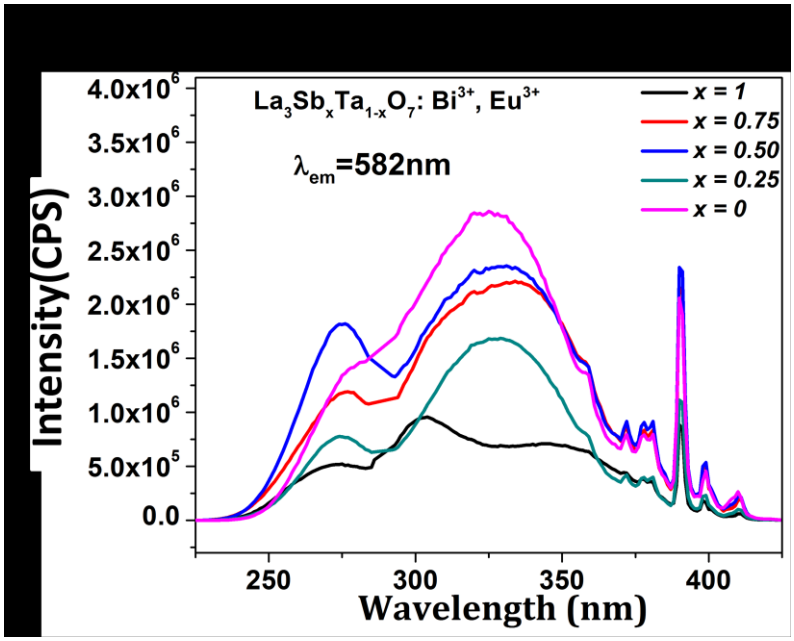

Fig.2 PLE spectra of LSTO: Bi^{3+}, Eu^{3+} samples at 582 nm emission wavelength

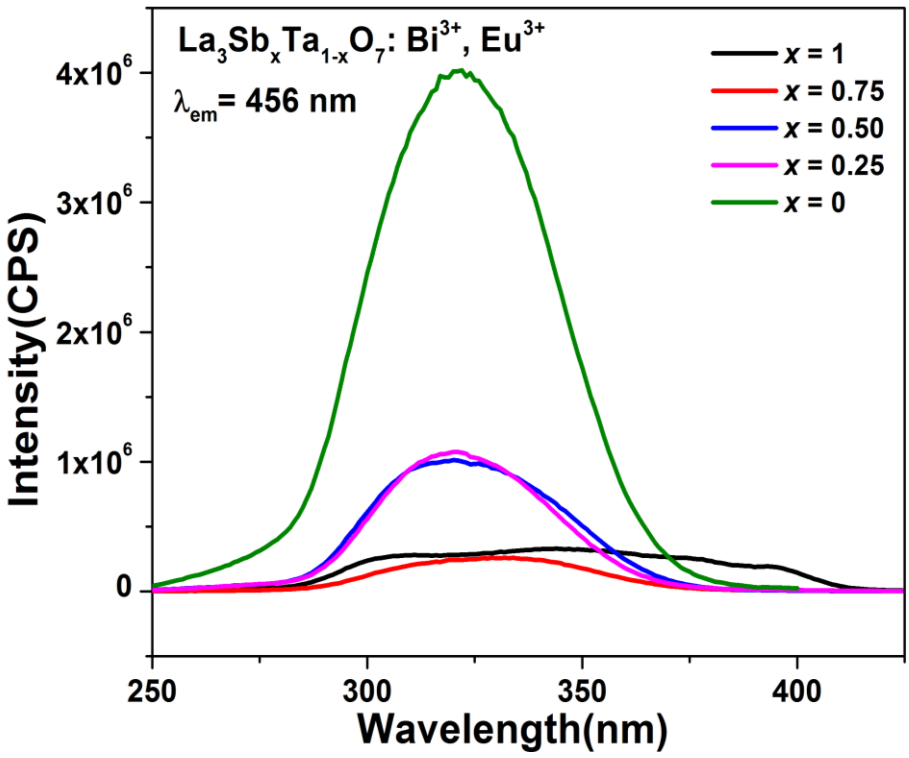

Fig.2 PLE spectra of LSTO: Bi^{3+}, Eu^{3+} samples at 582 nm emission wavelength

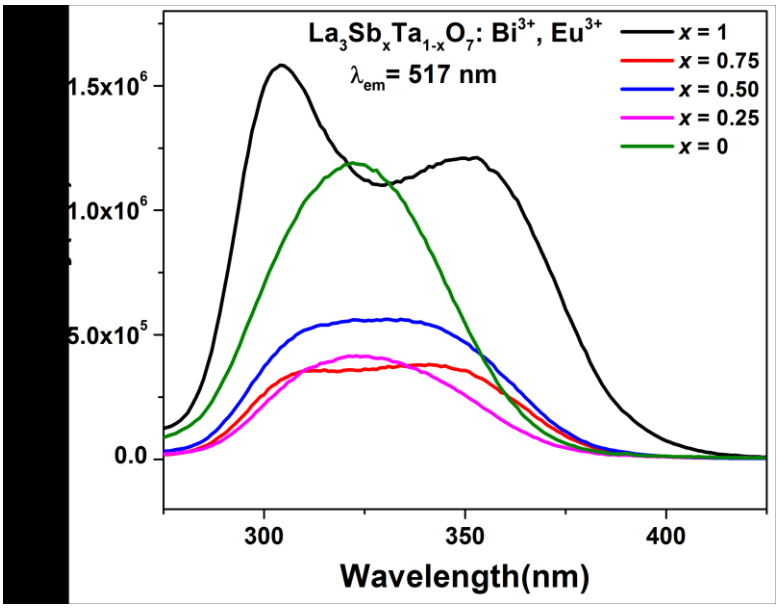

Fig.3 PLE spectra of LSTO: Bi^{3+}, Eu^{3+} samples at 517 nm emission wavelength

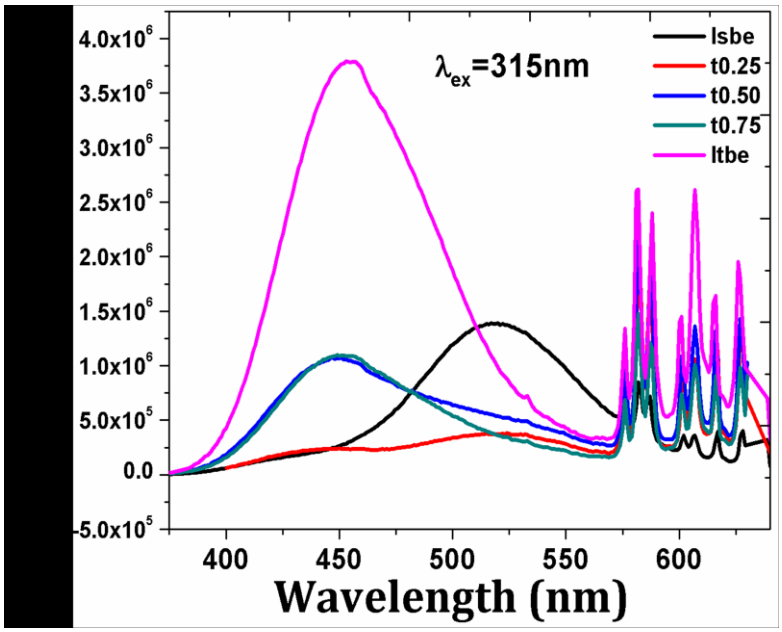

Fig.4 PL spectra of LSTO: Bi^{3+}, Eu^{3+} samples at 315 nm emission wavelength

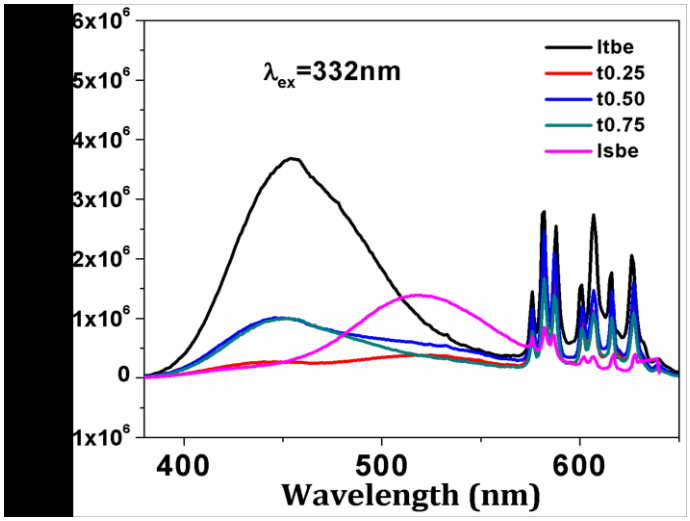

Fig.5 PL spectra of LSTO: Bi^{3+}, Eu^{3+} samples at 332 nm emission wavelength

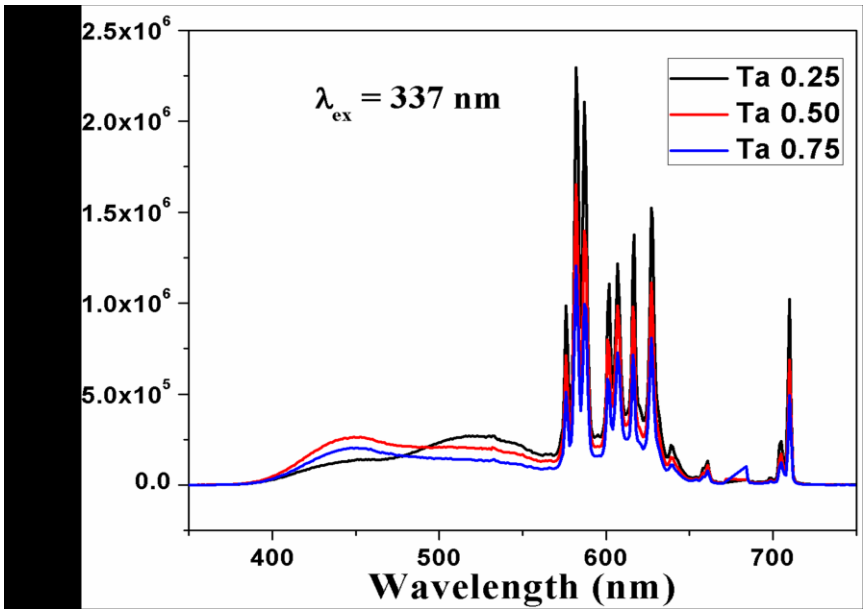

Fig.6 PL spectra of LSTO: Bi^{3+}, Eu^{3+} samples at 337 nm emission wavelength

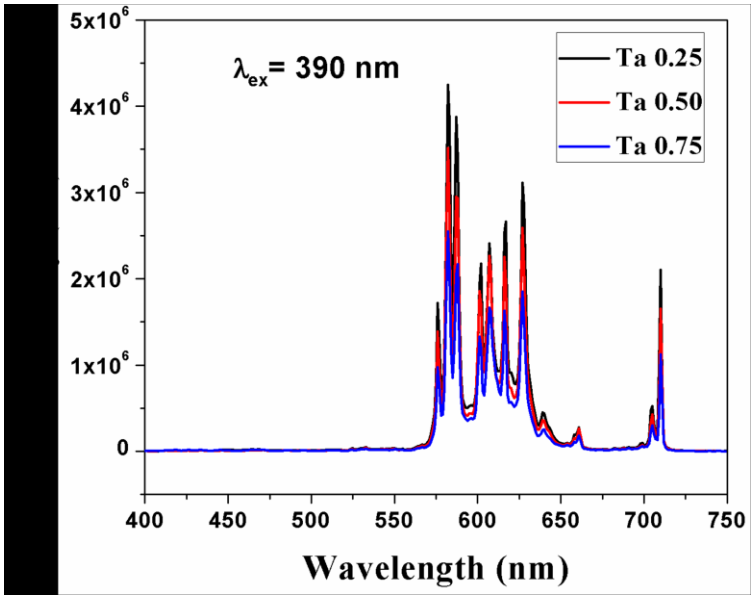

Fig.7 PL spectra of LSTO: Bi^{3+}, Eu^{3+} samples at 390 nm emission wavelength

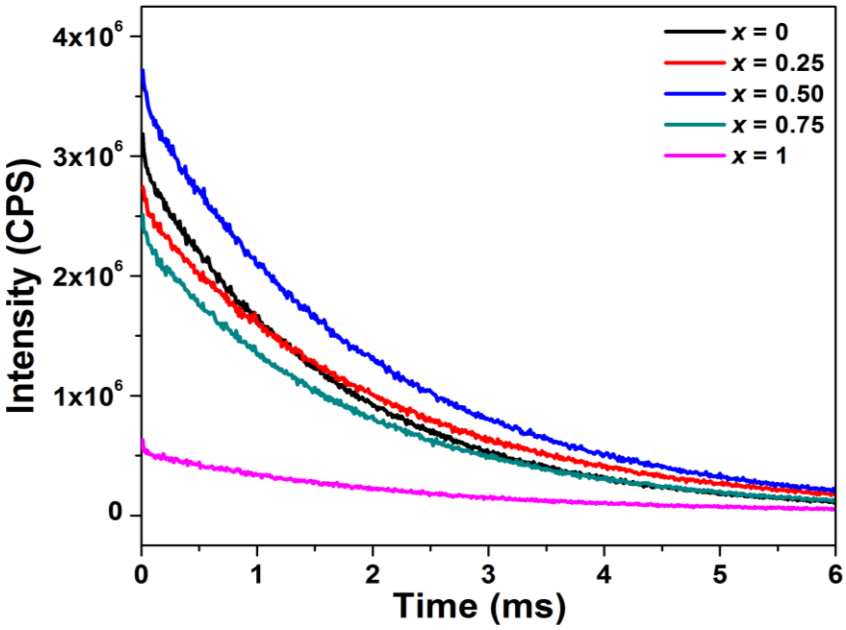

Fig.8 Lifetime decay curve of LSTO:Bi^{3+},Eu^{3+} samples

Table .1 Lifetime values of LSTO:Bi^{3+},Eu^{3+} samples

Composition x	***Lifetime (ms)***
LTBE	1.75±0.003
LT0.25S0.75BE	2.05±0.007
LT0.50S0.50BE	1.96±0.006
LT0.75S0.25BE	1.81±0.006
LSBE	1.87±0.007

Table.2 CIE values of LSTBE samples

Sample	CIE value
LTBE	(0.38,0.26)
LT0.25S0.75BE	(0.29,0.23)
LT0.50S0.50BE	(0.31,0.28)
LT0.75S0.25BE	(0.40,0.37)
LSBE	(0.30,0.49)

4.3.2. Eu^{3+} co-doped $La_3TaO_7:Bi^{3+}$

4.3.2.1 XRD analysis and crystal structure

A detailed structural study about La_3TaO_7 (LTO) was reported by Nicolas Preux et al (2010). in 2010. According to them, La_3TaO_7 is made up of chains of Ta-O octahedral linked by one oxygen atom in between chains of La-O and isolated lanthanum atoms. Three unique oxygen sites are there in the structure, O (3) sites belong to La-O chains and O (2) and O (1) sites are connected to apical and equatorial sites of TaO_6 octahedron respectively. It is an oxygen deficient fluorite type structure with one oxygen vacancy per unit cell. Likewise three different cation sites are there in this structure, a distorted cubic La^{3+} site, a distorted pentagonal bi pyramidal La^{3+} site, and an octahedral Ta^{5+} site(Z.H. Ming et al. 2017). In this crystal structure, tantalum prefers a six-fold coordination, and oxide positions are rather far from ideal tetrahedral sites of the fluorite. From their studies, they could find two cavities in the crystal, but the distance to other oxygen sites from these cavities was reported to be less than 2 - 3 Å, which is too small to accommodate an additional oxygen ion. But the expansion of unit cell and the creation of defects such as oxygen vacancies is expected through a judicious choice of substitution at La / Ta sites. Fig. 9 depicts the pictorial representation of a unit cell of La_3TaO_7.

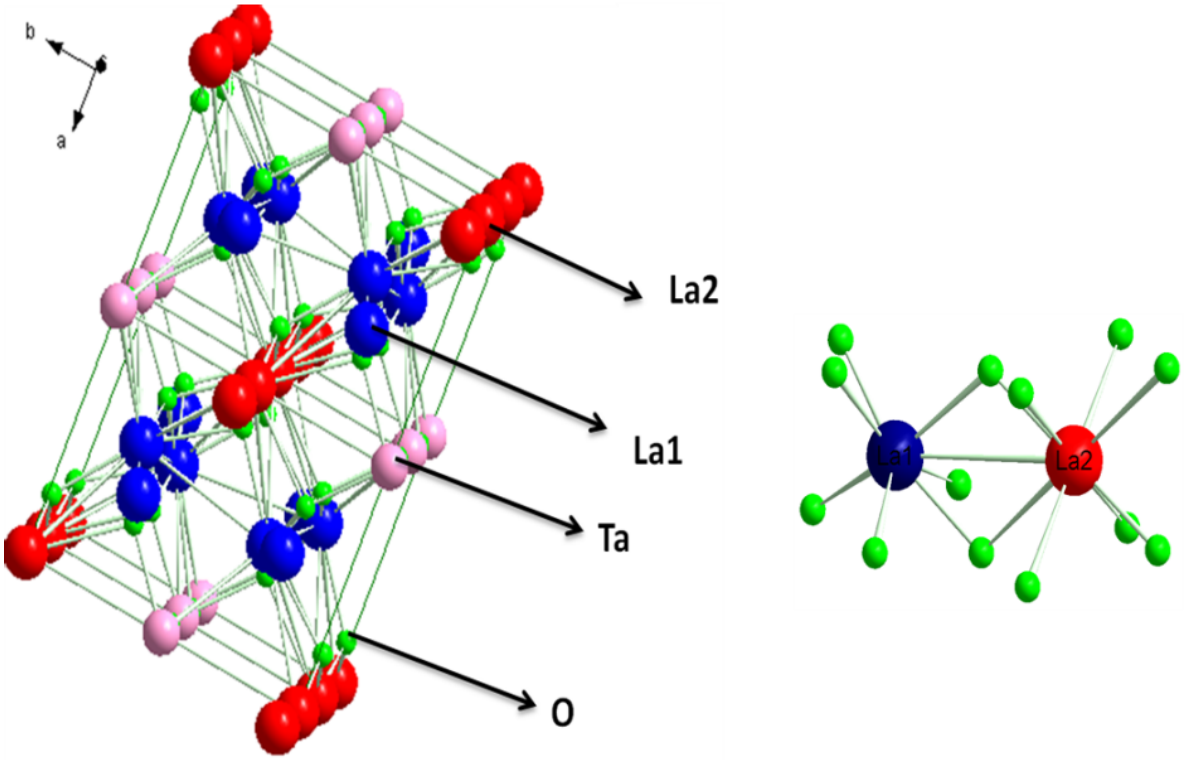

Fig. 9 Crystal structure of LTO

Powder X-ray diffraction measurements of the samples were carried out to check the crystalline phase purity of the prepared samples and their corresponding diffraction patterns are depicted in Fig. 10. All the diffracted peaks of the patterns coincide with the peaks of the standard data of La_3TaO_7 (JCPDS file No. 01-073-8085).

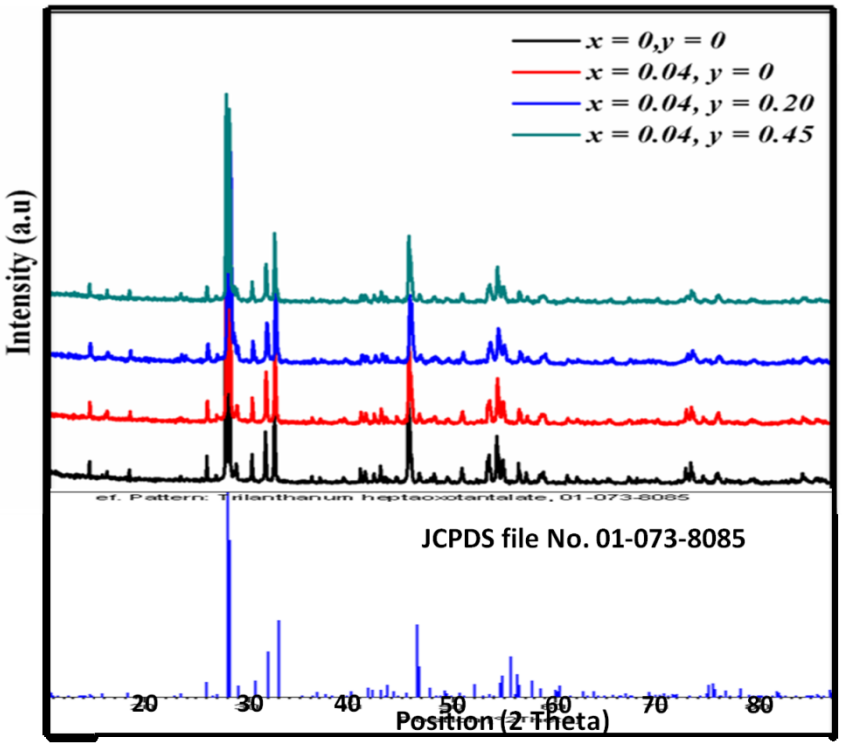

Fig. 10 Powder XRD patterns of LTO samples

It manifests the purity of the samples and it is confirmed that the dopants Bi^{3+} and Eu^{3+} are entered into the host lattice without changing the host structure. All the samples are crystallized into an orthorhombic structure with Cmcm space group. Considering the well matching ionic radii of Bi^{3+}, La^{3+} and Eu^{3+} ions (1.17 Å, 1.16 Å and 1.066 Å respectively), it can be confirmed that the dopants occupy La sites in the crystal. As the La^{3+} ions exhibit two coordinated sites, ie; VII and VIII, in the lattice, preferential occupation of dopants in these two sites are expected. Due to the more ionic nature and ionic size of Bi^{3+} ions, it is expected that Bi^{3+} ions will occupy La – VIII coordinated sites and Eu^{3+} ions will occupy La - VII coordinated sites (V.G.Suchithra et al. 2017). Further the Eu^{3+} luminescence which is discussed in the later part of the text also shows the behavior of VII coordinated occupancy. This type of preferential occupation has been reported in our earlier work of the similar system. All these results confirm the preferential occupation of Bi^{3+} and Eu^{3+} in the Lanthanum sites of respective coordination.

4.3.2.2 Morphological studies

Fig. 11 shows the typical scanning electron micrographs (SEM) of LTO: 0.04Bi^{3+}, *y*Eu^{3+} samples. The highly crystalline nature of the sample is evident from the SEM images. Particles have uniform particle size and they are almost spherical in nature. The average particle size is around 1µm. The particles are less agglomerated and uniformly distributed. EDS spectra and X-ray dot mapping images of a representative sample of LTO: 0.04Bi^{3+}, *y* Eu^{3+} samples are provided here (Fig. 12 and Fig. 13). They are confirming the uniform distribution of elements and the presence of all elements are confirmed. From these EDS studies, we can infer that both Eu^{3+} and Bi^{3+} ions are well present in the LTO matrix.

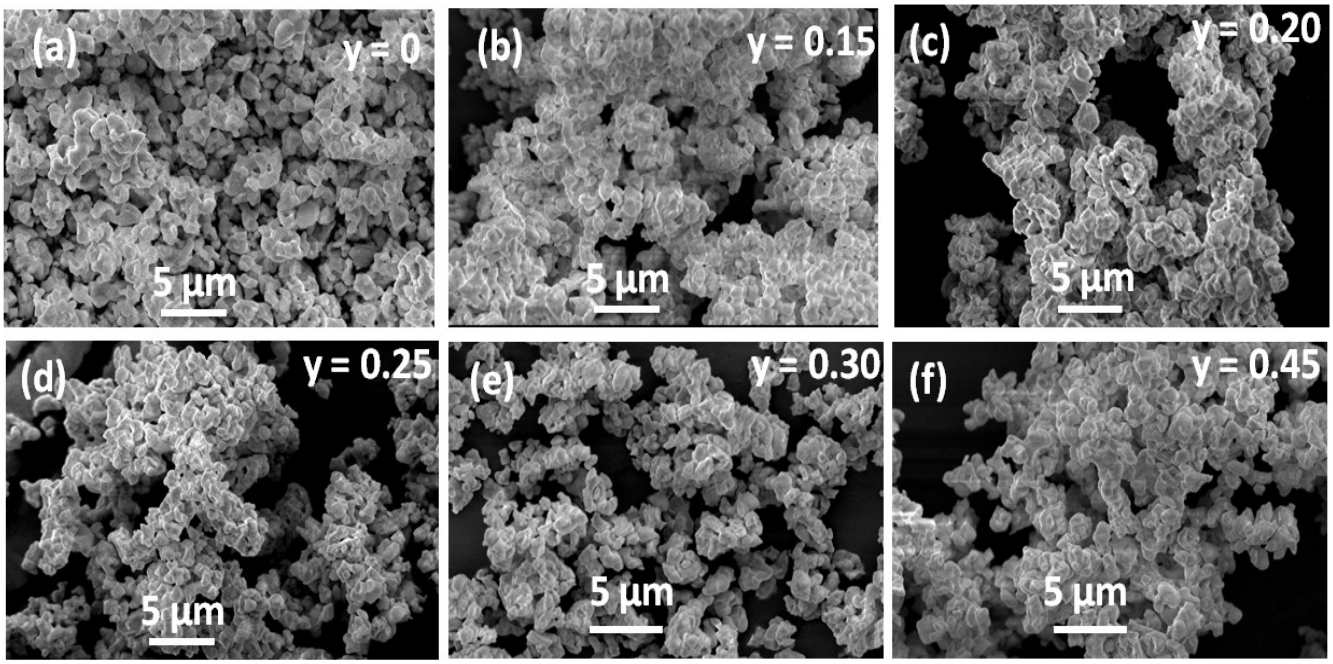

Fig. 11 SEM images of LTO: 0.04 Bi^{3+}, *y*Eu^{3+} samples

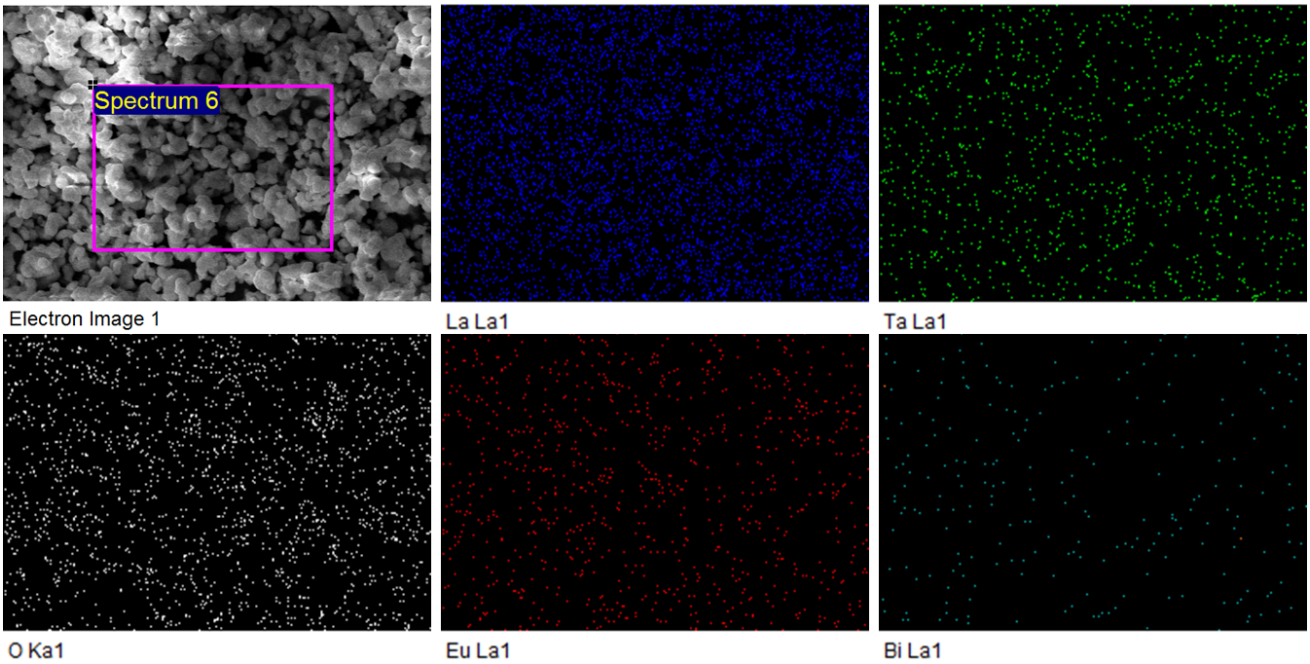

Fig. 12 X-ray dot mapping of LTO: 0.04 Bi^{3+}, 0.02 Eu^{3+}

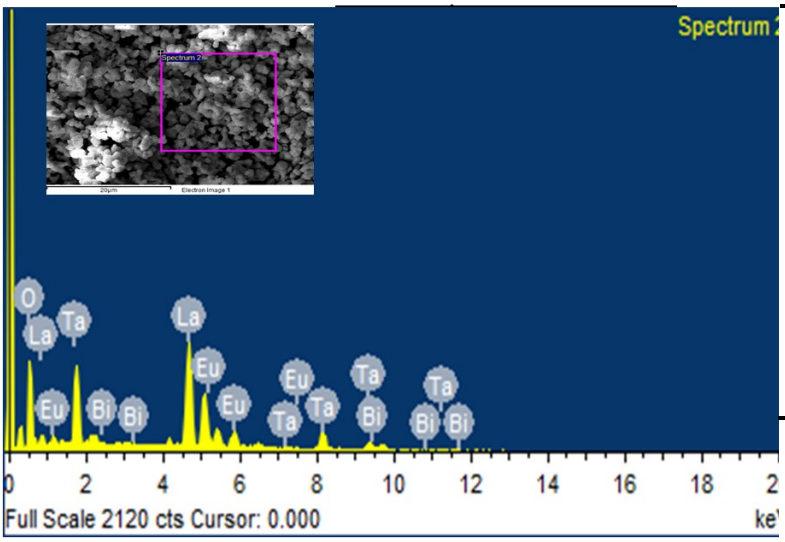

Element	Weight%	Atomic%
O K	18.38	67.93
La L	50.95	21.69
Eu L	6.49	2.53
Ta M	23.02	7.52
Bi M	1.17	0.33
Totals	100.00	

Fig. 13 EDAX image of LTO: 0.04 Bi^{3+}, 0.20 Eu^{3+}

4.3.2.3 Absorbance, Photoluminescence properties, energy transfer and chromaticity

The absorption spectra of Eu^{3+} co-doped LTO: Bi^{3+} samples are depicted in Fig. 14. Absorption occurs around 200 – 350 nm region with the maxima at 223 nm. For white LED application, it is desirable that the phosphor should have absorption around near UV region. Metal to ligand charge transfer in the matrix gives rise to these broad peaks in our samples. The bandgap values of the samples calculated by using the Shapiro's method are listed in table 3. The bandgap values exhibit a decreasing trend. A similar trend was observed in our earlier work, La_3SbO_7: Bi^{3+}, Eu^{3+} also. As there is a difference in the electronegativity values of the activator and sensitizer ions, i.e., Bi has a high electronegative value of 1.9, which very greater than that of Eu 1.31, the average electronegativity is reducing with increased Eu^{3+} content. It again confirms that Eu^{3+} ions are successfully doped into the system. As a result of this reduced electronegativity of the system, there will be an increase in the covalency and it affects the charge transfer mechanism among ligand ions.

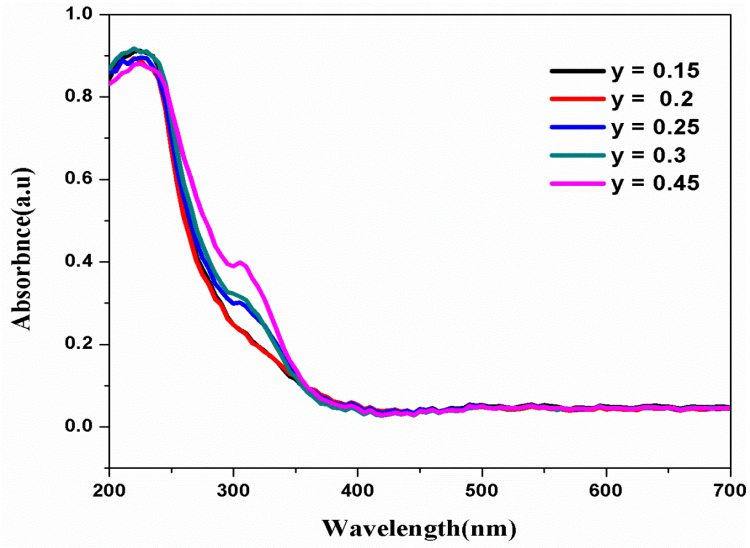

Fig. 14 Absorption spectra of LTO: $0.04Bi^{3+}$, yEu^{3+}

Table 3 Band gap values of LTO: $0.04Bi^{3+}$, yEu^{3+}

Concentration	***Band gap energy E_g (eV)***
$x = 0.04, y = 0.15$	4.03
$x = 0.04, y = 0.20$	3.74
$x = 0.04, y = 0.25$	3.45
$x = 0.04, y = 0.30$	3.30
$x = 0.04, y = 0.45$	3.14

A series of Bismuth alone doped samples were prepared. Their structural studies and optical studies were carried out for optimizing the Bismuth concentration. Bismuth concentration was varied from 0.04 to 0.075. Photoluminescence emission spectra of these samples are presented in Fig. 7. Luminescence studies show that the emission spectra is a double peaked broad spectra covering the visible rage from 350 nm to 600 nm and it is also noted that as the Bismuth content increases the two peaks in the emission spectra separates more. The overall emission intensity of emission spectra is decreasing with increased Bismuth content. Hence we optimized the Bismuth concentration at 0.04 and further Europium was co-doped with the samples.

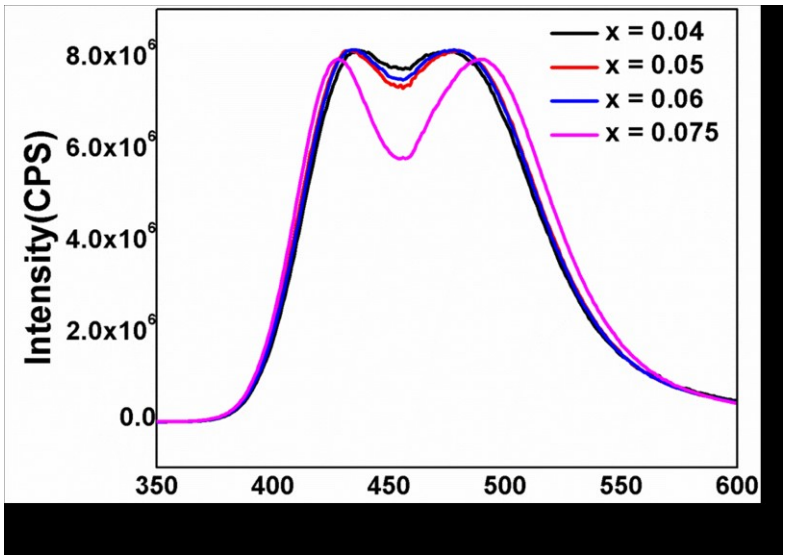

Fig. 15 Emission spectra of LTO: xBi^{3+}(x = 0.04, 0.05, 0.06, 0.075) samples

Fig. 16 displays excitation spectra of LTO host and LTO: 0.04Bi^{3+} sample for emission at 454 nm. The excitation spectra of Bismuth doped sample shows two excitation bands, with their peak intensities located at 302 nm and 340 nm, respectively. From the host excitation spectra it can be seen that the first excitation band around 302 nm corresponds to the host absorption of the tantalate group.

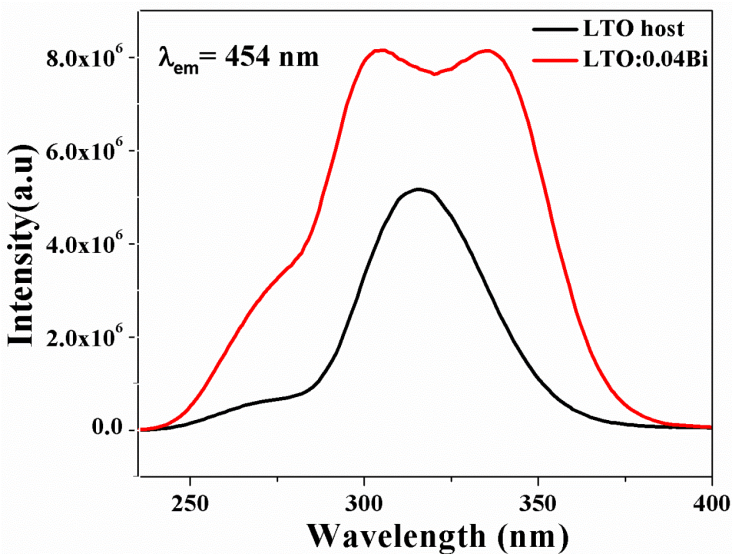

Fig. 16 Excitation spectra of LTO host and LTO: 0.04Bi^{3+} sample for an emission corresponding to 454 nm

The intensity of the two peaks is the same and a similar trend is maintained with different Bi^{3+} concentrations. Thus we can say that both the peaks are due to Bi^{3+} absorption. Since these peaks appear at 4.09 eV and 3.6 eV, i.e., with very small separation, both peaks may be aroused due to $^1S_0$ to $^3P_1$ transitions (Z.Yang et al. 2013). Similar results of the existence of two absorption bands for Bi^{3+} were reported in the case of Y_2O_3, YOCl and YBO_3 host lattices. Exciting the LTO: Bi^{3+} samples at 302 nm and 340 nm give broad emission spectra in blue-green region (Fig. 17) This broad nature of the emission band indicates that the activator ions strongly interact with the host lattice and the strong coupling of the electronic states with the vibrational mode of the lattice mainly leads to more or less broad bands in the spectrum (R.Mohan 2010). The inset of Fig. 16 depicts the host emission peak. From the figure it is clear that the host emission peak is sharper compared to Bismuth doped samples. The full width half maximum also increases with Bismuth doping. It is further noted that the emission intensity of Bismuth doped sample is much higher than the host emission, under the same excitation. It implies that the host sensitization is taking place in the system.

But as seen from Fig. 18 while increasing the excitation wavelength; there is a change in the emission levels of the activators (Bi^{3+}, Eu^{3+}). We have varied the excitation wavelength

from 300 nm to 350 nm. It is seen that the intensity of emission spectra remains almost the same up to the excitation wavelength of 340 nm and after that, it starts decreasing. Under the excitation of

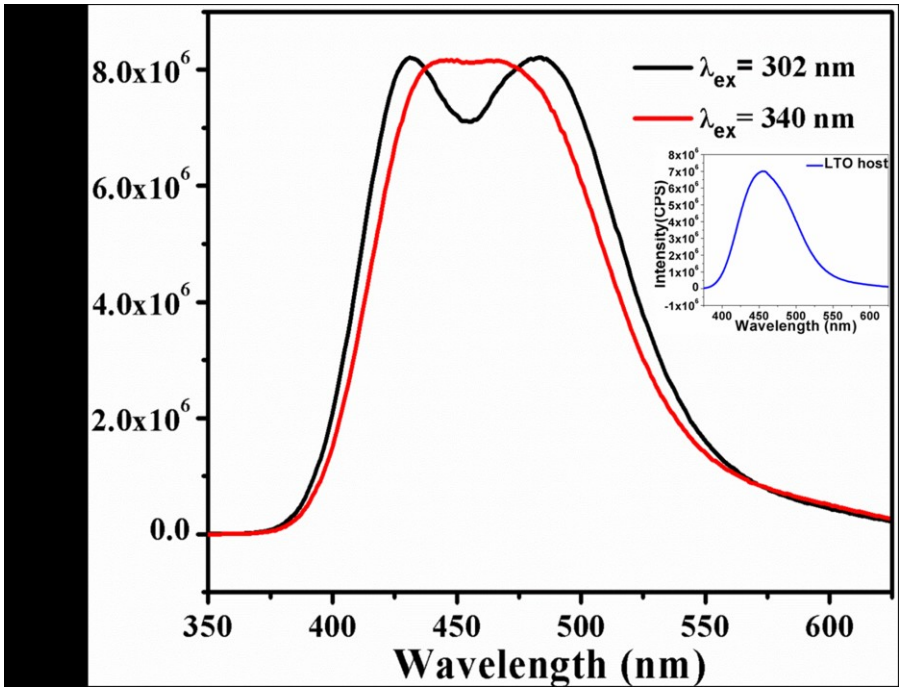

Fig. 17 Emission spectra of LTO: 0.04Bi^{3+} samples at different excitations, the inset shows host emission peak

302 nm, emission spectra have two emission peaks located at 434 nm and 477 nm due to the emissions of host and Bismuth respectively, and it becomes a broad single peak with reduced FWHM for only Bismuth excitations above 330 nm.

The emission spectra of Bi^{3+} doped LTO samples cover the region of visible spectra from 375 nm to 600 nm. As our objective is to develop a full color emission phosphor, we have co-doped Eu^{3+} ions into the system so that we will get emission peaks in the red region also along with Bi^{3+} emission peaks. The emission spectra of Eu^{3+} co-doped samples were observed for different excitation wavelengths of 270 nm, 336 nm, 394 nm and 407 nm. From Fig. 18, it is seen that emission spectra corresponding to Europium excitation are much weak compared to that of Bismuth excitations and we got better emission profile at an excitation of 336 nm. At this excitation, emission spectra consist of a broad peak covering the range 400 nm to 550 nm and it is followed by characteristic emission peaks

of Eu^{3+} ions. Also, it is interesting to note that the profile of Eu^{3+} peaks does not vary with different excitation wavelengths. According to our assumption of preferential site occupancy of Eu^{3+} ions occupy distorted VII coordinated La site

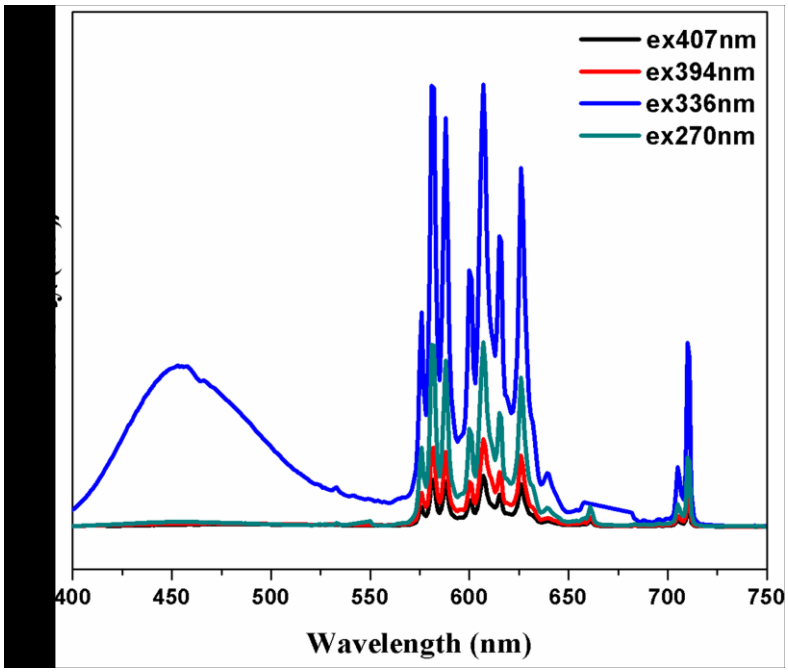

Fig. 18 PL and PLE spectra of LTO: Bi^{3+}, Eu^{3+}

and it results in many stark splitting in Eu^{3+} emission transitions $^5D_0$ to ^7F_J . Here we observed three peaks in magnetic dipole transitions and four peaks in electric dipole transitions. Previous reports on the same observation substantiate our results (Z.Yang et al. 2013, L.G.Jaconsohn et al. 2010, A.Wolfert et al. 1984, 1985, M.Janulevicius et al. 2016). As the Bi^{3+} ions have strong orbital coupling effect owing to its complex electronic structure, it interacts strongly with the corresponding coordination environment and this multiple splitting in Eu^{3+} peaks is a clear indication that Eu^{3+} is sensitized by Bi^{3+} ions. As indicated in Fig. 20 quenching of Bi^{3+} peaks is observed after y = 0.20 concentration of Eu^{3+} and a further reduction in the intensity of Bismuth peaks and enhancement of Europium peaks with increasing Eu^{3+} content up to the concentration of 0.45 indicates the efficient energy transfer between Eu^{3+} and Bi^{3+} centers. Europium peaks exhibit self

quenching after 0.45 and further increase in Europium concentration results in reduction in emission intensity of Europium peaks.

For energy transfer to take place, the sensitizer and activator ions have to show physical interaction. For this process, the emission profile of the sensitizer and absorption profile of activator should have a good overlap. The overlap between the excitation spectra of LTO: $Eu^{3+}$and the emission spectra of LTO: Bi^{3+} is depicted in Fig. 21. As indicated in the figure, the excitation peaks of LTO: Eu^{3+} consist of a broad excitation band in the range of 250 – 350 nm and the characteristic excitation peaks of Eu^{3+} ions in the range 350 – 500 nm. The broadband is due to the charger transfer from the Ta-O group to the Eu^{3+} ions and the sharp lines are associated with the intra-configurational $[Xe]4f^6 \rightarrow [Xe]4f^6$ transitions of Eu^{3+} ions. Excitation peak at 392 nm and 463 nm are attributed due to the $^7F_0 \rightarrow {}^5L_6$ and $^7F_0 \rightarrow {}^5D_2$ transitions, respectively. And these peaks show good overlap with the Bi^{3+} emission profile.

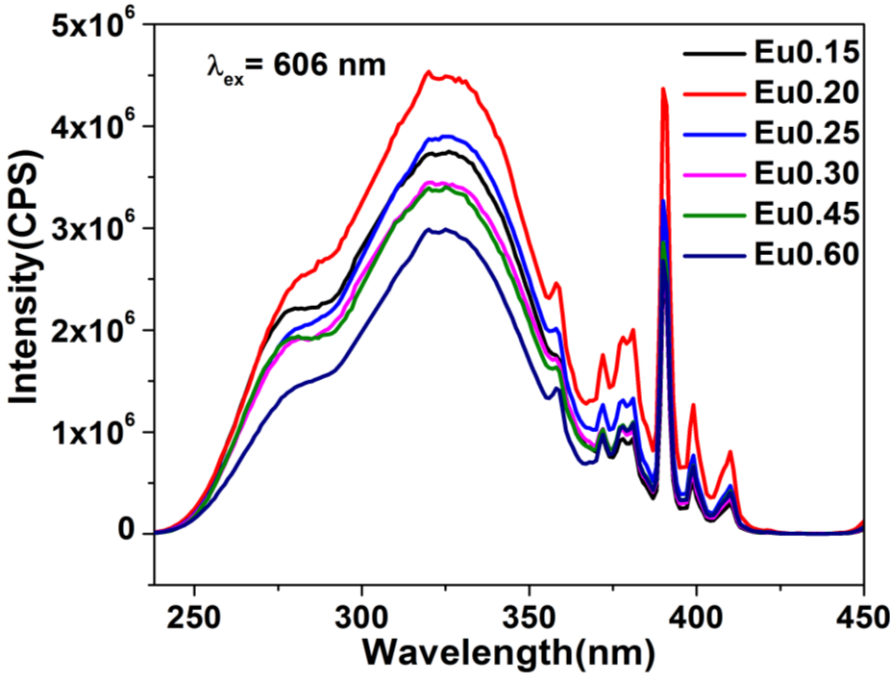

Fig. 19 PLE spectra of LTO: 0.04 Bi^{3+}, yEu^{3+}

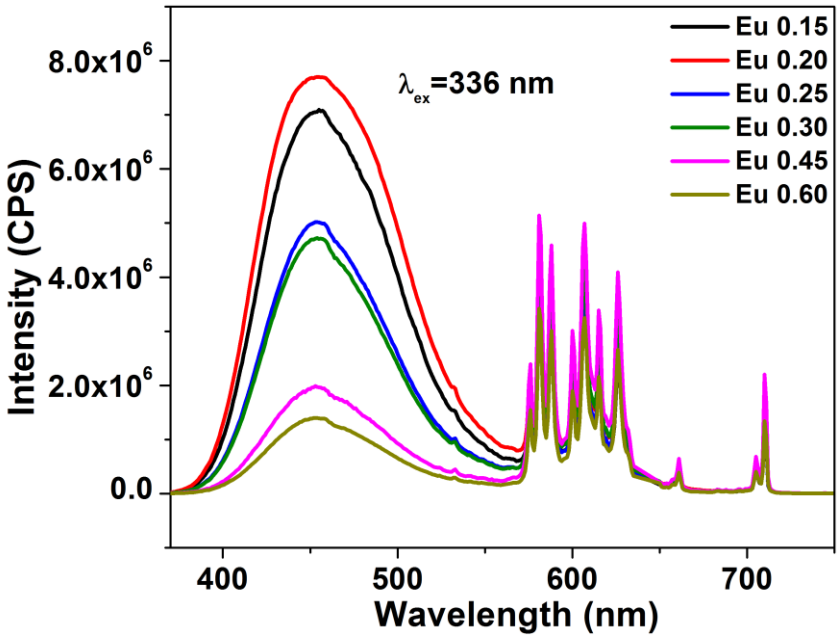

Fig. 20 PL spectra of LTO: 0.04 Bi^{3+}, *y*Eu^{3+}

This spectral overlap between the PL spectra of LTO: Bi^{3+} and the PLE spectrum of LTO: Eu^{3+} indicates that the LTO host may undergo an energy transfer between the sensitizer and the activator ions. The blue emissions of Bi^{3+} ions are reabsorbed by the Eu^{3+} ions and upon excitation of 394 nm, characteristic $^5D_0$ to ^7F_J (J = 0,1,2,3,4) transition emissions of Eu^{3+} ions occur. And it enhances the total emission at the same time. Whereas in reverse, there is no spectral overlap was observed between the emission spectrum of Eu^{3+} and excitation spectrum of Bi^{3+} ions. Thus we may say the inverse energy transfer process may not occur. Thus Eu^{3+} excitations will not give Bi^{3+} emission curves in Eu^{3+} co-doped LTO: Bi^{3+} system (R. C. Ropp. 2004).

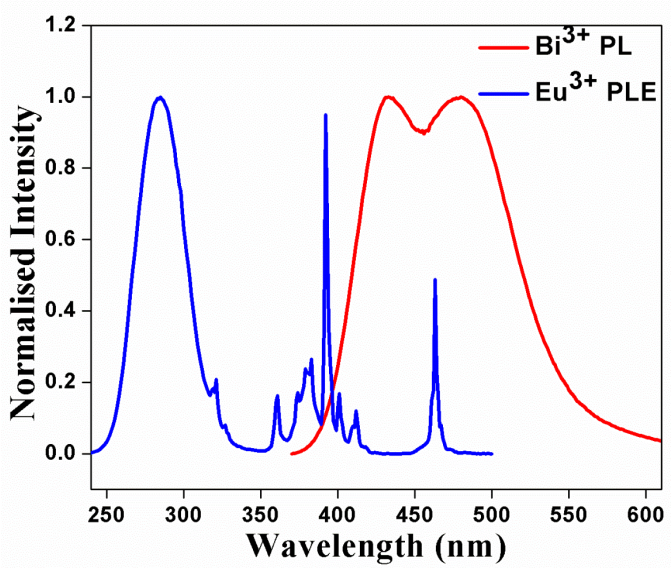

Fig. 21 Spectral overlap between PL spectra of LTO: $0.04Bi^{3+}$ and PLE of LTO: $y Eu^{3+}$

The existence of energy transfer between Bi^{3+} and Eu^{3+} can be confirmed from the lifetime measurement studies that sharp decreasing trend in the lifetime values for Bi^{3+} excitations (Table 4) is due to the increasing and decreasing radiative transitions arising from Eu^{3+} and Bi^{3+} centers respectively. A detailed investigation of the energy transfer mechanism existing in this phosphor was conducted. Energy transfer between sensitizer and activator can be written as

$$S^* + A \longrightarrow S + A^*$$

Where, the asterisks indicate excited state. The probability for energy transfer is given as

$W_{ET} = 2\pi / \hbar(\rho)[\phi_i |H| \phi_f]^2$

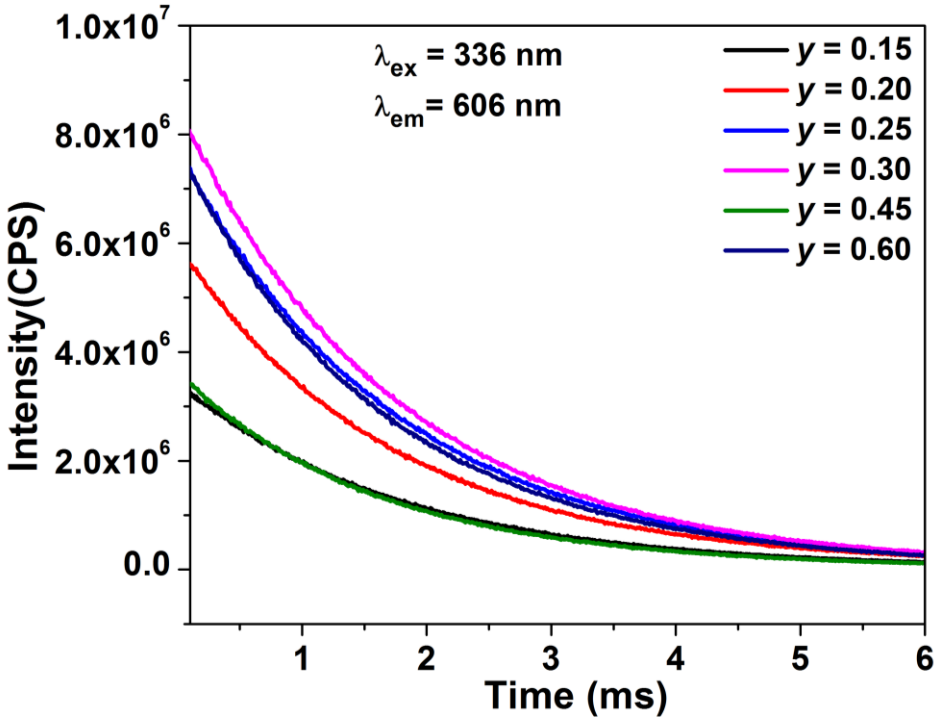

Fig. 22 Lifetime measurements of LTO: Bi^{3+}, Eu^{3+}

Table 4 lifetime values of LTO: Bi^{3+}, Eu^{3+}

Composition y	***Lifetime (ms)***
0.15	1.75 ± 0.003
0.20	1.71 ± 0.001
0.25	1.71 ± 0.002
0.30	1.71 ± 0.002
0.45	1.58 ± 0.003
0.60	1.52 ± 0.004

Where, ϕ_i = wave function of the initial state, ϕ_f = wave function of the final state, ρ = measure for density of initial and final states capable of interaction, H = operator coupling initial and final states.

The process of energy transfer occurs from a broadband emitting center to line absorber only when they are nearest neighbors and energy transfer in the case of a line emitter to broadband absorber occurs for distances up to 2 nm. Whereas, broadband emitter to broad band absorber energy transfer may happen for large distances of about 3.5 nm. There are mainly three mechanisms for energy transfer: radiation re-absorption, exchange interaction and electric multipolar interaction (K.Li et al. 2014). For radiation re-absorption, there should be a large overlap of excitation and emission spectra. And for exchange interaction, the critical distance should be of the order of 5 - 8 Å. Also, dipole-dipole interaction is common in smaller rare-earth ions and lower lying levels of larger rare-earth ions. Dipole- quadrupole interactions occur in higher lying levels of larger rare-earth ions. Whereas, quadrupole interactions occur only when involved states are highly perturbed (L.G.Van Uitert, 1967). The energy transfer process will dominate when $R_{SA} < R_0$ otherwise inherent decay of sensitizer ions is the most important process, where R_{SA} and R_0 are the distance between sensitizer and activator ions and distance at which transfer rate to the activator is equal to decay rate of sensitizer, respectively (S.He.2008).

Here we neglect the chance of radiation re-absorption and exchange interaction due to small overlap of excitation and emission spectra and comparatively large value of the critical distance between activator and sensitizer ion which is 19.5 Å > 5 - 8 Å, calculated using equation suggested by Blasse (G.Blasse. 1969, G.Blasse. 1994)

$$R_c = 2\left[\frac{3V}{4\pi X_c N}\right]^{\frac{1}{3}} \qquad \cdots\cdots\cdots\cdots\cdots\cdots (1)$$

Where X_c is the critical doping concentration of Bi^{3+} and Eu^{3+} ions; N is the total number of La sites per unit cell that can be occupied by Bi^{3+} and Eu^{3+} ions; V denotes the cell volume of the unit cell. Here X_c is 0.49, N is 2 and volume is 658.38 $Å^3$.

Further, the kind of multi-polar interaction scheme monitoring the energy transfer mechanism can be explored using Dexter's energy transfer formula (D.L.Dexter.1954, Z.Jiang et al. 2017) and Reisfield's approximation. According to them

$$\ln(\eta_o/\eta) \propto C \quad \cdots\cdots\cdots\cdots\cdots\cdots (2)$$

for exchange interaction and

$$\eta_o/\eta \propto C^{n/3} \text{ with } n = 6, 8, 10 \quad \cdots\cdots\cdots (3)$$

are related to dipole-dipole, dipole-quadrupole and quadrupole-quadrupole interactions, respectively; Where C is the total concentration of activator and sensitizer ions. η_o and η are luminescence quantum efficiency in the absence and presence of Eu^{3+} ions. The equation (2) can be rearranged into terms of luminescence intensities of the sensitizer in the absence and presence of the activator ion, respectively, using the relation $(\eta_o/\eta) \approx (I_{so}/I_s)$. Also, the energy transfer efficiency can be calculated using the equation (P.I.Paulose et al. 2003)

$$\eta_T = 1 - (I_s / I_{so}) \quad \cdots\cdots\cdots\cdots\cdots\cdots (4)$$

Fig. 24 depicts the fitted curves for the concentration Vs. ratio of PL intensity with and without activator. As seen from the figure better result for the curve fitting is obtained for n = 8. Hence we may conclude that dipole – quadrupole energy transfer is occurring in this system.

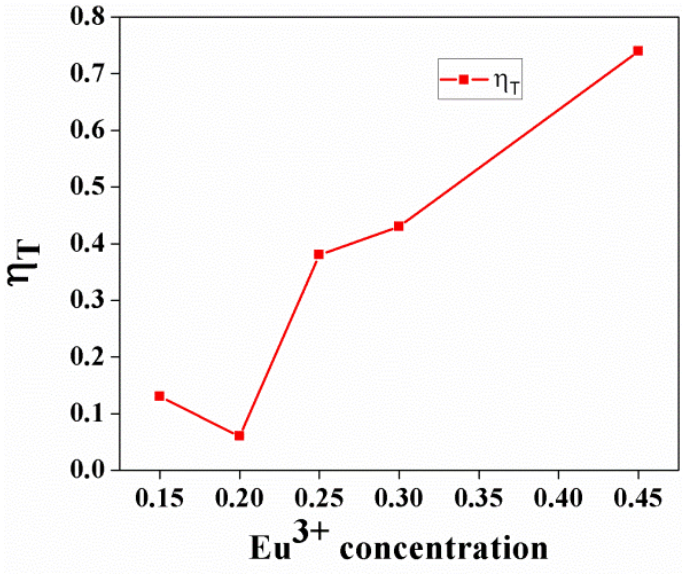

Fig. 23 Energy transfer efficiency determination plot

Table 5 CIE values of LTO : Bi^{3+}, Eu^{3+}

sample	**chromacity coordinates**
LTBE0.15	(0.38,0.26)
LTBE0.20	(0.22,0.20)
LTBE0.25	(0.25,0.19)
LTBE0.30	(0.27,0.21)
LTBE0.45	(0.21,0.17)

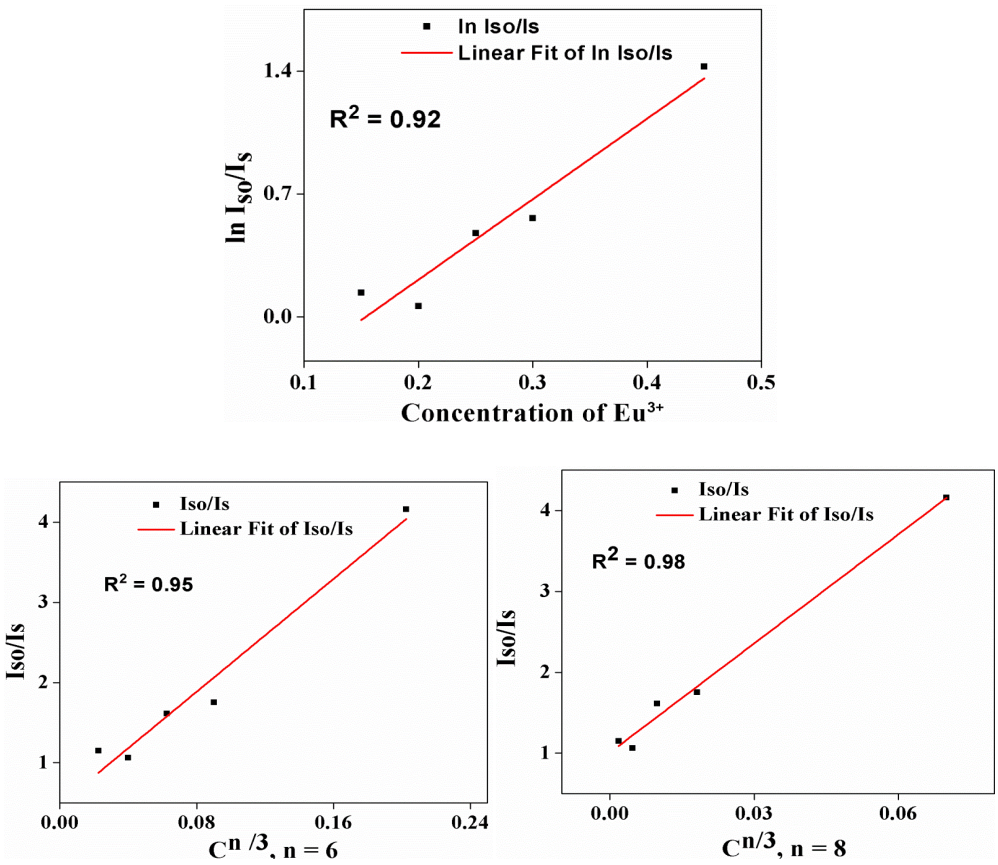

Fig. 24 Fitted curves of intensity ratios Vs concentration

The relative ratios between Bi^{3+} and Eu^{3+} ions not only control the energy transfer efficiency but also control the color tuning of the phosphor from blue to white region. CIE values of $LTBE_{0.15}$ sample falls near-ideal CIE coordinates of white light. CCT values of this sample calculated by McCamy's Formula

$$CCT = 449n^3 + 3525n^2 + 6823.3n + 5520.33$$

is 2523 K.

Conclusions

A new series of full color emission phosphors in Bi^{3+} and Eu^{3+} co-doped La_3TaO_7 weberite system was developed by the conventional high temperature ceramic method. The structural studies confirm the phase purity of the samples. Morphological studies also the requisite particle size around 1μm for LED phosphor applications. Presence of the doped elements in the matrix was confirmed from EDS analysis. Band gap values of the samples show a decreasing trend with increasing Eu^{3+} content. It indicates the effect of increase in covalency on charge transfer mechanism of ligand ions. Photoluminescence spectra give broad spectra of Bi^{3+} ions along with narrow bands of Eu^{3+} ions. Energy transfer existing between the Bi^{3+} and Eu^{3+} ions are confirmed from the luminescence emission spectra as well as from the decreasing trend in the lifetime values of the sample. The mechanism behind energy transfer was investigated and found to be due to dipole-quadrupole interactions. Calculated values of CIE and CCT values are well in agreement with observed results. Hence we propose the present system as a potential candidate for direct white emitting single phase phosphor for WLED applications.

Chapter 5

Novel $LaGaGe_2O_7$ single phase phosphors for WLED applications

The chapter consists of investigations on monoclinic structure $LaGaGe_2O_7$ with respect to luminescence aspects. The luminescence properties were investigated with Bismuth alone doped samples and then with Cerium Substituted and Europium co-doped samples. The effect of Europium co-doping was studied in detail. Bismuth alone doped samples produce emission in near UV/blue region only (382 nm). When Ce^{3+} was substituted to Ge site the emission spectra had a slight red shift but the average emission intensity got reduced. Eu^{3+} co-doping enhanced the emission spectra and modified the CIE values. There was good overlap of PLE and PL spectra of LaGaGe2O7:Bi^{3+}, $Eu^{3+}$and the energy transfer in this phosphor was established and is found to be due to dipole – quadrupole mechanism.

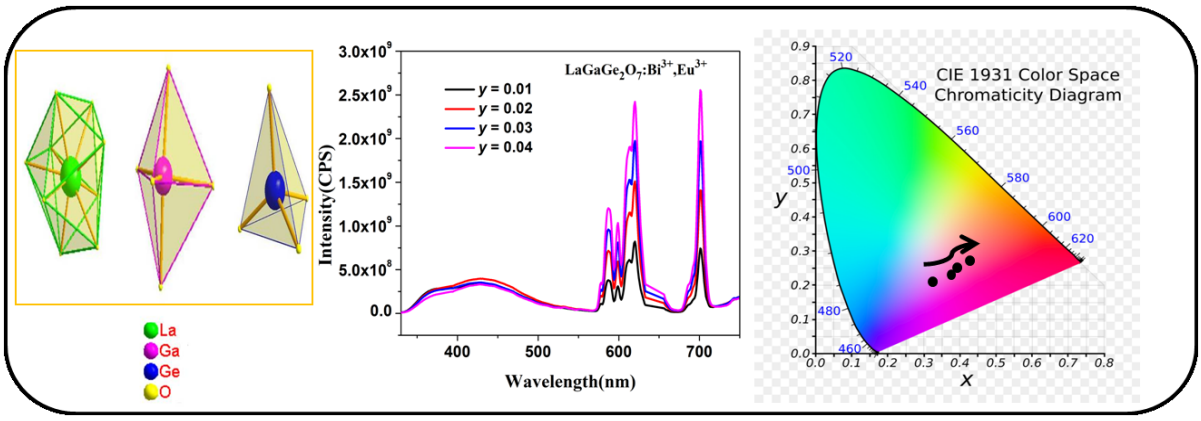

Introduction

The research interests in the field of inorganic phosphors are advancing day by day with new efforts to bring out new technologies with advanced features to overcome the existing issues. The currently using technology of combining YAG yellow phosphor with UV/ blue LEDs or by combining tricolor phosphors with UV LEDs is facing drawbacks such as poor color rendition due to spectral gap in green region, high correlated color temperature, color re-absorption among different phosphors, phosphor aging etc. to overcome these difficulties it will be a better option to develop a single phosphor material which cover the whole visible region of electromagnetic spectra so that it will be capable of full color emission when combined with UV/blue LED. Many reports are coming now on the development of single phase phosphors for white LED application based on energy transfer mechanism. It utilizes the energy transfer between activator and sensitizer ion to tune the color of preparing single phase phosphor. Different combinations of activator and sensitizer ions are there such as Bi^{3+}/Eu^{3+}, Ce^{3+}/Mn^{2+}, Eu^{2+}/Mn^{2+}, $Bi^{3}+/Sm^{3+}$ etc. In this chapter photoluminescence properties of Bi^{3+}/Eu^{3+} ions in monoclinic $LaGaGe_2O_7$ system are reported. Bi^{3+} ions were chosen because of its very peculiar features which may aid the luminescence mechanism of phosphor material. The ground state of Bi^{3+} is $6S^2$ electronic configuration. The excited states coming from nsnp configuration are $^3P_0$, $^3P_1$, $^3P_2$ and $^1P_1$ states. Transitions from $^1S_0$ to $^3P_0$ and $^3P_2$ are completely spin forbidden, if no other configurations are taken into account. The two energy states $^3P_1$ and $^1P_1$ are mixed by spin-orbit coupling. Therefore, only two transitions are expected to have reasonable absorption strength. Transitions from $^1S_0$ to $^3P_1$, $^1S_0$ to $^3P_2$, $^1S_0$ to $^1P_1$ are termed as A band, B band and C band respectively. Charge transfer bands which have high energy than C band are coined as D band. Emission properties of Bi^{3+} ions vary with host lattice. *Rambabu et al.(2013)* have reported the greenish-yellow luminescence of Bi^{3+} ions in lanthanide vanadate phosphors. Whereas red luminescence in scandium vanadates and blue emission in calcium antimonates were reported by *Fengwen Kang et al*. (2014) and *Shiyue Yao et al.* (2016) respectively. The Bi^{3+} ions are usually used as sensitizers along with Ln activators (Eu^{3+}, Sm^{3+}, Er^{3+}). The resonance type energy transfer from Bi^{3+} ions to Ln ions could result in highly enhanced emissions of the Ln ions in Bi^{3+}/Ln co-doped materials.

Eu^{3+} ions will be a suitable co-dopant for Bi^{3+} ions owing to their emission in red region due to the 4f – 5d transitions. There are many reports on different phosphors utilizing energy transfer mechanism between Bi^{3+}/Eu^{3+} ions to produce full color emission from a single phase phosphor (Hongpeng Zhou et al.2014, Renping Cao etal.2016,Kang.F.W. et al. 2015). The monoclinic structure $LaGaGe_2O_7$ was studied for structural aspects and in the field of pigments (A A Kaminskii et al.2013). No reports on this systems is available on this system for luminescence studies to date. Similar systems like $YInGe_2O_7$, $LaAlGe_2O_7$, was reported with Bi^{3+} and Ln^{3+}(Gd^{3+}, Tb^{3+}, Eu^{3+}, Sm^{3+} and Dy^{3+}) luminescence (Yeou - Yih Tsai et al. 2012, Yu-Chun Li et al. 2006, 2007). In this present study along with the photoluminescence studies the structural characterizations as well as the morphological studies were carried out. CIE values of the prepared phosphors were calculated and are found to be very close to ideal values. A detailed study of energy transfer mechanism existing in this phosphor was conducted and it is reported.

Experimental

The monoclinic phosphors $LaGaGe_2O_7$: $x$$Bi^{3+}$, $y$$Eu^{3+}$ and $LaGaGe_2O_7$: $x$$Bi^{3+}$, $y$$Ce^{3+}$ were synthesized by the conventional solid state reaction method using La_2O_3, Ga_2O_3, GeO_2, CeO_2 Bi_2O_3 and Eu_2O_3 (99.9% purity; Sigma-Aldrich, Steinheim, Germany) as the starting materials. The required stoichiometric amounts of these materials were weighed and then thoroughly wet mixed in an agate mortar with acetone as the wetting medium. The mixing is followed by drying in an air oven at a temperature of 100°C. This process of mixing and drying was repeated thrice to obtain a homogeneous product. The obtained mixture was initially calcined at 1100°C twice and then followed by 1200°C for 6h in an alumina plate in an air atmosphere furnace each time. The calcined product was then ground into a fine powder for carrying further characterization.

The crystalline structure and the phase purity of the samples were analyzed by recording the X-ray powder diffraction (XRD) pattern using a PANalytical X'Pert Pro diffractometer having a Ni filtered Cu-Kα radiation with an X-ray tube operating at 40 kV, 30 mA and 2θ varying from 10 to 90° in 0.016 steps. The morphology of powder particles was studied using a scanning electron microscope (Carl Zeiss EVO 18) operated at 20 kV. The X-ray

microchemical analysis and elemental mapping of the samples were carried out using a Silicon Drift Detector-X-MaxN attached with the SEM. The selected-area electron diffraction (SAED) patterns and high-resolution electron microscopy of the samples were taken using a TECNAI 30G2 S-TWIN transmission electron microscope (FEI, The Netherlands) operating at 300 kV. Absorbance studies of the samples were carried out using a Shimadzu UV-3600 UV-Vis spectrophotometer in the 200-500 nm wavelength range using barium sulfate as a reference. The photoluminescence spectra of the prepared samples were obtained using a Spex-Fluorolog DM3000F spectrofluorimeter with a 450 W xenon flash lamp as the exciting source. The luminescence lifetime of the phosphors was recorded using the phosphorimeter attached to a Fluorolog®3 spectrofluorimeter. All the measurements were carried out at room temperature.

Results and discussion

Luminescence properties of Bismuth doped LaGaGe2O7

Powder X-ray diffraction studies

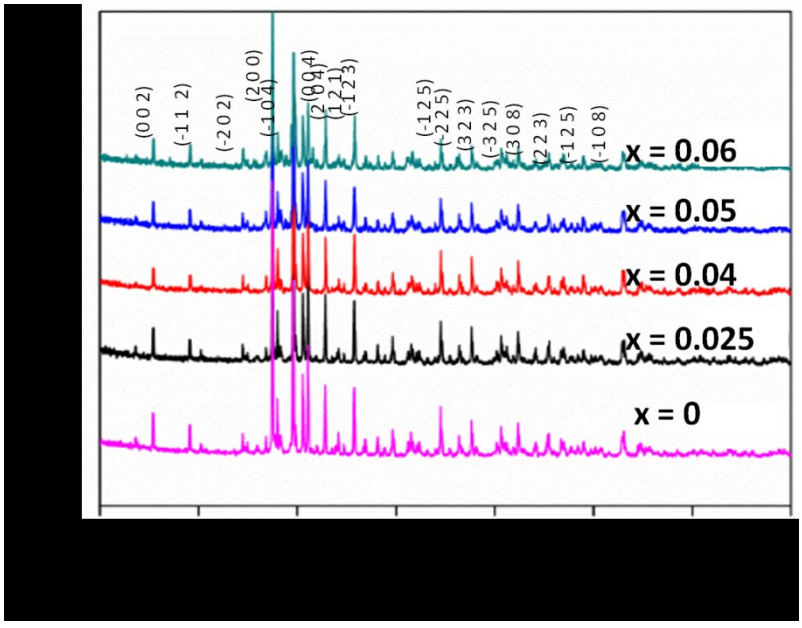

Fig.1 XRD patterns of $LaGaGeO_7$: xBi^{3+} samples

Figure depicts the powder x-ray diffraction patterns of Bismuth doped $LaGaGe_2O_7$ for different concentrations. All the samples are phase pure and they are crystallized into monoclinic structure with space group $P2_1/c$. the patterns are in well agreement with standard pattern of ICDD No. 00-041-0969. In this system the rare earth ions are separated by GaO_5 and Ge_2O_7 polyhedra. And oxygen have 9- fold coordination around rare earth ion. The unit cell of the system consist of four La^{3+}, four Ga^{3+}, eight Ge^{4+} and 14 O^{2-} ions occupied in the 4e positions of C_1 symmetry.

Photoluminescence studies

Photoluminescence studies of Bismuth aloe doped samples were analyzed. The excitation emission spectra of the sample for different excitations and emissions are depicted in figure 2 and figure 3.

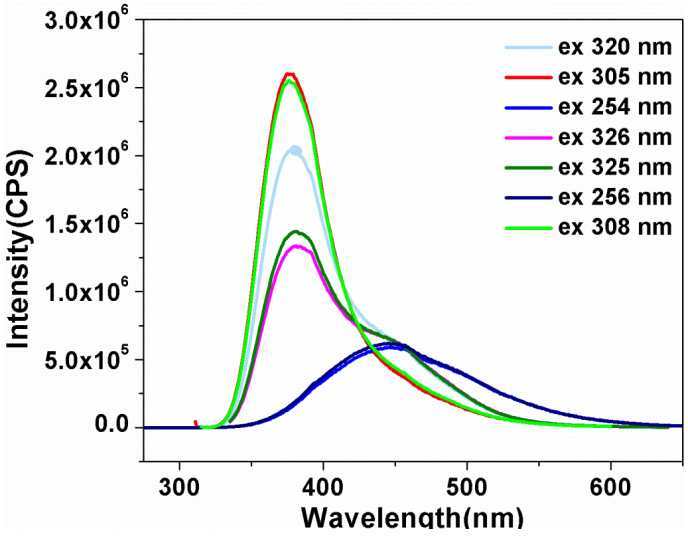

Fig.2 Emission spectra of LGG : Bi^{3+} sample for different excitations

Emission spectrum was recorded for different excitation wavelengths ranging from 254 nm to 326 nm. It is clear from figure 2 that emission spectra are very narrow for the excitation wavelengths corresponding to Bi^{3+} emissions. Similar results were reported in Bi^{3+} doped La_2MgGeO_6 system by (Wie Xie et al.2018). Hence it is not much suitable for broad emission applications such as pc-WLED applications. Emission spectrum is comparatively broad for 254 nm excitation, but intensity is very poor. Thus it was very essential to think of substituting a rare earth ion. In this present case there

is emission only in the blue region of visible spectra. Thus a suitable substituent is needed to cover the green emission also. Hence for this purpose Ce^{3+} was used. Cerium was substituted to Germanium site.

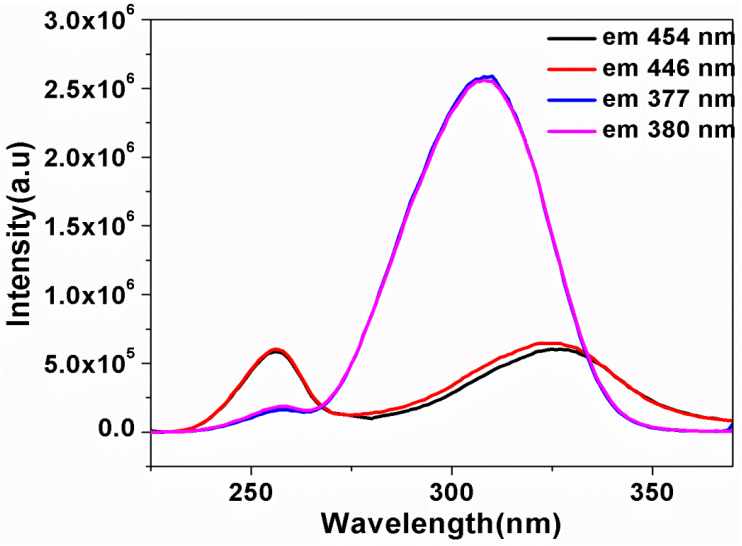

Fig.3 PLE of LGG: Bi^{3+} for different emission wavelengths

Effects of Cerium substitution into Monoclinic $LaGaGe_2O_7$

Powder X-Ray diffraction studies

The powder XRD pattern of cerium substituted $LaGaGe_2O_7$:Bi^{3+} sample is shown in figure 4. The cerium substituted sample also crystallizes into monoclinic structure with space group $P2_1/c$. The phase purity of the sample was confirmed from XRD analysis. Then photoluminescence property of the prepared sample was studied. Figure 5 and figure 6 indicate the excitation and emission spectra of the cerium substituted samples.

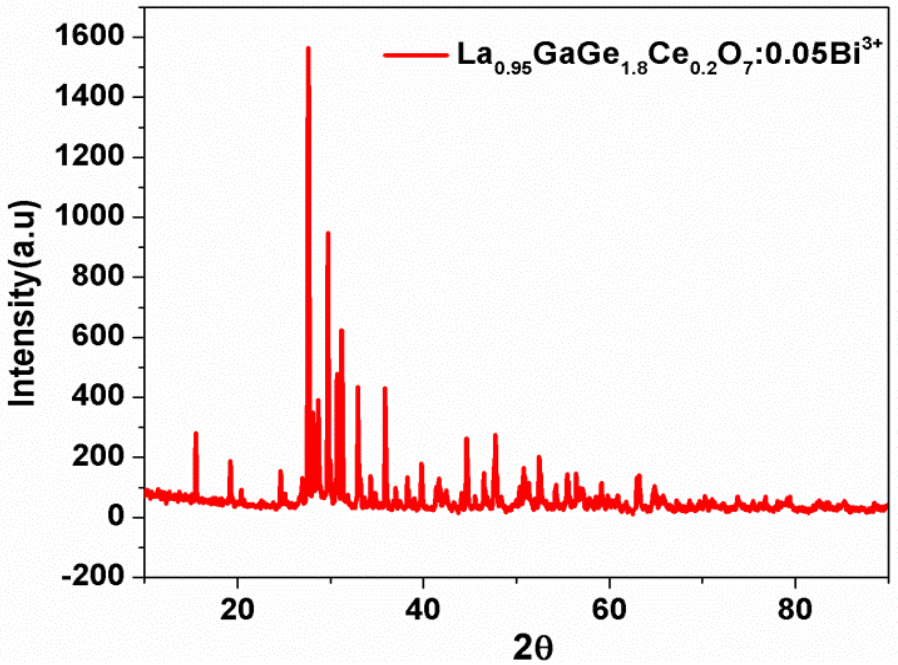

Fig. 4 Powder XRD pattern of cerium substituted $LaGaGe_2O_7:Bi^{3+}$ sample

Photoluminescence studies

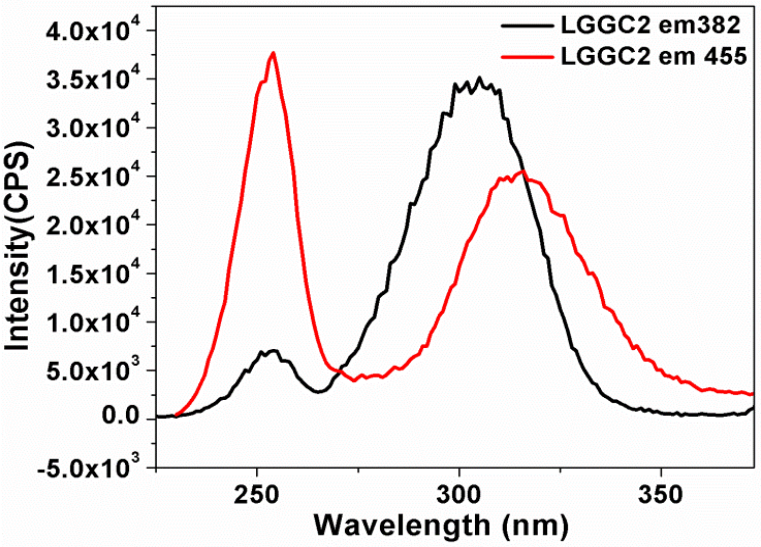

Fig. 5 Excitation spectra of $La_{0.95}GaGe_{1.8}Ce_{0.2}O_7$ sample for

λ_{em} =382 nm and λ_{em} = 455 nm

The excitation spectrum consists of two narrow peaks whereas the emission spectrum is much broad compared to LGG: Bi samples. Better emission is recorded for 254 nm

excitation other than Bi^{3+} excitation. Comparing with figure 4 it is evident that Cerium substitution introduces an additional peak around 500 nm for the Bismuth excitation (315 nm). But the host emission is not much sensitized by the substitution of Cerium into germanium site. Also comparing the two results it is evident that photoluminescence intensity of Cerium substituted samples are much less than that of LGG: Bi^{3+} samples. Hence we dropped the cerium substitution studies with these results and further studies were carried out with Eu^{3+} co-doping.

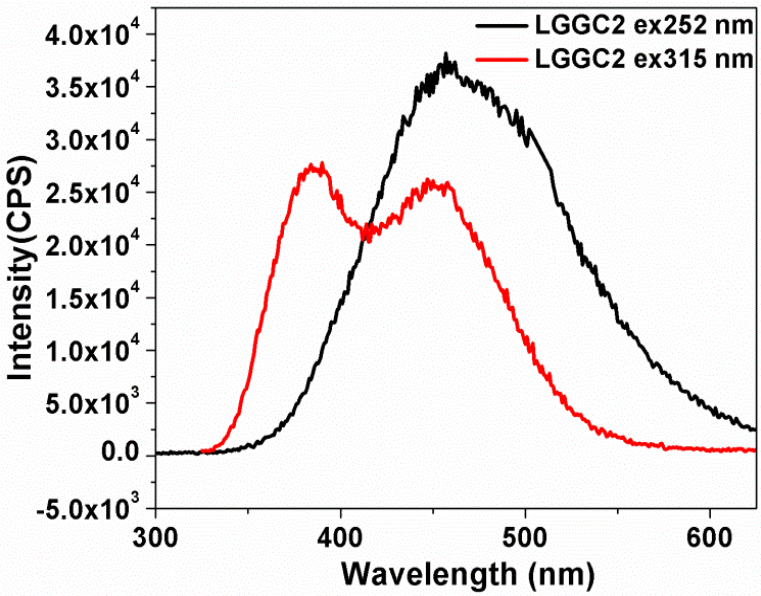

Fig. 6 Emission spectra of $La_{0.95}GaGe_{1.8}Ce_{0.2}O_7$ sample for

λ_{ex} =252 nm and λ_{ex} = 315 nm

Europium co-doping and photoluminescence studies

The powder XRD results (Fig.7) confirms the phase purity of the samples. And all the samples were crystallized into monoclinic structure.

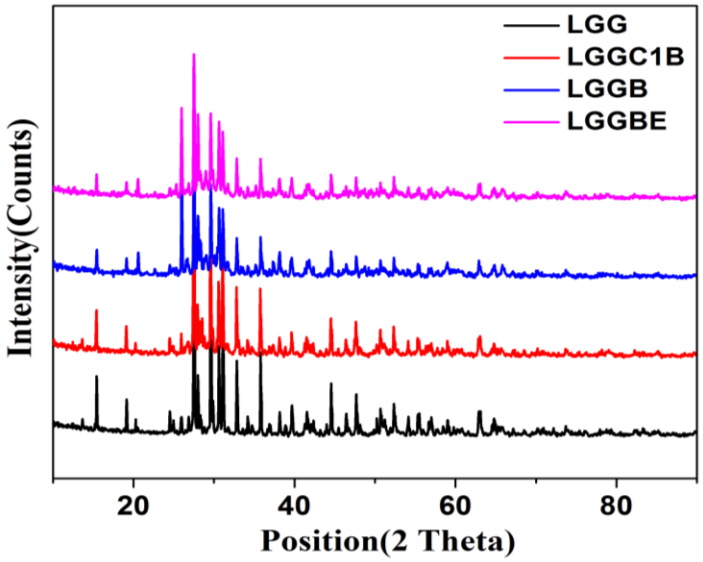

Fig. 7 Powder XRD patterns of LGG: xBi^{3+}, yEu^{3+} samples

Morphological studies

Figure 8 shows the SEM images of LGG: xBi^{3+}, yEu^{3+} samples. Agglomerative nature of particles is clear from the SEM images. Also the particles have irregular shape. Reduction in particle size is noticed with increasing Europium content. It is assumed that difference in ionic radius between lattice atoms and substitution atoms results in distortion of the lattice and it may induced a local non- uniform strain. And it may be reason for reduction in particle size. The uniform distribution of all the elements in the matrix is confirmed from the X-ray dot mapping images.

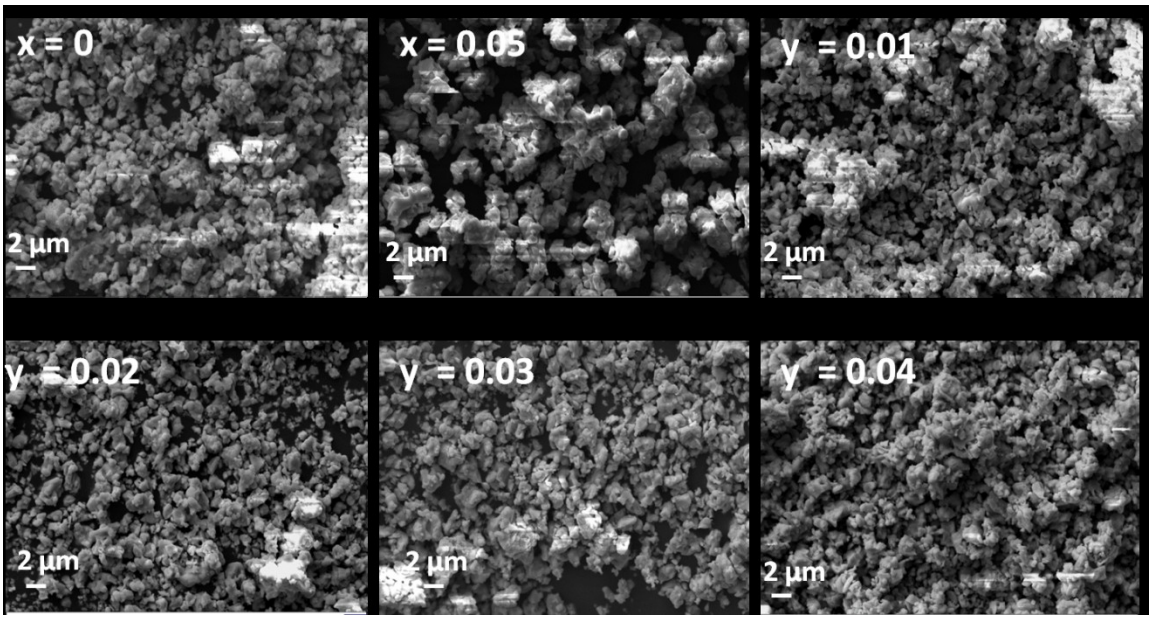

Fig. 8 SEM images of $LaGaGe_2O_7$: $0.05Bi^{3+}$, yEu^{3+} samples

The EDS spectra (Fig.10) provide the chemical analysis of the samples and the presence of all the elements in the matrix is confirmed from EDS analysis. Also the experimental data is in well agreement with the calculated atomic weight ratios.

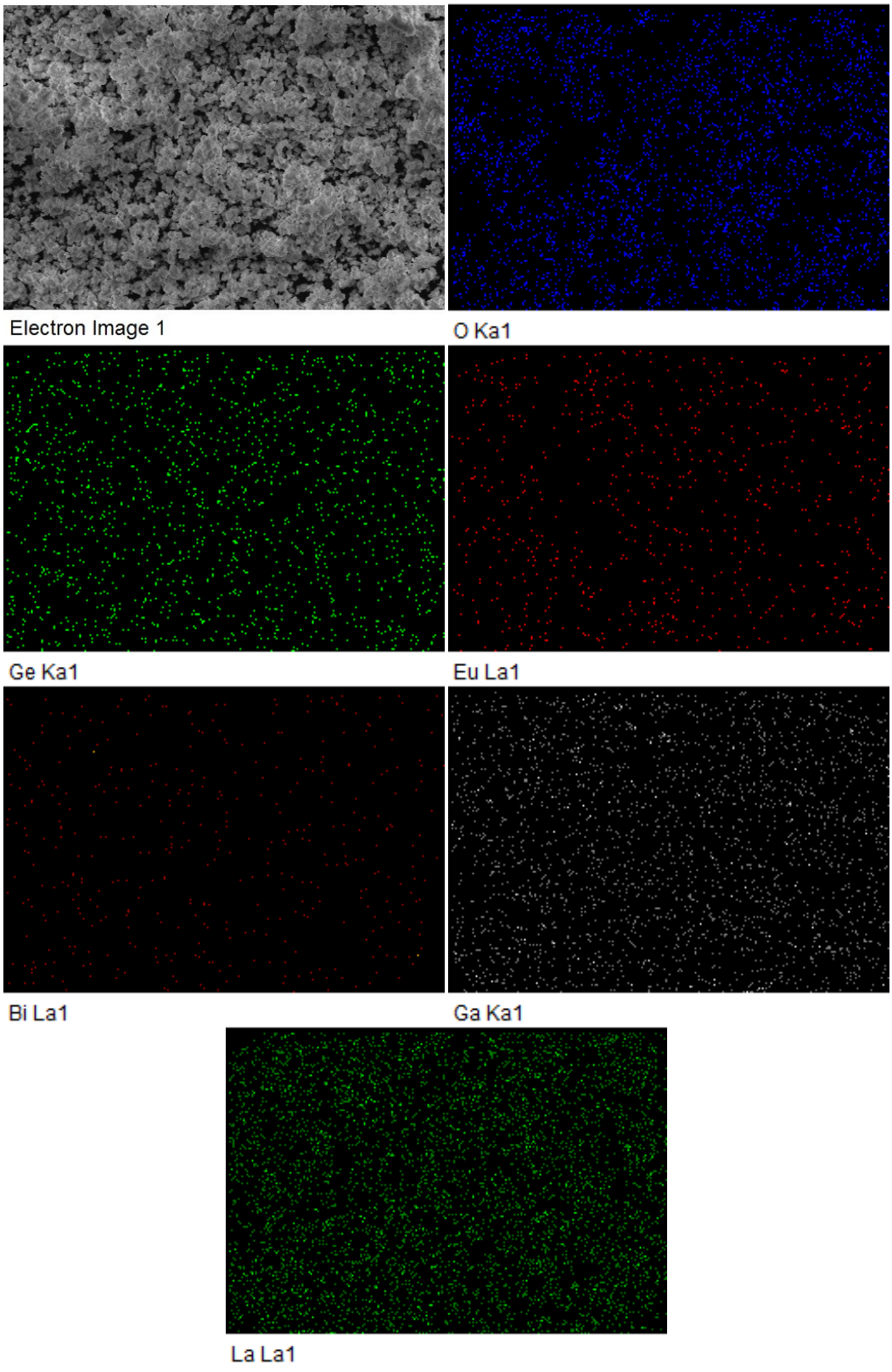

Fig. 9 X-ray dot mapping images of $LaGaGe_2O_7$: $0.05Bi^{3+}$, $0.04yEu^{3+}$ samples

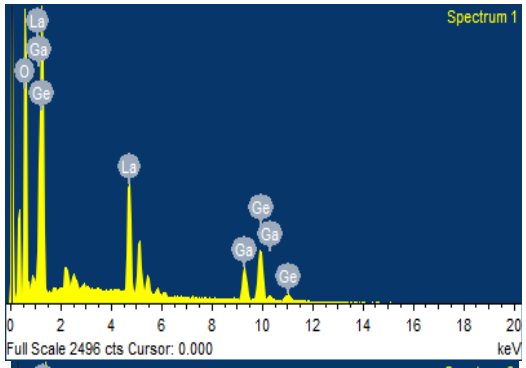

Element	Weight%	Atomic%
O K	28.28	68.12
Ga K	15.65	8.65
Ge K	30.30	16.08
La L	25.77	7.15
Totals	100.00	

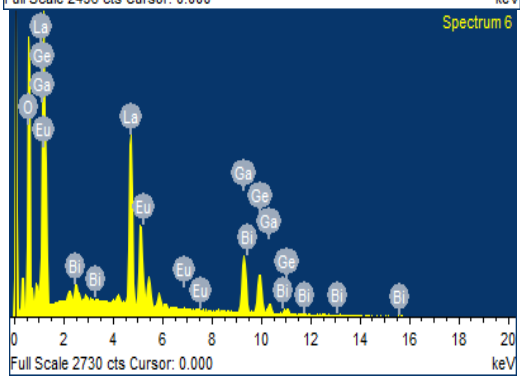

Element	Weight%	Atomic%
O K	18.07	55.85
Ga K	24.60	17.45
Ge K	20.21	13.76
La L	34.58	12.31
Eu L	0.33	0.11
Bi M	2.21	0.52
Totals	100.00	

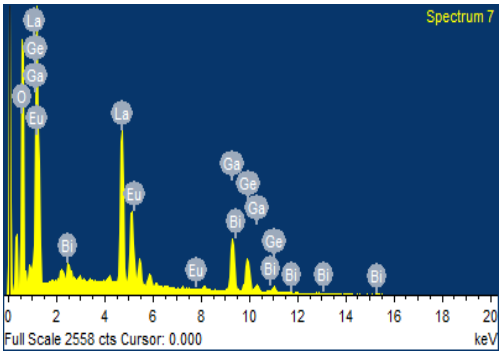

Element	Weight%	Atomic%
O K	23.19	63.77
Ga K	22.65	14.30
Ge K	17.73	10.75
La L	32.40	10.26
Eu L	0.94	0.27
Bi M	3.09	0.65
Totals	100.00	

Fig.10 EDS spectra of LGG: Bi^{3+}, Eu^{3+} samples

Absorbance

The absorption spectra for LGG: 0.05Bi^{3+}, *y* Eu^{3+}samples were recorded and it is displayed in figure11. The LGG samples show strong absorption in the UV region (200 nm – 300 nm). Two main absorption peaks are noticed in the absorption spectra. One major peak is around 250 nm and a shoulder peak at 300 nm. The peak around 250 nm is attributed due to the host absorption and peak around 300 nm can be assigned due to optical absorption of Bi^{3+} ions owing to $1S_0$ to $3P_1$ transitions (A band) of Bi^{3+}. This 'A' band is allowed due to

the spin orbit interaction. The band gap values of these samples are calculated and it falls around 3 eV.

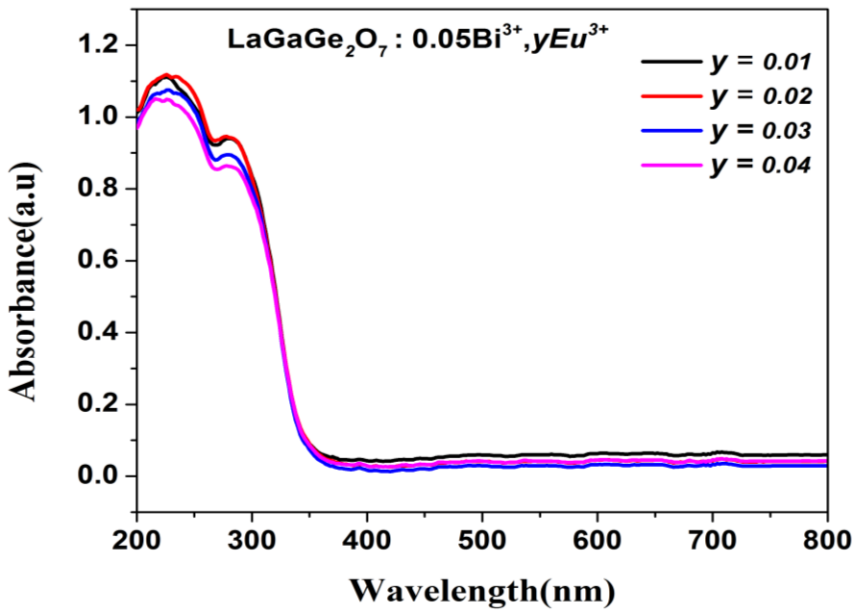

Fig.11. Absorption spectra for LGG: Bi^{3+}, yEu^{3+} samples

Table.1. Band gap energy of LGG: Bi^{3+}, yEu^{3+}.

Composition	Bandgap
x = 0.05, y = 0.01	3.33
x = 0.05, y = 0.02	3.31
x = 0.05, y = 0.03	3.35
x = 0.05, y = 0.04	3.31

Photoluminescence and Energy Transfer

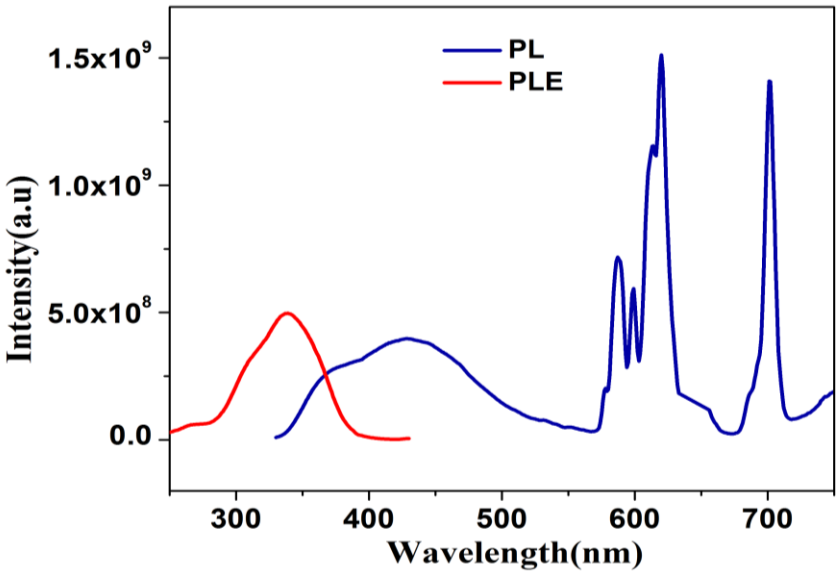

Fig.12. PLE and PL spectra for LGG: Bi^{3+}, Eu^{3+} sample

Photoluminescence studies of the LGG: Bi^{3+}, Eu^{3+} samples were studied. The overlap of excitation and emission spectra is depicted in figure 12. There is good overlap between the excitation and emission spectra. It is a clear indication of existence of energy transfer between Bi^{3+} / Eu^{3+} ions. The excitation spectrum is broad in nature and covers the visible region up to 400 nm. It is very suitable for WLED application. The emission spectra spans from 350 nm to 700 nm. The emission spectra consist of broad peak in the blue – green region aroused due to the $3P_1$ to $1S_0$ transitions of Bismuth ions and characteristic peaks of Eu^{3+} ions in the 600 nm -700 nm region. Thus the emission spectrum covers the whole visible region from 400 nm -700 nm. Thus it is a very suitable candidate for white LED application. The emission and excitation spectra for the series of samples were recorded and it is shown in Figure 13 and figure 14.

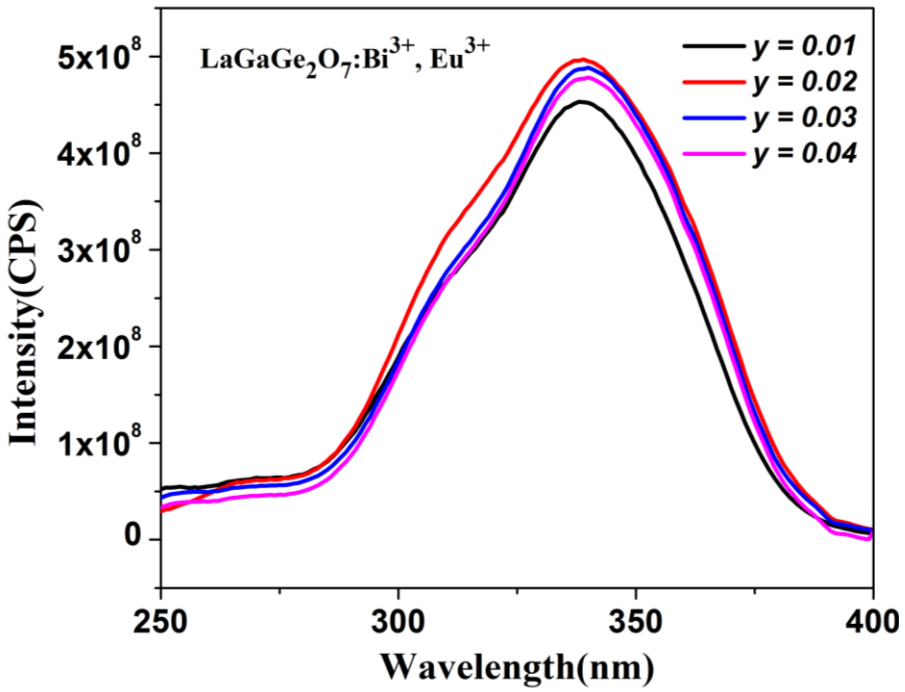

Fig.13 PLE spectra of $LaGaGe_2O_7$: Bi^{3+}, Eu^{3+} samples at an emission wavelength of 452 nm

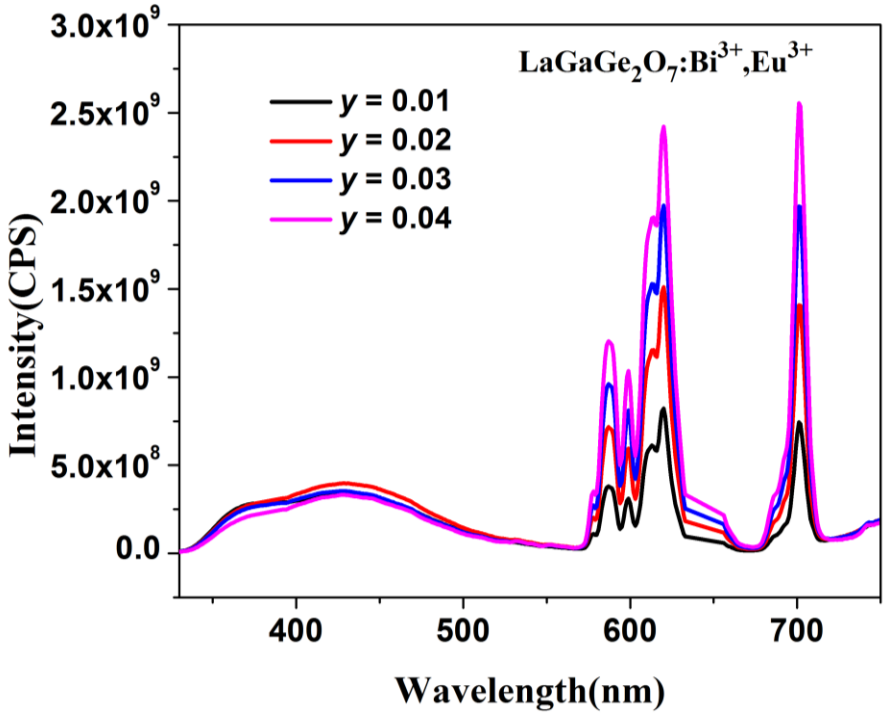

Fig.14 PL spectra of $LaGaGe_2O_7$: Bi^{3+}, Eu^{3+} samples

The photoluminescence excitation spectra in figure 13 show the broad nature of absorption. It is a very desirable feature for WLED application. The broadness is increasing with increasing Europium content. The emission spectra in figure 14 show peaks covering the whole visible region of electromagnetic spectra. There are broad peaks covering the blue –green region and sharp peaks in the red region. The broad peaks are attributed to the 1S – 3P Bismuth transitions and sharp peaks arise due to the 4D – 5F transitions of Europium ions. The Bismuth peaks exhibit concentration quenching after y = 0.02 concentration of Europium. Also the Europium peak intensity enhances with increasing Europium content. This is a clear indication of effective energy transfer existing between Bi^{3+} and Eu^{3+} ions.

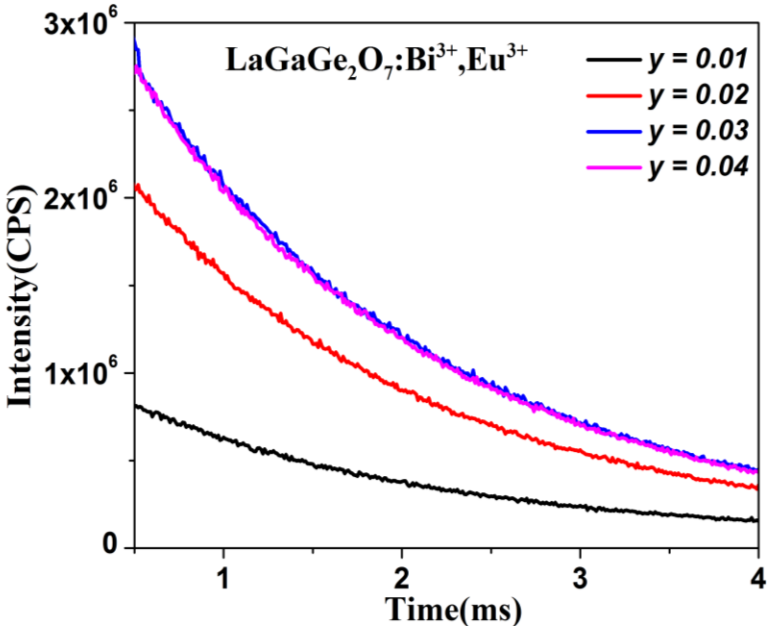

Fig.15 Lifetime decay curves of $LaGaGe_2O_7$: Bi^{3+}, Eu^{3+} samples

Lifetime decay curves show exponential behavior. All the curves were fitted with single exponential function,

$$I = A \exp(-x/\tau)$$

Where I is intensity, A is fitting parameter, x is concentration and τ is decay time. The decay time is defined as the time needed for the emission intensity decreasing to 1/e (~ 37%). The lifetime values of the samples are recorded in table 2. Any particular trend is noticed in the lifetime values. Thus any hint about energy transfer is not understood from the lifetime decay values.

Table.2. Lifetime values LGG: 0.05Bi^{3+}, *y*Eu^{3+} samples

Composition	Lifetime (ms)
x = 0.05, y = 0.01	1.45
x = 0.05, y = 0.02	1.64

x = 0.05, y = 0.03	1.43
x = 0.05, y = 0.04	1.58

The CIE values of the samples were calculated and listed in table 3. Also the values are plotted in CIE diagram and it is represented in figure 16.

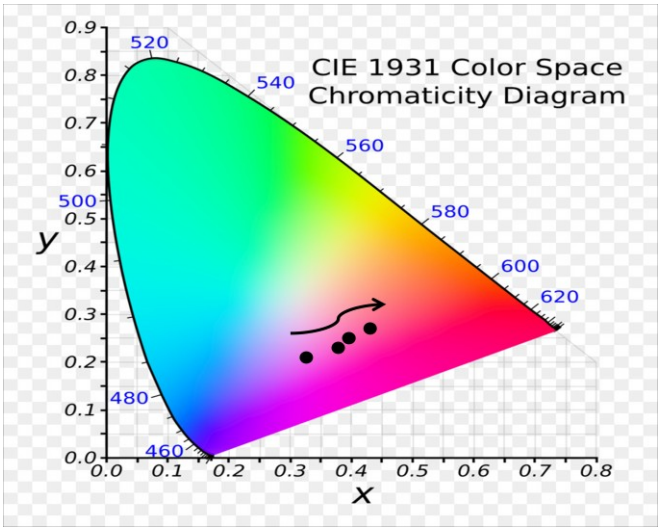

Fig.16 CIE diagram of LGG: Bi^{3+}, Eu^{3+} samples

Table 3. CIE values of LGG: Bi^{3+}, Eu^{3+} samples

Composition	CIE values
x = 0.05, y = 0.01	(0.32,0.20)
x = 0.05, y = 0.02	(0.38,0.22)
x = 0.05, y = 0.03	(0.43,0.23)
x = 0.05, y = 0.04	(0.48,0.25)

Further the energy transfer mechanism existing in this phosphor was investigated using Dexter's energy transfer formula for exchange and multipolar interactions and Reisfeld's approximation. The ratio $\ln(\eta_o/\eta)$ α C is plotted to find whether there exist exchange interaction, here C is the total concentration of Bi^{3+} and Eu^{3+} ions and η_o/η α $C^{n/3}$ plots were worked out and fitted parameters of the plots were noticed. n = 6, 8, 10 are related to dipole-dipole, dipole- quadrupole and quadrupole - quadrupole interactions respectively. The ratio η_o/η approximately calculated by the ratio of relative luminescence intensities, ie; (I_{so}/I_s). The plots made from this theory are depicted in figure 17.

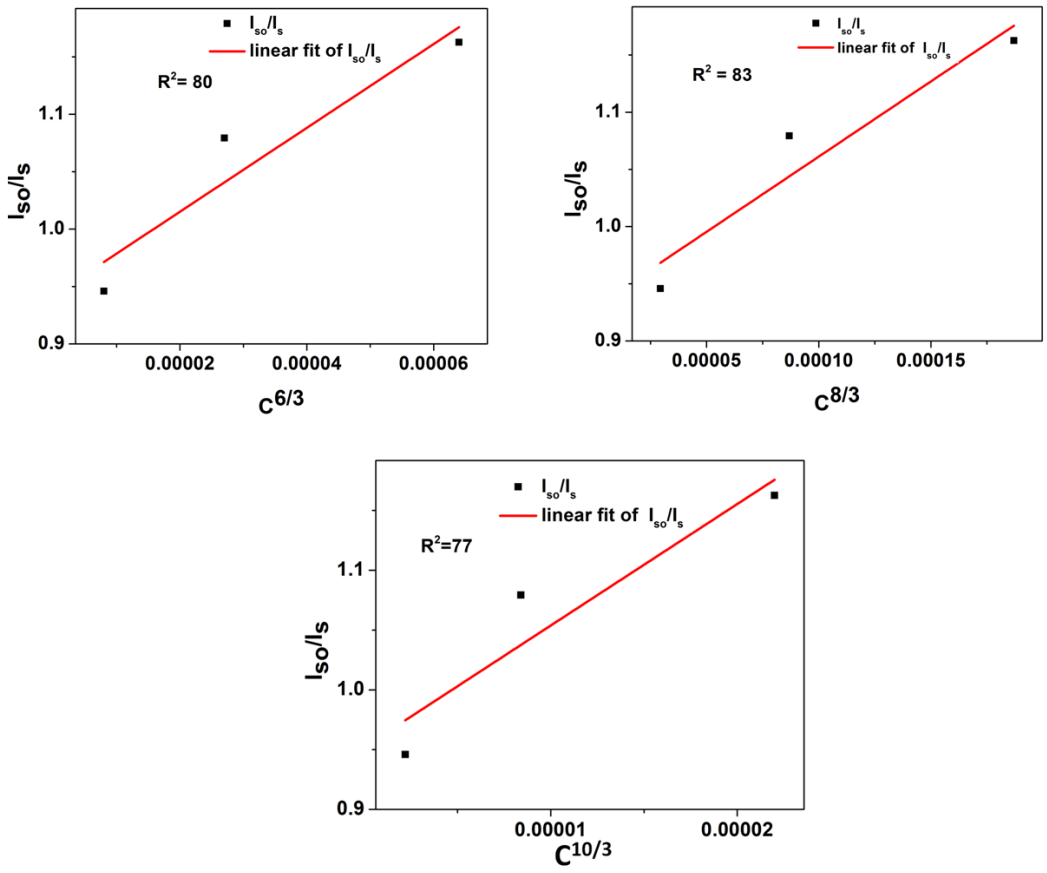

Fig.17 Fitted curves of dependence of I_{so}/I_s on $C^{n/3}$ for n = 6, 8, 10

and total concentration of Bi^{3+} and Eu^{3+} ions.

It is clear from the diagram that better fit is obtained for n = 8. Thus the energy transfer mechanism existing in this phosphor is dipole – quadrupole type.

Conclusions

Monoclinic system $LaGaGe_2O_7$ was synthesized via solid state reaction method. Phase purity of the samples was ensured from powder x-ray diffraction patterns. Absorption strength of the samples in the UV region was analyzed. Morphological characteristics of the samples were understood from SEM analysis. Presence of each element in the matrix was confirmed from EDS analysis. X-ray dot mapping images ensure the uniform distribution of elements in the matrix. Photoluminescence studies were conducted for Bismuth alone doped LGG samples, Cerium substituted samples and Europium co-doped samples. These studies reveal that Bismuth alone doped samples give emission in blue region only. When Cerium substitution was made in the Germanium site and Bismuth was doped into it, the luminescence results do not produced expected results. It reduces the overall emission intensity. Thus the idea of Cerium substitution was dropped and the study continued with Europium co-doping. It exhibited the full color emission nature with a broad peak in the blue region and Europium characteristics peaks in the red region. But the in the green region the spectrum has a shallow region thus the CIE values of the samples vary a little from the ideal values of white light. Lifetime decay curves were recorded and fitted with single exponential curve fitting. The decay time was also recorded. The energy transfer mechanism was analyzed using Dexter's formula and it was found that the dipole – quadrupole type energy transfer exists in this phosphor.

Chapter 6

Full color emission in Pyrochlore type phosphor $La_2Y_{0.66}Sn_{0.66}Sb_{0.66}O_7$: Bi^{3+}, Eu^{3+}

In this chapter the influence of Eu^{3+} co-doping in the system which results in the full color emission was studied. The pyrochlore system $La_2Y_{0.66}Sn_{0.66}Sb_{0.66}O_7$ produce good luminescence results. For Bi^{3+} alone doped samples with the emission and excitation spectra are broad with 520 nm and 322 nm emission and excitation wavelengths respectively. Eu^{3+} add red component to the phosphor and emission spectra of this phosphor covers the whole visible spectral range up to 700 nm with broad peaks along with sharp narrow characteristic peaks of Eu^{3+}. The samples have good absorption strength in the UV region. Calculated CIE values are very close to ideal value (0.33, 0.33). Any particular kind of energy transfer mechanism was not identified in this phosphor.

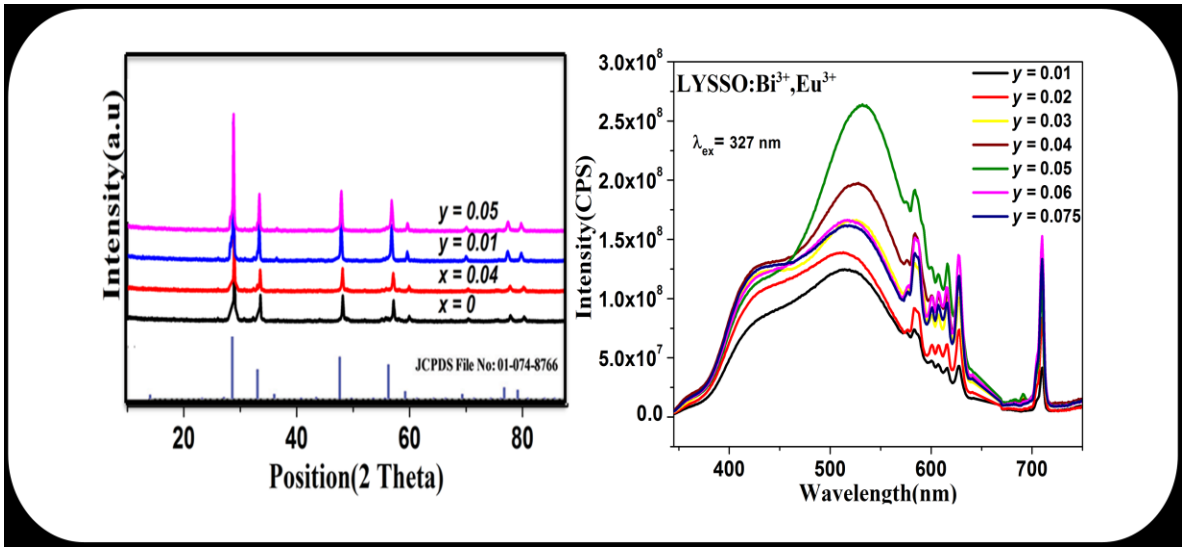

6. 1 Introduction

The journeys to new inventions have never found an end. Advancements in technologies make human life better day by day. In lighting industry the efforts to bring low cost novel inorganic phosphor materials for white light generation is still a hot topic of research. Solid state lighting technology has brought many advantages in lighting industry, as it is highly efficient, energy saving, compactable and environmental friendly. The technology has replaced conventional lighting sources such as incandescent lamps, halogens and even CFLs with LEDs due its superior properties. The currently using technology for white light generation in industry is either by combining tri color phosphors or by using UV/blue LEDs with yellow phosphor. But both of these methods possess disadvantages such as color re absorption among phosphors, phosphor aging, and gaps in emission profile etc. These disadvantages results in poor color temperature and low color rendering properties. To develop a phosphor with appropriate color temperature as well as good color rendering properties is still a key challenge in this area. The concept of single phase phosphors can introduce a lot of improvements in this area to fulfill the research efforts. As it is a single material which is capable of producing full color emission in visible region it can overcome the existing issues in this area. Also it will be of low cost and high efficiency. Currently many research efforts are going on to produce novel single phase phosphors out of inorganic materials.

There are numerous reports on pyrochlore based materials for phosphor applications. Pyrochlores are gaining so much attention because of high chemical and thermal stability, lattice stiffness, ability to form with diverse range of elements and ability to tolerate both cation and anion disorders.[1-4] The general formula of Pyrochlore is $A_2B_2O_7$. It has a cubic symmetry with space group Fd3m.[5] The ions with f–d or d–d electron configurations are the best choices of activators in phosphors because they could emit visible and broad-band light under the influence of crystal field and nephelauxectic effect.[6-7] Among different trivalent ions including rare earth ions, Bi^{3+} ions are recently getting attention in the field of luminescence, due to their host dependent luminescence properties. Bi^{3+} luminescence arise due to the transitions between $^1S_0$ to $^nP_1$ (n = 1, 3). The Bi^{3+} ions are capable of

producing emission in UV, visible as well as near infra red spectral region due to 6s6p to $6s^2$ transitions. Due to the nS2 electronic configuration Bi^{3+} ions give rise to broad excitation and emission bands. This property of Bismuth ions is very useful in the production of full color emitting phosphors. The recent studies on single phase phosphors have reported that the concept of full color emission can be realized by employing the energy transfer mechanism instead of using a single dopant method. [8-10] This is much effective when the optical absorption of the activator ion is weak. From the literature it is observed that Eu^{3+} ions are the best choice to co-dope with Bi^{3+} ions to obtain full color emission. The peculiar properties of Eu^{3+} ions to give emission in red region of the visible spectra make it a potential candidate for this purpose. Eu^{3+} ions posses a simple energy level scheme compared to other rare earth ions. The transitions of Eu^{3+} ions are hypersensitive and hence they strongly depend on the chemical surroundings.[11] According to Jude- oflet theory the electronic transitions of Eu^{3+} ions from $^5D_0$ to lower lying levels with J = 0, 3 or 5 are both electric and magnetic dipole forbidden. But due to the J- mixing effect induced by crystal field some weak transitions from $^5D_0$ to lower lying levels are observed. This makes Eu^{3+} ions an optical probe to investigate coordination environment around cations in crystalline lattice.[12]

In the present work Bi^{3+} ions were doped into La site of pyrochlore system $La_3YSnSbO_{10.5}$. The photoluminescence properties of the samples were analyzed after confirming the phase pure nature through powder X-ray patterns. As the luminescence of Bismuth alone doped samples don't cover the whole visible range, Eu^{3+} was co-doped in to the matrix and the new luminescence results were recorded. It was found that Europium co-doping improves the luminescence behavior of the samples and the spectra covers the whole visible range of electromagnetic spectra. The CIE values of the samples were calculated and it falls very close to ideal CIE values of white light (0.33, 0.33).

Experimental

The pyrochlore type phosphors $La_3YSnSbO_{10.5}$: $x$$Bi^{3+}$, $y$$Eu^{3+}$ were synthesized by the conventional solid state reaction method using La2O3, SnO2, Sb_2O_5, Bi_2O_3 and Eu_2O_3 (99.9% purity; Sigma-Aldrich, Steinheim, Germany) as the starting materials. The required stoichiometric amounts of these materials were weighed and then thoroughly wet mixed in

an agate mortar with acetone as the wetting medium. The mixing is followed by drying in an air oven at a temperature of 100°C. This process of mixing and drying was repeated thrice to obtain a homogeneous product. The obtained mixture was initially calcined at 1400°C for 6h in a alumina plate in an air atmosphere furnace. The calcination was repeated at 1500°C for 6h with intermittent grinding until a phase pure compound was obtained. The calcined product was then ground into a fine powder for carrying further characterization.

The crystalline structure and the phase purity of the samples were analyzed by recording the X-ray powder diffraction (XRD) pattern using a PANalytical X'Pert Pro diffractometer having a Ni filtered Cu-Kα radiation with an X-ray tube operating at 40 kV, 30 mA and 2θ varying from 10 to 90° in 0.016 steps. The morphology of powder particles was studied using a scanning electron microscope (Carl Zeiss EVO 18) operated at 20 kV. The X-ray microchemical analysis and elemental mapping of the samples were carried out using a Silicon Drift Detector-X-MaxN attached with the SEM. The selected-area electron diffraction (SAED) patterns and high-resolution electron microscopy of the samples were taken using a TECNAI 30G2 S-TWIN transmission electron microscope (FEI, The Netherlands) operating at 300 kV. Absorbance studies of the samples were carried out using a Shimadzu UV-3600 UV-Vis spectrophotometer in the 200-500 nm wavelength range using barium sulfate as a reference. The photoluminescence spectra of the prepared samples were obtained using a Spex-Fluorolog DM3000F spectrofluorimeter with a 450 W xenon flash lamp as the exciting source. The luminescence lifetime of the phosphors was recorded using the phosphorimeter attached to a Fluorolog®3 spectrofluorimeter. All the measurements were carried out at room temperature.

Results and discussion

Powder X-ray diffraction studies

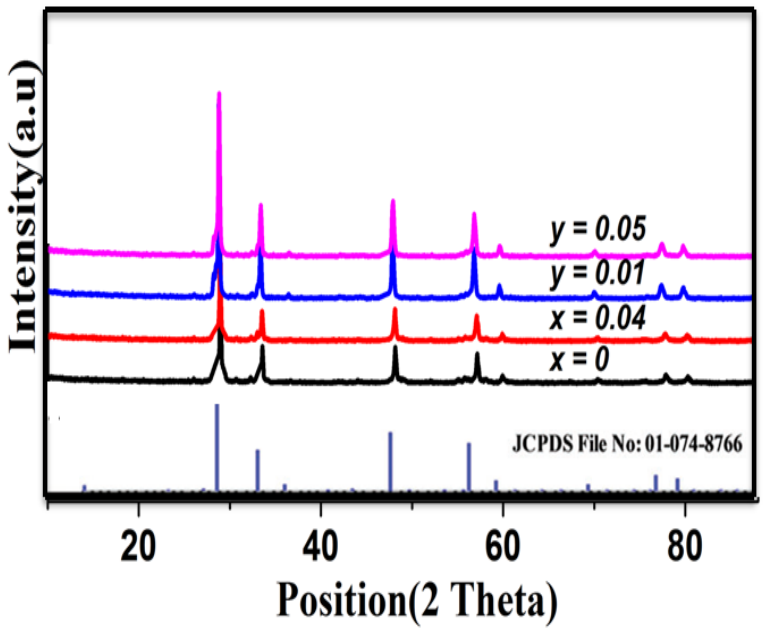

Fig.1. XRD pattern of LYSSO : xBi^{3+}, yEu^{3+}

((a)x = 0, (b)x = 0.04, (c)x = 0.04, y = 0.01, (d)x = 0.04, y = 0.05)

The figure shows the powder x-ray diffraction patterns of the $La_3YSnSbO_{10.5}$: xBi^{3+}, yEu^{3+} phosphors calcined at 1500^{o}C/6hr. All the peaks are in well match with JCPDS File no: 01-074-8766. The crystalline nature of the samples can be confirmed from the sharp intense peaks present in the XRD pattern. All the samples are crystallized into cubic pyrochlore structure with space group Fd3m. In the general formula $A_2B_2O_7$ of pyrochlore "A'' denotes large cations in 8 fold coordination and "B" denotes smaller cations in octahedral coordination.[5] And the oxygen atoms have two distinct sites: 48f(x_{48f}, 1/8, 1/8) and 8b(1/8, 1/8, 1/8) sites. The oxygen ions in the 48f sites are bounded tetrahedrally to two "A" and "B" cations, while the oxygen ions in the Sb sites are bonded tetrahedrally to four 'A' cations.[13-15] These two polyhedra comprise D_{3d} symmetry. For pyrochlore

structure, the x value lies between 0.309 and 0.355, while it is equal to 0.375 for defect fluorite. Hence the x parameter determines the polyhedral distortion and structural deviation from ideal pyrochlore structure.[16-18] The size difference between the cations in "A" and "B" sites is supposed to be the factors which stabilize the pyrochlore structure. The order – disorder transformations at elevated temperatures in pyrochlore structures can be modified by the incorporation of the cations differing in valence or size from the host cations of the pyrochlore structure.[19] According to the previous reports on pyrochlore system the stability of this system depends on the radius ratio of "A" and "B" site cations, with the ideal pyrochlore stable in the region of r_A/r_B =1.46 - 1.78. Materials with radius ratio of nearly 1.2 are found to crystallize with the defect fluorite structure.[20] In this study the ionic radius of Bi^{3+} and Eu^{3+} ions are 1.17A˚ and 1.066 A˚. And that of La^{3+} is 1.16 A˚. Due to the matching values of ionic radii it is expected that the Bi^{3+} and Eu^{3+} ions occupy La site in the lattice.

Morphological studies

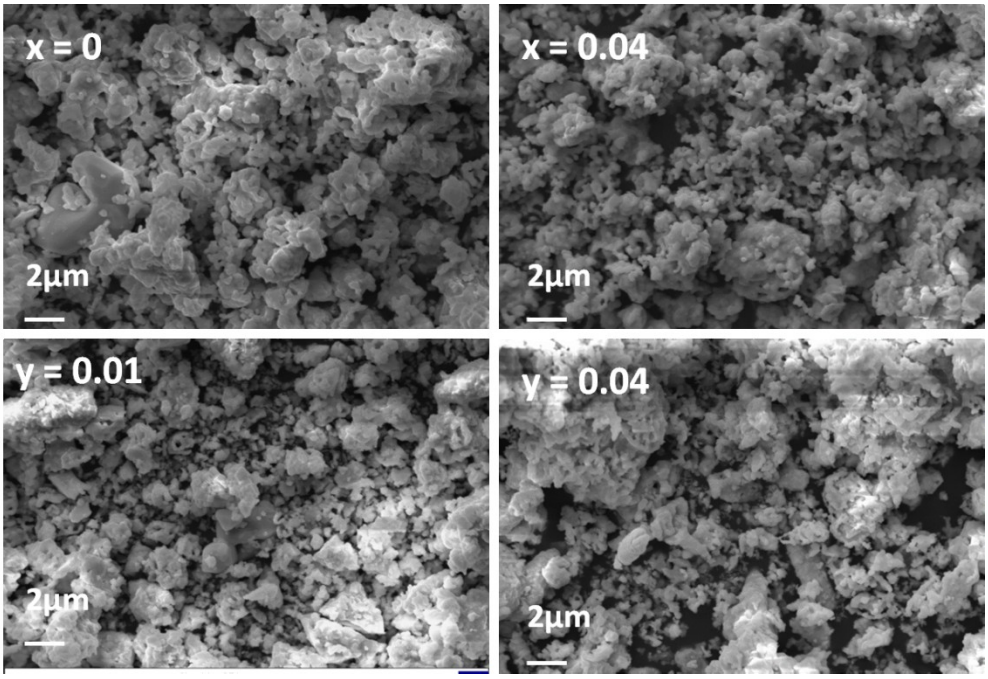

Fig.2.SEM images of LYSSO: *x*Bi^{3+}, *y*Eu^{3+} samples

Fig.2. shows the SEM images of LYSSO: xBi^{3+}, yEu^{3+} samples. From SEM analysis it is noticed that the particles are highly agglomerative in nature and the agglomeration increases with increase in Europium content. The average particle size is found to be less than 1 µm. The EDS spectra of the samples LYSSO: xBi^{3+}, yEu^{3+} for (a) x = 0, y = 0 (b) x = 0.04(c) x =0.04, y =0.05 are depicted in Fig. 3. The presence of all the expected elements is confirmed from the EDS spectra. Atomic weight percentages obtained from the experimental analysis of all elements are in accordance with the calculated stoichiometric ratios. The X-ray dot mapping images represented in figure 4 confirms the uniform distribution of all the elements in the matrix.

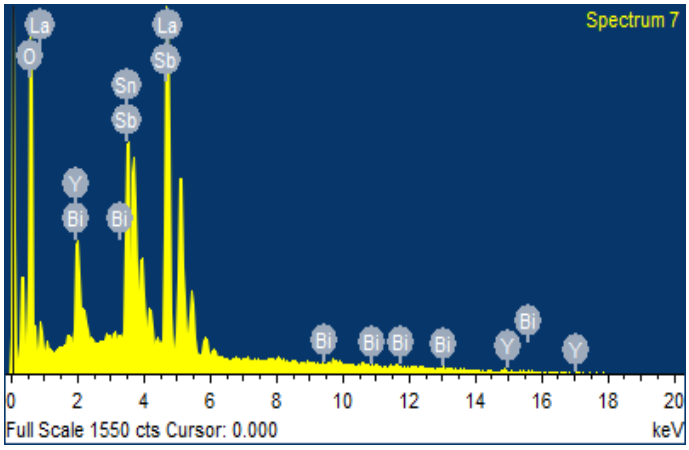

Element	Weight %	Atomic %
O K	23.68	70.97
Y L	6.56	3.54
Sn L	15.25	6.16
Sb L	11.27	4.44
La L	42.97	14.83
Bi M	0.28	0.06
Totals	100.00	

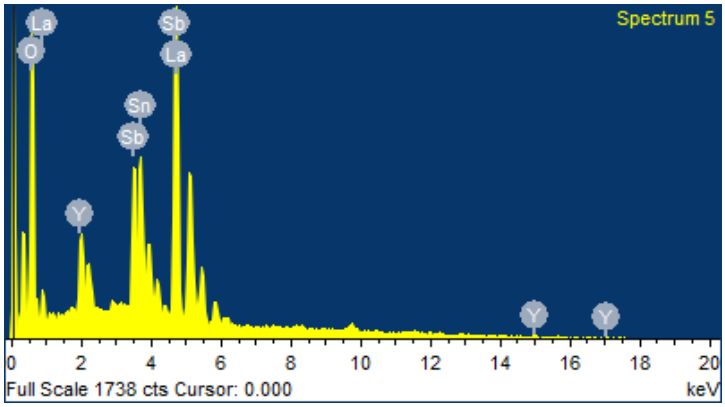

Element	Weight %	Atomic %
O K	24.08	71.58
Y L	5.84	3.13
Sn L	12.86	5.15
Sb L	11.44	4.47
La L	45.78	15.67
Totals	100.00	

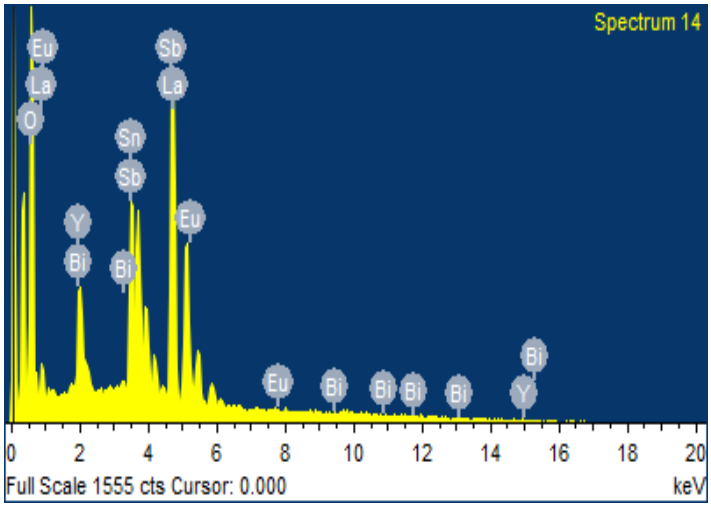

Element	Weight %	Atomic %
O K	27.33	74.77
Y L	6.34	3.12
Sn L	14.47	5.34
Sb L	10.80	3.88
La L	40.30	12.70
Eu L	0.34	0.10
Bi M	0.42	0.09
Totals	100.00	

Fig.3.EDS spectra for LYSSO: xBi^{3+}, yEu^{3+} for (a) x = 0, y = 0 (b) x = 0.04(c) x =0.04, y =0.05

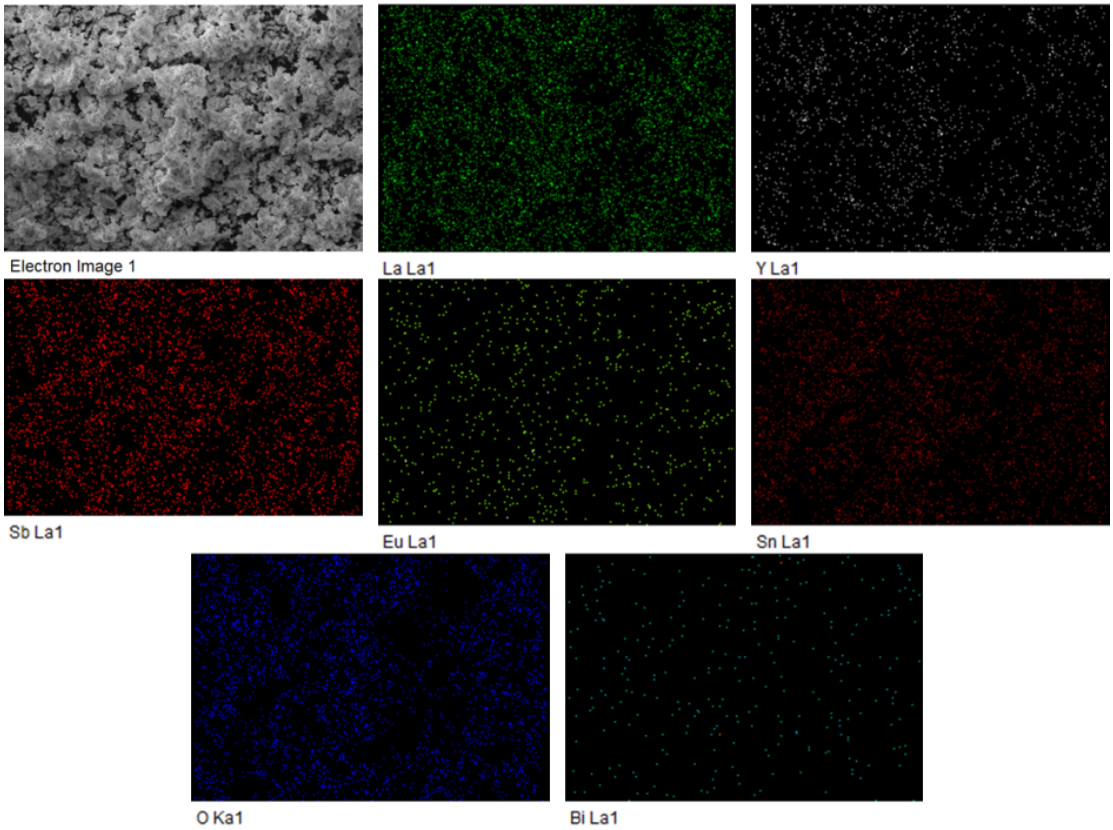

Fig.4.X-ray dot mapping images of LYSSO: xBi^{3+}, yEu^{3+} for (x = 0.04, y = 0.05)

Absorbance

The absorption spectra for LYSSO: 0.04Bi^{3+}, *y* Eu^{3+}samples were recorded and it is displayed in Fig.5. The LYSSO samples show strong absorption in the UV region (200 nm – 300 nm). The first peak below 250 nm may be aroused due to the metal to ligand charge transfer mechanism and the second peak close to 300 nm may arise due to the 1S0 to 3P1 transitions of Bi^{3+} ions. The band gap values of the samples were calculated by Shapiro's method of extrapolating the onset of absorption band to x axis. The calculated band gap values are listed in table 1. The band gap values exhibit a sharp decreasing trend. The difference in electro negativity of dopants ions with Lanthanum ions may cause an average reduction in Lanthanum site and thus increase in covalency will be followed. This will create irrefutable effects on the charge transfer mechanism of ligand ions. These may be the major reason for reducing trend in bandgap values.

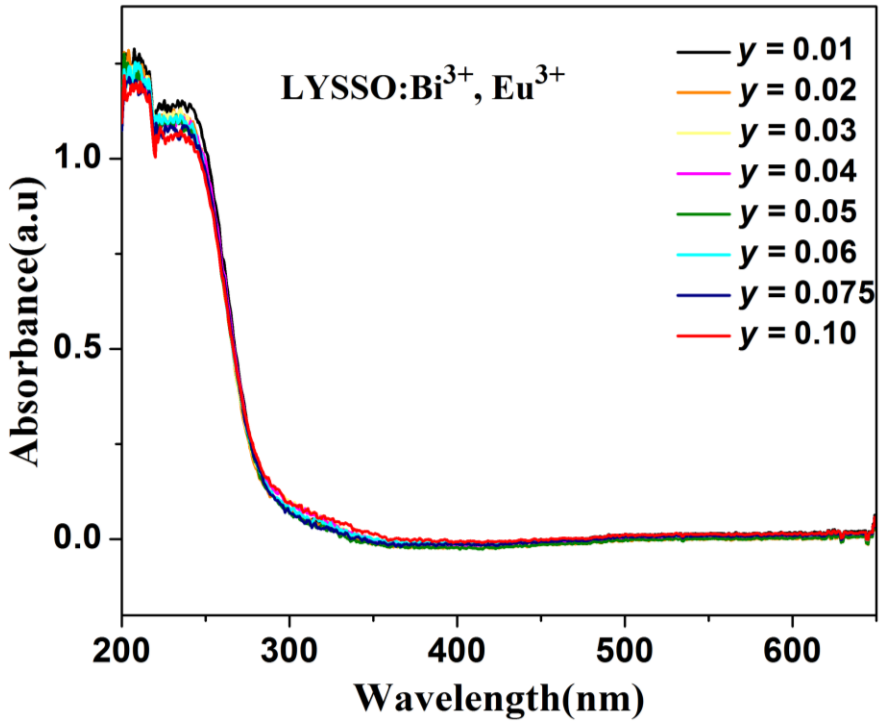

Fig.5. Absorption spectra for LYSSO: 0.04Bi^{3+}, *y*Eu^{3+}(0.01 to 0.075)

Table.1. Band gap energy of LYSSO: 0.04 Bi^{3+}, yEu^{3+} (0.01 to 0.075) samples

Concentration	*Band gap energy, E_g (eV)*
$x = 0.04, y = 0.01$	4.1
$x = 0.04, y = 0.02$	4.0
$x = 0.04, y = 0.03$	3.9
$x = 0.04, y = 0.04$	3.9
$x = 0.04, y = 0.05$	3.9
$x = 0.04, y = 0.06$	3.8
$x = 0.04, y = 0.075$	3.7

Photoluminescence studies

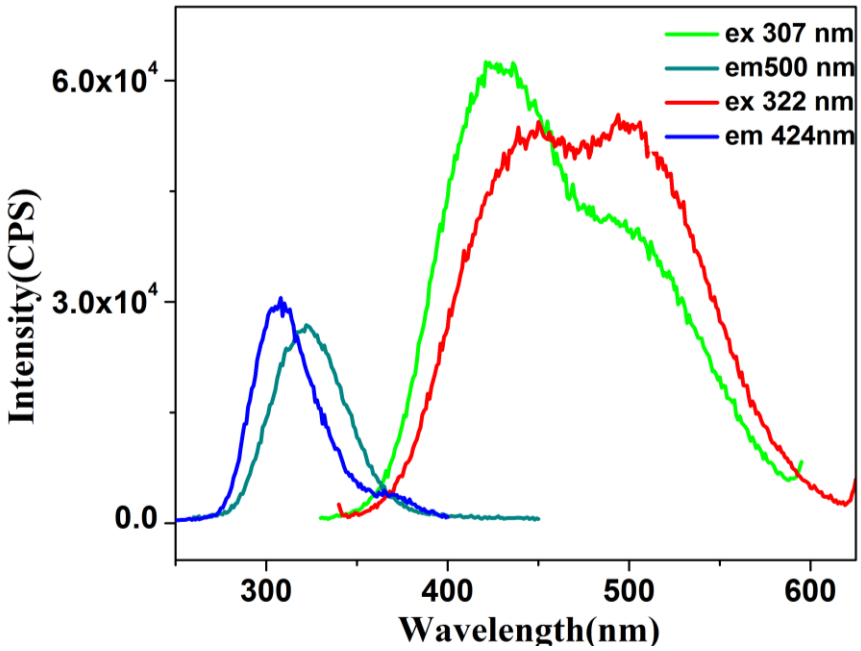

Fig.6. PL and PLE spectra for LYSSO: 0.04Bi^{3+} samples for different excitation (307 nm, 322 nm) and emission (424 nm, 500 nm) wavelengths

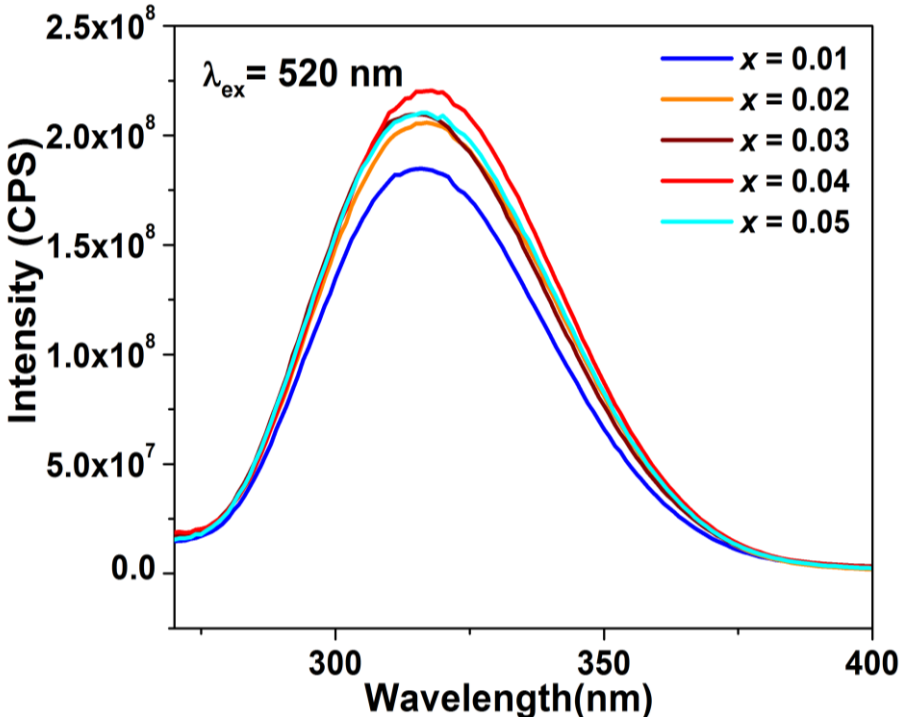

Fig.7. PLE spectra for LYSSO: xBi^{3+} samples for emission at 520 nm

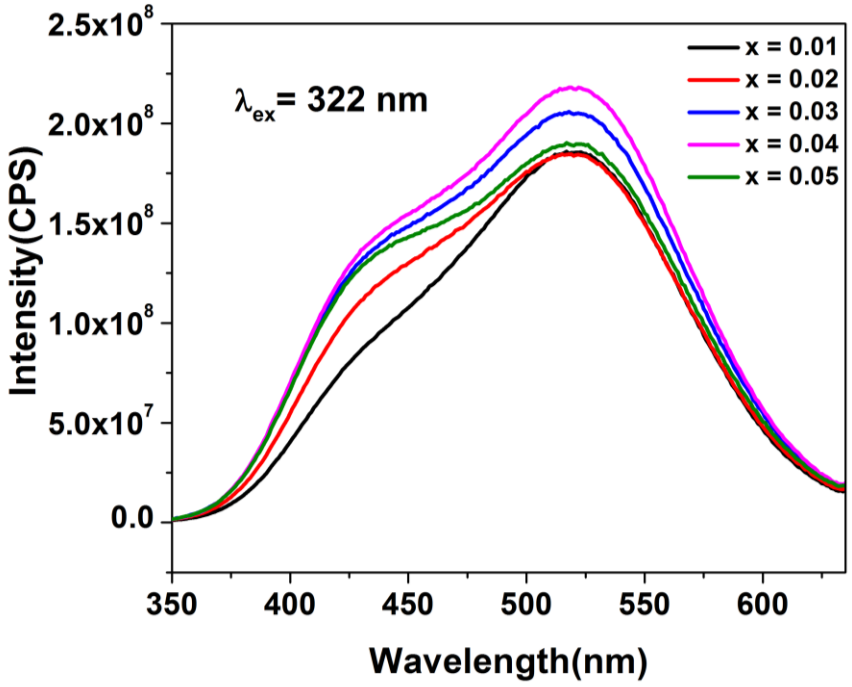

Fig.8. PL spectra for LYSSO: xBi^{3+} samples for excitation at 322 nm

Fig. 6 represents the combined spectrum of excitation and emission for different excitation (307 nm, 322 nm) and emission (424 nm, 500 nm) wavelengths. It is seen from the figure that excitation spectra for the emission wavelength 424 nm is more intense and when the emission wavelength is increased to 500 nm intensity of the peak decreases and also there is a red shift in the spectra. From the figure it is clear that the emission profile changes with excitation wavelength. Intensity also varies with different excitation wavelength. The emission spectra corresponding to excitation 307 nm is more intense compared to emission spectra corresponding to 322 nm excitation. The emission spectra corresponding to 307 nm excitation covers 350 nm to 600 nm, whereas the emission spectra for 322 nm excitation covers the 350 nm to 610 nm region. Both the spectra are broad in nature. Figure 7 and figure 8 depicts the PLE nd PL spectra for the whole series of Bismuth alone samples. It is evident from these figures that both the excitation and emission peaks have broad nature and it is very suitable for WLED applications. Since the aim of the study is to develop full color emission it is necessary obtain an emission spectra covering the whole visible region. Hence Eu^{3+} is co-doped into the system so that red emission along with broad Bi^{3+} emission can be combined to obtain the desired full color emission.

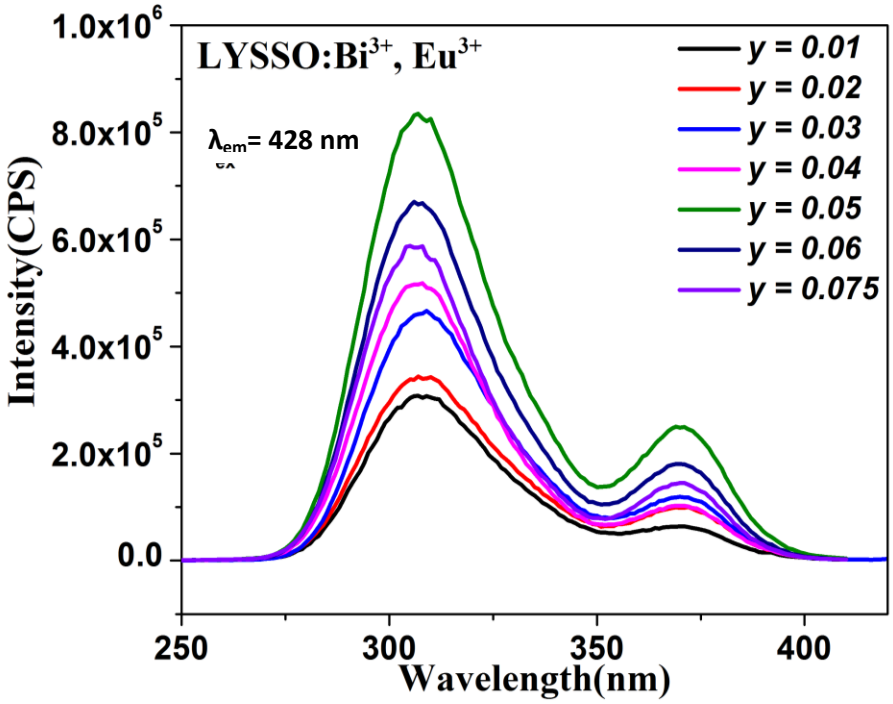

Fig.9. PLE spectra of LYSSO: $0.04Bi^{3+}$, yEu^{3+} samples

Thus Eu^{3+} ions were co-doped into the matrix by keeping the optimum concentration of Bi^{3+} ions at 0.04. Eu^{3+} concentration was varied from 0.01 to 0.075. Fig. 9 represents the excitation spectra of the Eu^{3+} co-doped samples corresponding to 428 nm emission. The excitation spectrum is broad covering the electromagnetic spectra from 275 nm to 400 nm. The spectra consist of two peaks centered at 327 nm and 375 nm. The first peak is more intense than the second peak. The excitation band around 375 nm is appeared with Eu^{3+} co-doping. Bi^{3+} alone doped samples have excitation around 300 nm only.

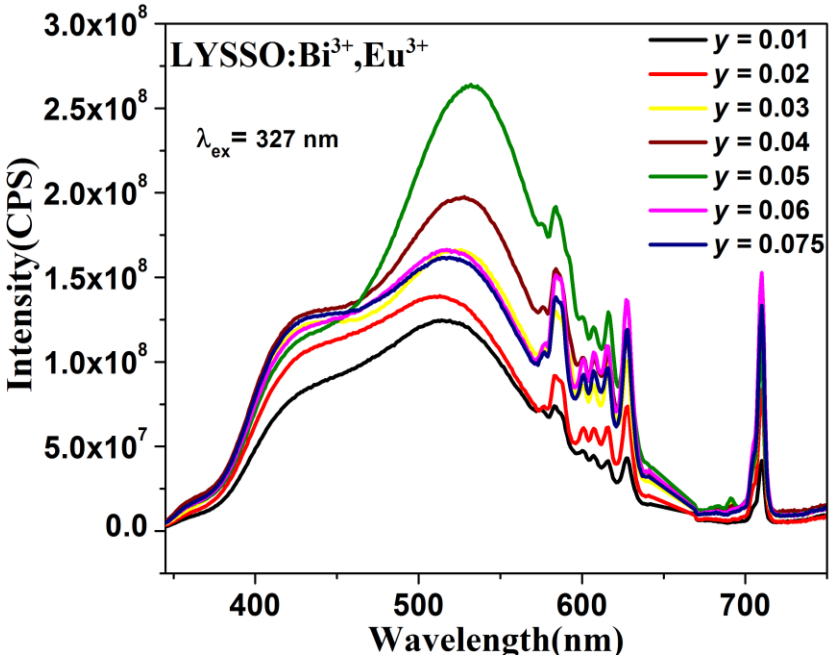

Fig.10.PL spectra of LYSSO: 0.04Bi^{3+}, *y*Eu^{3+} samples

The emission spectra corresponding to excitation wavelength 327 nm is shown in fig.10. The spectra cover the whole visible region starting from near UV region. This property is very indeed for single phase phosphor for WLED application. The emission intensity is increasing with Eu^{3+} concentration up to y = 0.05. Thereafter emission intensity of Bismuth peaks quenches with higher concentrations of Eu^{3+} and the intensity of Europium peaks increases up to the concentration y = 0.06. Thus the decreasing trend in Bismuth peaks and increasing trend in Europium peaks with increased Europium content says there exists energy transfer between Bismuth and Europium ions. The CIE values for the samples were calculated. The calculated values are very close to the ideal CIE values of white light (0.33, 0.33). A pictorial representation of calculated CIE values is represented in the color

coordinate diagram in fig. 11. As the spectra cover the whole visible region and the calculated CIE values are very close to ideal values the prepared phosphor is a good candidate for WLED application.

Table.2. CIE values of LYSSO: 0.04Bi^{3+}, yEu^{3+} samples

Concentration	CIE values
$x = 0.04, y = 0.01$	(0.27,0.36)
$x = 0.04, y = 0.02$	(0.27,0.34)
$x = 0.04, y = 0.03$	(0.29,0.36)
$x = 0.04, y = 0.04$	(0.30,0.37)
$x = 0.04, y = 0.05$	(0.32,0.42)
$x = 0.04, y = 0.06$	(0.30,0.36)
$x = 0.04, y = 0.075$	(0.29,0.35)

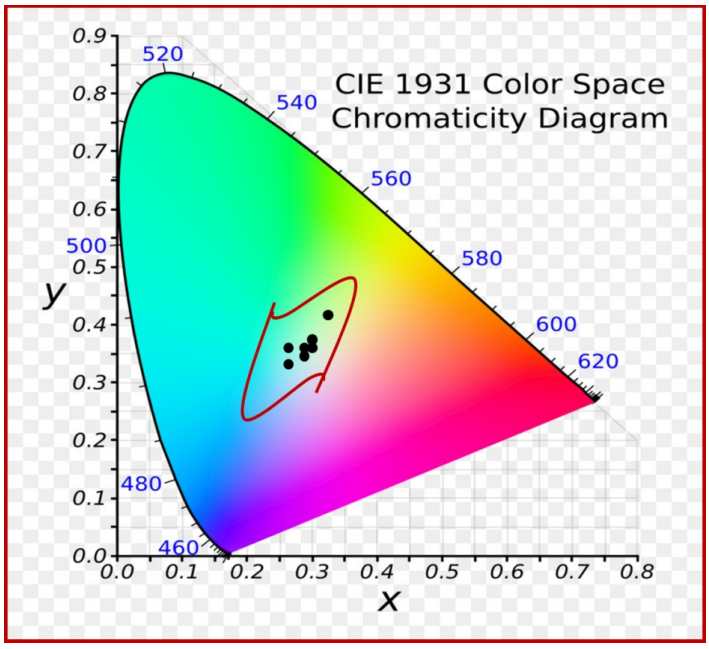

Fig.11.CIE diagram of LYSSO: 0.04Bi^{3+}, yEu^{3+} samples

The study was further progressed with efforts to understand the energy transfer mechanism existing in the phosphor. Lifetime decay curves were recorded and it is depicted in fig. 12. Decay rates were recorded for excitation wavelength 327 nm and emission wavelength 616 nm.

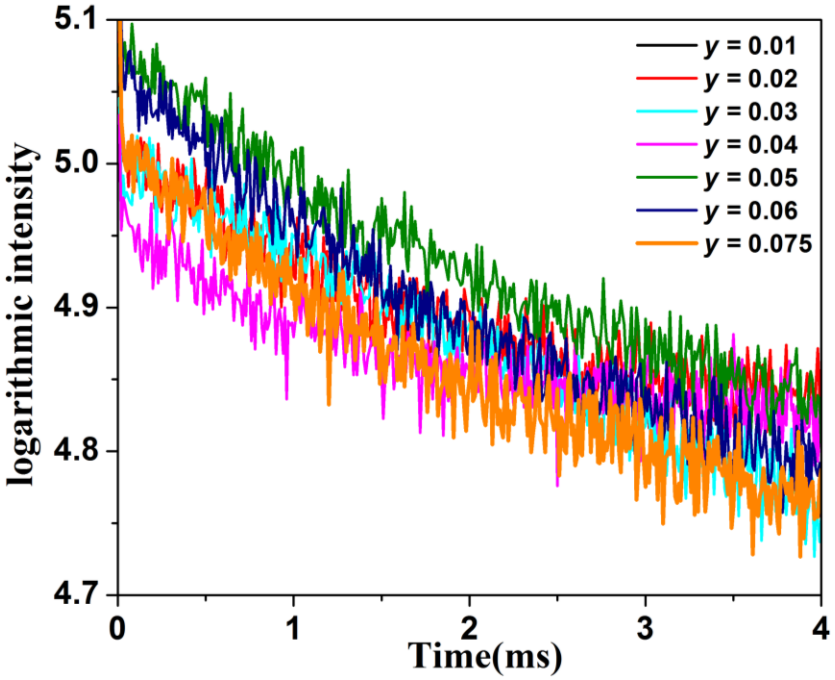

Fig.12. Lifetime decay curves of LYSSO: 0.04Bi^{3+}, *y*Eu^{3+} samples

Table.3. Lifetime values of LYSSO: 0.04Bi^{3+}, *y*Eu^{3+} samples

Concentration	Lifetime
$x = 0.04, y = 0.01$	2.65
$x = 0.04, y = 0.02$	1.55
$x = 0.04, y = 0.03$	1.55
$x = 0.04, y = 0.04$	1.13
$x = 0.04, y = 0.05$	2.05
$x = 0.04, y = 0.06$	1.88
$x = 0.04, y = 0.075$	1.85

As the decay rates show a continuous decreasing tendency the existence of effective energy transfer between the activator and sensitizer ions can be confirmed. The resonant type energy transfer between activator and sensitizer ions depends on the distance between them. The critical distance between the activator and sensitizer ions can be calculated using the equation suggested by Blasse,

$$R_c = 2[\frac{3V}{4\pi X_c N}]^{\frac{1}{3}} \qquad \cdots\cdots\cdots\cdots\cdots\cdots (1)$$

Where, X_c is the critical doping concentration of Bi^{3+} and Eu^{3+} ions; N is the total number of La sites per unit cell that can be occupied by Bi^{3+} and Eu^{3+} ions; V denotes the cell volume of the unit cell. Here X_c is 0.1, N is 1 and volume is 1239.80200 $Å^3$. The calculated value of R_c is 28.72. Since it is greater than 5 - 8 Å the possibility for energy transfer by exchange interaction can be neglected

Conclusions

Pyrochlore system $La_2Y_{0.66}Sb_{0.66}Sn_{0.66}O_7$ was synthesized via solid state reaction method. Phase purity of the samples was ensured from powder x-ray diffraction patterns. Absorption strength of the samples in the UV region was analyzed. Morphological characteristics of the samples were understood from SEM analysis. Presence of each element in the matrix was confirmed from EDS analysis. X-ray dot mapping images ensure the uniform distribution of elements in the matrix. Photoluminescence studies were conducted for Bismuth alone doped samples as well as Europium co-doped samples. These studies reveal that Bismuth alone doped samples produce broad emission peak in the blue – green region of visible spectra. The spectral absence in the red region was compensated with Europium co-doping. Europium co-doped samples produce full color emission covering the whole visible region with a broad peak in blue green region and characteristics sharp peaks of Europium in the red region. CIE values of the samples falls very close to the ideal values of white light. Lifetime decay measurements were recorded and decay time was also tabulated. The existence of any type of energy transfer such as dipole – dipole, dipole – quadrupole, etc… couldn't find out in this system of phosphors. As the emission spectra cover the whole visible region and CIE values are very close to the ideal value, this phosphor can be suggested as a potential candidate for WLED application.

Chapter 7

Conclusions And Future Aspects

This chapter summarizes the major conclusions derived from the work based on Synthesis and Photoluminescence Properties of Bi^{3+} activated Novel Single Phase Full Color Emitting Phosphors for White Light Emitting Diode Applications. A comparison of CIE values obtained from each chapter is also included in this chapter. These conclusions may be utilized to construct pc WLEDs and to develop new phosphors with suitable alterations to improve the optical properties. The future scope of the present work is also mentioned

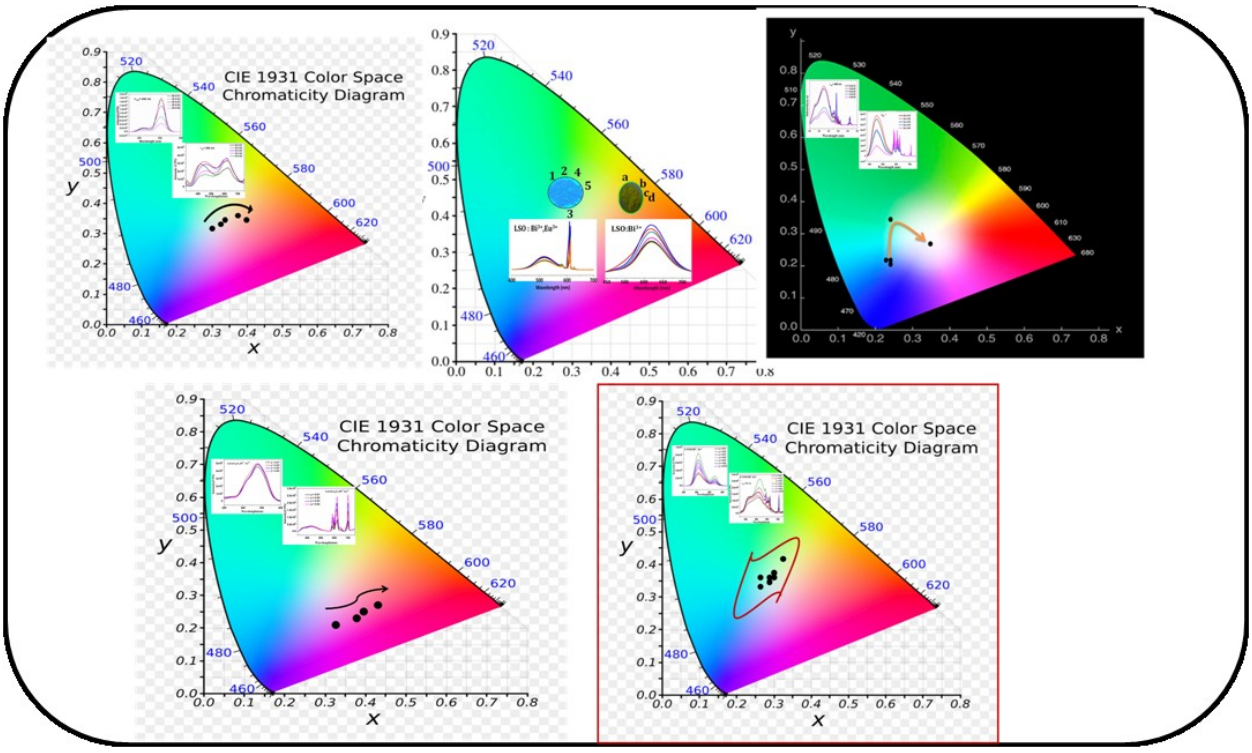

7.1 Conclusions

Series of Bi^{3+} doped phosphors were synthesized with different cationic modifications of host lattice. Their structural and optical properties were analyzed through different characterization techniques. Energy transfer mechanism underlying the luminescence behavior was studied in detail for each phosphor. The major conclusions drawn from the whole study is included below.

Studies on photoluminescence properties of weberite type phosphors with different cationic modifications were conducted. *A* site was varied with different rare earths La, Y, Gd and Lu. Better morphology and photoluminescence properties were obtained for Lanthanum. Hence Lanthanum ions were fixed in the *A* site and different metal ions were tried on *B* site. B site was varied with Sb, Ta and Nb. Compared to Antimony and Tantalum, Niobium in the *B* site gave full color emission covering the whole visible spectra. Thus the further part of the chapter discusses morphology and photoluminescence properties of Niobium based samples. The spherical morphology of the samples was revealed from SEM analysis. And full color emission property exhibited in photoluminescence produce CIE values very close to ideal values of white light.

Color - Tunable Phosphors in Weberite Type System, $La_3SbO_7:Bi^{3+}$, Eu^{3+} for Near-UV LED Applications were developed. Structural, morphological and luminescence results were studied. Spherical morphology is obtained for the samples orthorhombic crystal structure. Band gap as well as lifetime values exhibited a reducing trend which indicate the existence of energy transfer mechanism existing in the phosphor and it was studied in detail. it is found to the existence of energy transfer dipole-quadrupole mechanism.

New full color emitting phosphor through energy transfer in Bi^{3+} and Eu^{3+} co-doped La_3TaO_7 weberite system were developed through *B* site modifications. Effect of partial substitution was studied and better results were confirmed for Ta alone samples in B site. Further studies were carried out with La_3TaO_7 system. . Structural, morphological and luminescence results were studied. Spherical morphology is obtained for the samples orthorhombic crystal structure. Band gap as well as lifetime values exhibited a reducing trend which indicate the existence of energy transfer mechanism existing in the phosphor

and it was studied in detail. it is found to the existence of energy transfer dipole-quadrupole mechanism.

Novel $LaGaGe_2O_7$ single phase phosphors were developed for WLED applications. Bismuth alone doped samples produce emission in UV/ blue region of visible spectra. Cerium substitution was made to tune the PL properties. But desired results couldn't obtained from Cerium substitution. Thus further study was carried out with Europium co-doping. Europium co-doped samples exhibited full color emission with a small gap in green region of the visible spectra. CIE values of the samples were calculated and the energy transfer mechanism underlying the luminescence behavior of the phosphor was studied in detail. Best fit was obtained for n = 8. And thus energy transfer by dipole-quadrupole mechanism is found to be exists in this system.

Full color emission in Pyrochlore type phosphor$La_2Y_{0.66}Sn_{0.66}Sb_{0.66}O_7$ was studied. Phase purity of the samples was confirmed from powder XRD analysis and SEM analysis was performed to understand the morphology of the samples. EDS and X-ray dot mapping results were analyzed to understand the presence of elements and uniform distribution of the elements. Photoluminescence study shows that the emission spectrum covers the whole visible region from 400 nm to 700 nm. And the CIE values show very close resemblance with ideal values of white light. Thus this Pyrochlore phosphor is proposed to be an ideal candidate as direct white emitting single phase phosphor for WLED applications.

7.2 Future scope

- Temperature dependent luminescence behavior of the prepared phosphors should be studied in detail
- Understanding on effect of different characterization techniques on particle size and to luminescence behavior is needed
- Introducing different combinations of co-dopants to produce maximum full color emission
- Incorporation of developed phosphors on suitable near UV/Blue LED chips

References

Lei Chen, Chun-Che Lin , Chiao-Wen Yeh and Ru-Shi Liu, "Light Converting Inorganic Phosphors for White Light-Emitting Diodes", *Materials,* 3(**2010**), 2172-2195.

Ropp RC "Luminescence and the solid state", 2nd edn., *Elsevier Publishers* B. V., The Netherlands,(**2004**).

K. N. Shinde et al., "Phosphate Phosphors for Solid-State Lighting", *Springer Series in Materials Science*, 174(**2013**), Springer-Verlag Berlin Heidelberg.

Hong-Tao Sun, Jiajia Zhou, Jianrong Qiu, "Recent advances in bismuth activated photonic materials", *Progress in Materials Science,* 64, (**2014**), 1–72.

A. M. Srivatava, A. Szarowski, "On the Quenching of Bi^{3+} Luminescence in the Pyrochlore Gd2GaSbO7", *Journal of Solid State Chemistry,* 146(**1999**), 494-498.

V. G. Suchithra, Padala Prabhakar Rao, and B. A. Aswathy, "Color - Tunable Phosphors in Weberite Type System, $La_3SbO_7:Bi^{3+}$, Eu^{3+} for Near-UV LED Applications",Chemistry Select, 2,(**2017**), 7602– 7611.

D.S. McClure, C. Pedrini, "Excitons trapped at impurity centers in highly ionic crystals" Phys.Rev.B 32(**1985**), 8465.

A.M. Srivastava, Luminescence of Eu^{3+}, Tb^{3+} and Bi^{3+} in the Weberite $NaGdSb_2O_7$, J.Luminescence. 69(**1996**), 301.

Nakamura S, Mukai T, Senoh M. "Candela-class high-brightness InGaN/AlGaN doubleheterostructure blue-light-emitting diodes". *Appl. Phys. Lett.* 64(**1994),** 1687–89.

Mengmeng Shang, Chunxia Li* and Jun Lin* "How to produce white light in a single-phase host?" ***Chem. Soc. Rev., (*2014**)*,43, 1372

F.B.Xiong, C.Y.Han H.F. Lin, Y.P.Wang, H.Y.Lin, H.X.Shen, W.Z.Zhu., "White light emission from novel host-sensitized single-phase Y_2WO_6: Ln^{3+} (Ln^{3+}=Eu^{3+}, Dy^{3+}) phosphors", Volume 42, (**2016**), 13841-13848.

G.H. Dieke, H.M. Crosswhite, "The Spectra of the Doubly and Triply Ionized Rare Earths", *Applied Optics*, **2** (**1963**), 675-686.

N. Sabbatini, M. Guardigli, J.M. Lehn, "Luminescent lanthanide complexes as photochemical supramolecular devices", *Coordin Chem Rev*, 123 (1993) 201-228.

J.C.G. Bünzli, G.R. Choppin, " *Lanthanide probes in life, chemical, and earth sciences : theory and practice"*, Elsevier, Amsterdam ; New York, **1989**.

J. Holsa, M. Lastusaari, M. Marysko, M. Tukia, "A few remarks on the simulation and use of crystal field energy level schemes of the rare earth ions"**,** *J Solid State Chem*, 178 (**2005**) 435-440.

B.R. Judd,"Optical Absorption Intensities of Rare-Earth Ions"*Phys. Rev.*, 127 (**1962**) 750.

G.S. Ofelt, "Intensities of crystal spectra of rare-earth ions" *J. Chem. Phys.*, **37** (**1962**) 511-520.

G.S. Ofelt, "Structure of the f^6 Configuration with Application to Rare-Earth Ions", *J. Chem. Phys.*, 38 (**1963**), 2171-2180.

S. Cotton, "Lanthanide and actinide chemistry", Wiley, Chichester, England;Hoboken, NJ, (**2006)**

H.J. Rossell, J. Solid State Chem. 2 (1979) 115.

L. Cai, S. Denev, V. Gopalan, J.C. Nino, J. Am. Ceram. Soc. 93 (2010), 875.

L. Cai, J.C. Nino, J. Solid State Chem. 184 (2011) 2263.

C.R. Stanek, "Atomic scale disorder in fluorite and fluorite related oxides", Ph.D Thesis, University of London, London (**2003**).

Zhengwen Yang, Jiayan Liao, Shenfeng Lai, " Energy transfer and photoluminescence properties in Bi^{3+} and Eu^{3+} co-doped $ZnGa_2O_4$", *Mater.Express,* 3(**2013**),350-354.

Renping Cao, ting Fu, Dedong Peng, "synthesis, energy transfer and tunable emission properties of srSb2O6:Eu3+, Bi3+ phosphor", Spectrochimica Acta Part A: Molecular and Biomolecular spectroscopy, 169(**2016**), 192-196.

A.K. Harari, L. Mazerolles, D. Michel, F. Robert, "Structural description of La_3NbO_7", *J. Solid state Chem.*116 (1995) 103.

Blasse G., Grabmair B. C., "Luminescent Materials", *Springer*, Berlin, (**1994**).

Blasse G., "Energy transfer in oxidic phosphors", *Phys. Lett. A*, 28 (**1968**) 444-445**.**

Blasse G., "Handbook on the Physics and Chemistry of rare-earths", *North Holland Publishing Company*, Netherlands, (**1979**).

Chen M., Tanner D. B., Nino J. C., "Infrared study of the phonon modes in bismuth pyrochlores", *Phys. Rev. B*, 72 (**2005**) 054303-8.

Ege A., Ayvacikli M., Dinçer O., Satılmış S. U., "Spectral emission of rare earth (Tb, Eu, Dy) doped Y2Sn2O7phosphors" *J. Lumin.,* 143 (**2013**) 653-656.

Jing X., Gibbons C., Nicholas D., Silver J., Zhang X., Vecht A., Frampton C. S., "Blue luminescence in yttrium and gadolinium niobates caused by bismuth. The importance of non-bonding ns2 valence orbital electrons", *J. Mater. Chem.*, 9 (**1999**) 2913-2918.

Jones E. D., "Light emitting diodes for general illumination", *OIDA report*, **2001**

Hou J., Yin X., Fang Y., Huang F., Jiang W., "Novel red-emitting perovskite-type phosphor CaLa1-*x*MgM'O6:*x*Eu3+ (M' = Nb, Ta) for white LED application", *Opt. Mater*., 34 (**2012**) 1394-1397.

L. Cai, J.C. Nino, **"**Complex ceramic structures. I. Weberites", *Acta Cryst. B*, 65 **(2009)** 269.

Justel T., Nikol H., Ronda C., "New developments in the field of luminescent materials for lighting and displays", *Angew. Chem.,* 37 (**1998**) 3084-3103.

Kennedy B. J., Hunter B. A., Howard C. J., "Structural and bonding trends in tin pyrochlore oxides", *J. Solid State Chem*., 130 (**1997**) 58-65.

Liu X. M., Lin J., "Enhanced luminescence of gadolinium niobates by Bi3+ doping for field emission displays", *J. Lumin*., 122 (**2007**) 700-703.

Khan N., Abas N., "Comparative study of energy saving light sources", *Renewable Sustainable Energy Rev.*, 15 (**2011**) 296-309.

Lee S. K., Chang H., Han C. H., Kim H. J., Jang H. G., Park H. D., "Electronic structures and luminescence properties of YNbO4 and YNbO4:Bi", *J. Solid State Chem*., 156 (**2001**) 267-273.

Li K., Zhang Y., Li X. J., Shang M. M., Lian H. Z., Lin J., "Host-sensitized luminescence in $LaNbO4:Ln^{3+}$ (Ln^{3+} = Eu^{3+}/Tb^{3+}/Dy^{3+}) with different emission colors, *Phys. Chem. Chem. Phys.,* 17 (**2015**) 4283-4292.

Liu G. K., Jacquier B., "Spectroscopic properties of rare earths in optical materials", *Springer*, (**2005**).

Kaufman J. E., Christensen J. F., "Lighting Handbook", *Waverly Press*, Maryland, (**1972**)
McCamy C. S., "Correlated color temperature as an explicit function of chromaticity coordinates", *Color Res. Appl*., 17 (**1992**) 142-144.

McCauley R. A**.,** "Structural characteristics of pyrochlore formation", *J. Appl. Phys.*, 51 (**1980**) 290-294.

Wang J., Cheng Y., Huang Y., Cai P., Kim S. I. and Seo H. J., "Structural and luminescent properties of red-emitting Eu^{3+}-doped ternary rare earth antimonates R_3SbO_7 (R = La, Gd, Y)", *J. Mater. Chem. C*, 2 (**2014**) 5559–5569.

Ye S., Xiao F., Pan Y. X., Ma Y. Y., Zhang Q. Y., "Phosphors in phosphor-converted white light-emitting diodes: Recent advances in materials, techniques and properties", *Mater. Sci. Eng. R,* 71 (**2010**) 1-34.

Minervini L., Grimes R. W., "Disorder in pyrochlore oxides", *J. Am. Ceram. Soc*., 83 (**2000**) 1873-1878.

Subramanian M. A., Aravamudan G., Rao G. V. S., "Oxide pyrochlores-A review" *Prog. Solid State Chem*., 15 (**1983**) 55-143.

Ofelt G. S., "Intensities of crystal spectra of rare-earth ions." *J. Chem. Phys*., 37 (**1962**) 511-520.

Y. Hinatsu, Y. Doi, "Magnetic properties and structural transitions of fluorite-related rare earth osmates Ln_3OsO_7(Ln= Pr, Tb)", *J. Solid State Chem*, 198 (**2013**) 176.

E. Grey, W.G. Mumme, T.J. Ness, R.S. Roth, K.L. Smith, "Structural relations between weberite and zirconolite polytypes—refinements of doped 3T and 4M $Ca_2Ta_2O_7$ and 3T $CaZrTi_2O_7$", *J. Solid State Chem.* 174 (**2003**) 285.

W.T. Fu, D.J. W. Ijdo, " On the crystal structures of Ln_3MO_7 (Ln= Nd, Sm, Y and M= Sb, Ta)—Rietveld refinement using X-ray powder diffraction data", *J. Solid State Chem.* 182 (2009) 2451.

R.C Severence, A.H. Fox, S.J. Mugavero, M.D. Smith, "Synthesis and Crystal Structures of Two Polymorphs of Trilanthanum Iridium Septaoxide (La_3IrO_7)", J. Chem *Crystallogr*. 41(**2011**) 496.

S.A. Kovyazina, L.A. Perelyaeva, I.A. Leonidov, Yu. A. Bakhteeva, "High-Temperature Structural Disorder in R_3NbO_7", *J.Struct. Chem.* 44 (**2003**) 975.

M.A. Subramanian, G. Aravamudan G.V. SubbaRao, "Oxide pyrochlores—a review", *Prog. Solid State*, Chem. 15 (**1983**) 55.

L. Cai, J.C. Nino, **"**Synchrotron and neutron powder diffraction study of phase transition in weberite-type Nd_3NbO_7 and La_3NbO_7", J. Solid State Chem. 184 **(2011),** 2263.

H.J. Rossell, **"**Fluorite-related phases Ln_3MO_7, Ln= rare earth, Y or Sc, M= Nb, Sb, or Ta: II. structure determination", *J. Solid State Chem.* 2 (**1979**)**,** 115.

K.P.F. Siqueria, R.M. Borhes, E. Granado, L.M. Malard, A.M. de Paula, R.L. Moreira, E.M. Bittar, A. Dias, Crystal structure of fluorite-related Ln_3SbO_7 (Ln= La–Dy) ceramics studied

by synchrotron X-ray diffraction and Raman scattering**,** *J. Solid State Chem*. 203 (**2013**), 326-332.

K.P.F. Siqueira, J.C. Soares, E. Granado, E.M. Bittar, A.M. de Paula, "Synchrotron X-ray diffraction and Raman spectroscopy of Ln_3NbO_7 (Ln= La, Pr, Nd, Sm-Lu) ceramics obtained by molten-salt synthesis", J.Solid State Chem. 209 (**2014**) 63.

R.C Severence, A.H. Fox, S.J. Mugavero, M.D. Smith, "Synthesis and Crystal Structures of Two Polymorphs of Trilanthanum Iridium Septaoxide (La_3IrO_7)" , J. Chem Crystallogr. 41(**2011**), 496.

J.E. Greedan, N.P. Raju, A. Wegner, A study of the structure and electronic and thermal properties of quasi-one-dimensional La3MoO7, J. Solid State Chem. 129, (**1997**), 320 - 327.

L. Cai, J.C. Nino, Phase formation and dielectric properties of Ln2 (Ln′0.5 Nb0. 5) 2O7 (Ln= rare earth element),J. Eur. Ceram. Soc. 30 (**2010**) 307.

L. Cai, "Fundamental structure-dielectric property relationships in fluorite-related ceramics", PhD Thesis, University of Florida, (**2010**)

Simas Šakirzanovas, PhD thesis, Vilnius university Center for physical sciences and technology Institute of chemistry Simas Šakirzanovas, Vilnius, 2011.

D. Yanyan, Z. Yuan, H. Keke, W. Shan, Y. Long, F. Shouhua, DaltonTrans. 42 (**2013**) 8041.

W Xie, Y Mo, C Zou, F Kang, G Sun, "Broad color tuning and Eu^{3+}-related photoemission enhancement via controllable energy transfer in the La_2MgGeO_6: Eu $^{3+}$, Bi $^{3+}$ phosphor", *Inorg.chem.front.*,(**2018**),1076-1084.

G. Li, Y. Tian, Y. Zhao, J. Lin, Recent progress in luminescence tuning of Ce^{3+} and Eu^{2+}-activated phosphors for pc-WLEDs, Chem. Soc. Rev. (**2015**), 44, 8688–8713.

L. Chen, C. C. Lin, C. W. Yeh, R. S. Liu, Light converting inorganic phosphors for white light-emitting diodes,Materials (**2010**), 3, 2172–2195.

F. Kang, Y. Zhang, M. Peng, Controlling the Energy Transfer via Multi Luminescent Centers to Achieve White Light/Tunable Emissions in a Single-Phased X2-Type $Y_2SiO_5:Eu^{3+},Bi^{3+}$ Inorg. Chem. (**2015**), 54(4), 1462–1473.

Y. Feng, J. Huang, L. Liu, J. Liu, X. Yu, Enhancement of white-light-emission from single-phase Sr 5 (PO 4) 3 F: Eu 2+, Mn 2+ phosphors for near-UV white LEDs,Dalton Trans. 2015, 44, 15006–15013.

F. B. Xiong, C. Y. Han, H. F. Lin, Y. P. Wang, H. Y. Lin, H. X. Shen, W. Z. Zhu, White light emission from novel host-sensitized single-phase Y2WO6: Ln3+ (Ln3+= Eu3+, Dy3+) phosphors,Ceram. Int. 2016, 42, 13841–13848.

T. Linda Francis, P. Prabhakar Rao, S. K. Mahesh, T. S. Sreena, S. Parvathi Babu, Effect of host structure on the photoluminescence properties of Ln3TaO7: Eu3+ red phosphors, Opt. Mater. 2016, 52, 134–143.

M. Wakeshima, Y. Hinatsu, Magnetic properties and structural transitions of orthorhombic fluorite-related compounds Ln3MO7 (Ln= rare earths, M= transition metals), J. Solid State Chem. 2010, 183, 2681–2688.

Z. M. Li, L. G. Deng, S. C. Zhao, S. Q. Zhang, C. Y. Guo, J. Y. Liang, H. Yue, C. Y. Wan, Crystal structure of Ba 2 (La 0.727 Ba 0.182 M 0.091) MO 6 (M= Nb, Sb, Bi): symmetry nuance identified in photoluminescence and IR spectroscopy studies, Luminescence 2016, 32, 462–467.

A. M. Srivastava, On the luminescence of Bi3+ in the pyrochlore Y2Sn2O7, Mater. Res. Bull. 2002, 37, 745–751.

Z. Jiang, J. Gou, X. Yu, X. Su, Y. Duan, Z. Sun, L. Duan, Luminescence and energy transfer of single-phase and color-tunable Ca2Y3Sb3O14: Bi3+, Eu3+ phosphor for white light-emitting diodes, J. Alloys Compd.
2015, 650, 598–603.

G. Blasse, A. Bril, Investigations on Bi^{3+}-Activated Phosphors,J. Chem. Phys. 1968, 48, 217–222.

X. Y. Huang, X. H. Ji, Q. Y. Zhang, Broadband Downconversion of Ultraviolet Light to Near-Infrared Emission in Bi^{3+}–Yb^{3+}-Codoped Y_2O_3 Phosphors, J. Am. Ceram. Soc. 2011, 94[3], 833–837.

L. Wang, Q. Sun, Q. Liu, J. Shi, Investigation and application of quantitative relationship between sp energy levels of Bi3+ ion and host lattice, J. Solid State Chem. 2012, 191, 142–146.

U. Rambabu, S. D. Han, Synthesis and luminescence properties of broad band greenish-yellow emitting LnVO4: Bi3+ and (Ln1, Ln2) VO4: Bi3+ (Ln= La, Gd and Y) as down conversion
Ceram. Int. 2013, 39, 701–708.

F. Kang, X. Yang, M. Peng, L. Wondraczek, Z. Ma, Q. Zhang, J. Qiu, Red Photoluminescence from Bi^{3+} and the Influence of the Oxygen-Vacancy Perturbation in $ScVO_4$: A Combined Experimental and Theoretical Study, J. Phys.Chem. C. 2014, 118, 7515-7522.

S. Yao, L. Chen, Y. Huang, W. Li, Enhanced luminescence of CaSb2O6: Bi3+ blue phosphors by efficient charge compensation,Mater. Sci. Semicond. Process. 2016, 41, 265–269.

X. Y. Liu, H. Guo, Y. Liu, S. Ye, M. Y. Penga, Q. Y. Zhang, Thermal quenching and energy transfer in novel Bi 3+/Mn 2+ co-doped white-emitting borosilicate glasses for UV LEDs,J. Mater. Chem. C.
2016, 4, 2506–2512.

Y. Chen, J. Wang, C. Liu, X. Kuang, Q. Su, A host sensitized reddish-orange $Gd_2MoO_6:Sm^{3+}$ phosphor for light emitting diodes, Appl. Phys. Lett. 2011, 98, 081917(1)-081917(3).

H. Zhou, Y. Jin, M. Jiang, Q. Wang, X. Jiang, A single-phased tunable emission phosphor MgY 2 Si 3 O 10: Eu 3+, Bi 3+ with efficient energy transfer for white LEDs Dalton Trans. 2015, 44, 1102–1109.

Z. Tang, D. Wang, Y. Wang, W. U. Khan, S. Du, Photoluminescence of BaZrSi3O9: Bi3+ as a yellow emitting phosphor for White LEDs
Mater. Res. Bull. 2016, 83, 336–339.

H. T. Sun, J. Zhou, J. Qiu, Recent advances in bismuth activated photonic materials, Prog. Mater. Sci. 2014, 64, 1–72.

Z. Yang, J. Liao, S. Lai, H. Wu, Z. Fan, J. Qiu, Z. Song, Y. Yang, D. Zhou, Energy transfer and photoluminescence properties in Bi3+ and Eu3+ co-doped ZnGa2O4, Mater. Express 2013, 3, 350–354.

A. Huang, Z. Yang, C. Yu, Z. Chai, J. Qiu, Z. Song, Tunable and White Light Emission of a Single-Phased $Ba_2Y(BO_3)_2Cl:Bi^{3+},Eu^{3+}$ Phosphor by Energy

Transfer for Ultraviolet Converted White LEDs,J. Phys. Chem. C 2017,121, 5267-5276.

H. Zhou, Q. Wang, Y. Jin, Temperature dependence of energy transfer in tunable white light-emitting phosphor BaY 2 Si 3 O 10: Bi 3+, Eu 3+ for near UV LEDs, J. Mater. Chem. C 2015, 3, 11151–11162.

S. Khaja Hussain, J. S. Yu, Sol-gel synthesis of Eu3+/Bi3+ ions co-doped BaLa2WO7 phosphors for red-LEDs under NUV excitation and FEDs applications, J. Lumin. 2017, 183, 39–47.

I. V. B. Maggay, P. C. Lin, W. R. Liu, Thermal effects in (oxy) nitride phosphors, J. Sol. State Light. 2014, 1, 1–13.

Z. Jiang, X. Yu, J. Gou, L. Duan, X. Su, G. Fan, Y. Duan, Design, luminescence and energy transfer of single-phased color-tunable $YNbO_4$: Bi^{3+}, Eu^{3+} phosphor for UV pumped white light-emitting diodes, J Mater Sci: Mater, Electron. 2017, 28, 3630–3636.

L. Wang, K. Moon, S. H. Park, K. H. Kim, J. H. Jeong, Synthesis and photoluminescence of Bi 3+, Eu 3+ doped CdWO 4 phosphors: application of energy level rules of Bi 3+ ions, RSC Adv. 40, (**2016**), 3552–3560**.**

G. Blasse, B. C. Grabmaier, Luminescent Materials, Springer, 92–93, **1994**.

P. Chen, F. Mo, A. Guan, R. Wang, G. Wang, S. Xia, L. Zhou, Luminescence and energy transfer of the color-tunable phosphor $Li_6Gd(BO_3)_3$: Tb^{3+}/Bi^{3+}, Eu^{3+} Appl. Radiat. Isot. (**2016**), 108, 148–153

Jun Zhou, Quanlin Liu and Zhiguo Xia, Structural construction and photoluminescence tuning via energy transfer in apatite-type solid-state phosphors. J. Mater. Chem. C.6(**2018**), 4371-4383.

Qiyue Shao, Hao Ding, Leqi Yao, Junfeng Xu, Chao Liang and Jianqing Jiang , Photoluminescence properties of a ScBO3:Cr3+ phosphor and its applications for broadband near infrared LEDs. RSC Adv. **8**,12035, (**2018**).

Shaoan Zhang, Yihua Hu, Ren Chen, Xiaojuan Wang, Zhonghua Wang, Photoluminescence and persistent luminescence in Bi3+-doped Zn2GeO4 phosphors. Optical Materials **36**, 1830-1835, (2014).

G. Blasse, B.C. Grabmaier, Luminescence Materials vol. 2, (Springer, Berlin, Heidelberg, 1994), pp 28-29

L.L. Wang, Z.F. Lv, W.K. Kang, X.Y. Shangguan, J.S. Shi, Z.H. Hao, Applications oriented design of Bi3+ doped phosphors. Appl. Phys. Lett. **102** , 151909, (2013)

L.L. Wang, Q.L. Wang, X.Y. Xu, J.Z. Li, L.B. Gao, W.K. Kang, J.S. Shi, J. Wang, Energy transfer from Bi3+ to Eu3+ triggers exceptional long-wavelength excitation band in ZnWO4:Bi3+, Eu3+ phosphors Mater.Chem. C 1, 8033-8040, (2013)

Lili Wang, Qiang Sun, Qingzhi Liu, Jinsheng Shi, Investigation and application of quantitative relationship between sp energy levels of Bi3+ ion and host lattice. J.Solid State Chem.191,142-146, (2012)

R. Mohan, Green bismuth. Nat.Chem. **2**, 336, (2010)

Thomas Jüstel, Hans Nikol, and Cees Ronda, New Developments in the Field of Luminescent Materials for Lighting and Displays. Angew. Chem. Int. Ed. **37**, 3084 -3103, (1998)

Huang, J.; Yang, Z. W.; Yu, C. Y.; Chai, Z. Z.; Qiu, J. B.; Song, Z. G. Tunable and White Light Emission of a Single-Phased Ba2Y(BO3)2Cl: Bi3+, Eu3+ Phosphor by Energy Transfer for Ultraviolet Converted White LEDs. J. Phys. Chem. C. **121**, 5267-5276, (2017)

Mengmeng Jiao, Qinfeng Xu, Chuanlu Yang and Mingliang Liu, Electronic structure and photoluminescence properties of single component white emitting Sr3LuNa(PO4)3F : Eu2+, Mn2+ phosphor for WLEDs. J. Mater. Chem. C. **6**, 4435 - 4443, (2018)

Ropp RC, Luminescence and the solid state, 2nd edn(Elsevier Publishers B. V, 2004), 431-442

13. W. Xie, Y. Mo, C. Zou, F. Kang and G. Sun, Broad Color Tuning and Eu3+-related Photoemission Enhancement via the Controllable Energy Transfer in La2MgGeO6:Eu3+, Bi3+ Phosphor. Inorg. Chem.Front. **5**, 1076 - 1084, (2018)

Kisla P. F. Siqueira, Anderson Dias, Effect of the Processing Parameters on the Crystalline Structure of Lanthanide Orthotantalates. Mat. Res.**17**, 167-173,(2014)

Zhang Haoming, Feng Yan, Chen Xiaoge, Zhang Hongsong, Liu Yanxu, Tang An, Ren Bo, Thermal properties of La3TaO7 and La2AlTaO7 oxides. Ceramics International **43**, 755–759,(2017)

Nicolas Preux, Aure´ lie Rolle, Cindy Merlin, Messaoud Benamira, Marcin Malys, Claude Estournes,Annick Rubbens, Rose-Noelle Vannier, La3TaO7 derivatives with Weberite structure type. Possible electrolytes for solid oxide fuel cells and high temperature electrolysers. C. R. Chimie, **13**, 1351–1358,(2010)

V. G. Suchithra, Padala Prabhakar Rao, and B. A. Aswathy, Color - Tunable Phosphors in Weberite Type System, La3SbO7:Bi3+, Eu3+ for Near-UV LED Applications. Chemistry Select, **2**, 7602– 7611,(2017)

Zhigang Yang, Zhengyan Zhao, Yan Wen, Yuhua Wang, Structure and luminescence properties of Bi3+ activated Ca12Al14O32Cl2 phosphors. Journal of Alloys and Compounds. **559**,142–145, (2013)

L.G. Jacobsohn, B.C. Tappan, S.C. Tornga, M.W. Blair, E.P. Luther, B.A. Mason, B.L.Bennett, R.E.Muenchausen, The effect of hydrostatic pressure on the combustion synthesis of Y2O3:Bi nanophosphor.Opt. Mater. **32**, 652–656, (2010)

A. Wolfert, G. Blasse, Luminescence of the Bi3+ ion in compounds LnOCl (Ln = La, Y, Gd). Mater. Res.Bull. **19**, 67–75, (1984)

A. Wolfert, E.W.J.L. Omen, G. Blasse, Host lattice dependesnce of the Bi3+ luminescence in orthoborates *Ln*BO3 (with *Ln* = Sc, Y, La, Gd, or Lu). J. Solid State Chem. 59, 280–290, (1985)

Matas Janulevicius, Paulius Marmokas, Martynas Misevicius, Julija Grigorjevaite, Lina Mikoliunaite, Simas Sakirzanovas, Arturas Katelnikovas, Luminescence and luminescence quenching of highly efficient Y2Mo4O15:Eu3+ phosphors and Ceramics. Scientific Reports, **6**, 26098, (2016).

T. Linda Francis, P. Prabhakar Rao, S. K. Mahesh, T. S. Sreena, S. Parvathi Babu, Effect of host structure on the photoluminescence properties of Ln3TaO7:Eu3+ red phosphors. Opt. Mater. **52**, 134–143, (2016).

LIST OF PUBLICATIONS

1. "Color - Tunable Phosphors in Weberite Type System, La3SbO7:Bi3+, Eu3+ for Near-UV-LED Applications", **V.G. Suchithra**, Padala Prabhakar Rao, and B. A. Aswathy, ***Chemistry select*, 2017**, 2, 7602– 7611.

2. "New full color emitting phosphor through energy transfer in Bi^{3+} and Eu^{3+} co-doped La_3TaO_7 weberite system", **V.G. Suchithra,** Padala Prabhakar Rao, and B. A. Aswathy, ***Journal of Materials Science: Materials in Electronics*, , 2020,** 31, 5141–5151.

3. "New perovskite type orange red emitting phosphors, SrGd0.5Nb0.5O3:*x*Eu3+ for WLED applications", B.A. Aswathy, Padala Prabhakar Rao, and **V.G. Suchithra**, ***Materials Letters*, 2018**, 229, 182–184.

4. "New self charge compensating perovskite type red phosphors prepared via ball milling process for pc-white light emitting diode applications", B.A.Aswathy,P.Prabhakar Rao and **V.G.Suchithra, *Optics and Laser Technology,* 2020,**128,106217.

INTERNATIONAL/NATIONAL CONFERENCES ORAL/POSTER PRESENTATIONS

1. **Suchithra V. G.**, P. Prabhakar Rao, Aswathy B. A, *Morphological Assisted Luminescence Enhancement In Bismuth Doped Weberite Type Systems* ,Poster presented in National Conference on Emerging Trends in Science, Technology & Application of Electron Microscope (STAEM-2018) and 5th Annual Meeting of the

Academy of Microscope Science & Technology (AMST), India December 19 – 21, 2018, Trivandrum.

2. **Suchithra V.G**, P. Prabhakar Rao, B.A. Aswathy, *Photo Luminescence And Color Tunability Of Bi^{3+} Doped $Y_3sb_5o_{12}$ Phosphor,* poster presented in ICSTAR 2018 July 14,Tiruppathi.

3. **Suchithra V. G.**, P. Prabhakar Rao , *$La_{3-x-y}TaO_7$: xBi^{3+}, yEu^{3+} single phase phosphor for WLED Applications,* Oral presentation *at* National conference on luminescence and its applications 2018,Trivandrum.

4. **Suchithra V.G**, P. Prabhakar Rao, *Study Of Structural And Photoluminescence Properties Of Bi^{3+} Doped La_3Tao_7 Phosphor* Oral Presentation At National Conference On Critical And Strategic Materials For Advanced Technologies (CSMAT) 2017, Munnar.

5. **Suchithra V.G**, P. Prabhakar Rao, Linda Francis.T, Sreena.T.S, Parvathi.S.Babu, *Study of structural and photoluminescence properties of Ce^{3+} doped $SrLaGa_3O_7$ phosphor,* Poster presentation at National Seminar on Photonics and its Applications (NSPA-2015)December 9-11, 2015,Trivandrum.

.